ISSN 1173-5996

Exploratory Salt Water Experiments of Balcony Spill Plume Using Laser Induced Fluorescence Technique

BY

Ee Hieng Yii

Supervised by

Dr Charley Fleischmann

Fire Engineering Research Report 98/7
June 1998

This report was presented as a project report
as part of the M.E. (Fire) degree at the University of Canterbury

School of Engineering
University of Canterbury
Private Bag 4800
Christchurch, New Zealand

Phone 643 364-2250
Fax 643 364-2758

ABSTRACT

This report investigates the potential of applying salt water modelling using the Laser Induced Fluorescence (LIF) flow visualisation technique to study balcony spill plume phenomena. A 1/20 scale perspex model was used to conduct a series of salt water experiments. The testing parameters include two balcony settings (125mm and 250mm in model scale) and two spilling densities (0.5% and 1.0% of salt by weight).

Through the study, results showed that good flow visualisation could be achieved using the LIF technique. The main advantage of using the salt water modelling technique was the ease in modifying the model's geometry or testing conditions. These modifications would not result in huge changes in the data acquisition systems as in either the full or small scale fire tests.

The smoke layer within the compartment was simulated by the injection of a saline layer. By doing this, a quantitatively correct counter flow at the doorway was achieved, as in the real fire situation. This method also provided greater control over the injected flow and the flow was found to be repeatable.

From the results obtained, it was found that there was a small degree of entrainment at the rotational region of the balcony spill plume. It was also observed that the presence of the soffit at the opening would result in significant entrainment into the under-balcony flow layer. Smoke logging on the upper balcony was found to be more severe with a shorter balcony than a longer balcony; this was due to the local deepening effect.

The salt water results collected in this study could not be converted into the equivalent fire results at this stage. There are still many questions regarding the issue of scaling salt water results to full scale fire cases. Future research on the scaling laws needs to be done before the full potential of the salt water modelling technique could be utilised.

ACKNOWLEDGMENTS

I would like to thank my project supervisor Dr. Charlie Fleischmann for his enthusiasm and dedication on this project. His advice and suggestions were always available when needed.

To Associate Professor Andy Buchanan, I would like to thank Andy for his endless encouragement and support during my study. His enthusiasm has been inspirational.

To my friend, Mr. Jason Clement for his dedication of personal spare time in assisting me in my experiments and data processing. I wish to sincerely thank Jason for all the help he had given me. I also thank Ian Sheppard and Alan Poynter for their help with the model and equipment, Peter Coursey for his help with the computer and Dave MacPherson for preparing the dye. I would like to extend my thank to my friend, Mr. Ra Cleave for his help during my difficult time with Matlab software.

I thank my friends Per Olsson, Andre Lovett, Bill Wallace and Neil Gravestock for their supports, helps and laughs. Best wishes for you all in the future. I thank my family for their love and encouragement.

Special thanks to my friend, Dr. Anne Ditcher for proof-reading this report and many helpful comments.

I greatly appreciate the financial support provided by the New Zealand Fire Service Commission.

TABLE OF CONTENTS

LIST OF FIGURES

LIST OF TABLES

NOMENCLATURE

English Symbols

B	Experimental constant
b	Characteristic half-width of line plume
C_d	Discharge coefficient
c_p	Specific heat
D	Depth of gas stream beneath ceiling
D_f	Diameter of fire source
d_1	Effective height of clear layer above balcony
Fr	Froude Number
G	Ratio of length scales cubed, Equation (3.15)
g	Gravitational constant
H	Height of soffit of balcony above fire or Height of compartment in salt water scaling equations
h	Height of salt water model compartment
h_v	Height of vent above balcony
k	Thermal conductivity
L	Width of fire compartment opening, length of line source or Characteristic length of heat source in salt water scaling equations
l	Characteristic length of salt water source
M	Mass flow rate of gases
δM	Mass per second of air entrained into free ends of plume
m	Mass flow rate per unit width of gas stream
Pr	Prandtl Number
$\tilde{p}$	Pressure perturbation about hydrostatic
p'	Dimensionless buoyancy on plume axis
Q	Heat output, heat flux or Volumetric flow rate
Re	Reynolds Number

Sc	Schmidt Number
T	Absolute gas temperature
ΔT_{max}	Temperature rise on plume axis at height x
ΔT	Temperature rise on plume axis
t	Time
U	Velocity
$\bar{u}$	Mean velocity
u	Vertical gas velocity
v	Horizontal velocity of gas
W	Width of gas flow
x	Height above edge of balcony
$\bar{x}$	Position vector in salt fire situation
Y	Mass fraction of salt
z	Height above effective source of plume

Greek Symbols

α	Entrainment constant for plume (=0.16 for double sided plume)
α'	Entrainment constant for air mixing into gases rotating around a horizontal edge
θ	Excess temperature of gases above ambient temperature
Δ	Depth of effective line source below real source
ρ	Density
κ_M	Profile correction factor for mass flow (approx. 1.3)
κ_Q	Profile correction factor for heat flux (approx. 0.95)
λ	An empirical thermal plume constant (λ=0.90)
μ	Dynamic viscosity
υ	Kinematic viscosity
ζ	Perturbation scale

Subscripts

0	A source property
1	An ambient property
c	Variable evaluated at highest point in a flow (but outside any boundary layer)
G	A property of the equivalent Gaussian source
g	Fire situation
in	Entering the compartment
out	Out going from the compartment
r	A property evaluated at an arbitrary height above the balcony
s	Salt water situation
w	Variable evaluated in the horizontal flow at opening

Superscripts

*	Non-dimensional

ABBREVIATIONS

- BRE Building Research Establishment
- CFD Computational Fluid Dynamics
- Glab Global Lab® Image software, Version 2, 1992
- IMS Industrial Methylated Spirits
- LES Large Eddy Simulation
- LIF Laser Induced Fluorescence
- Matlab Matlab® for Windows software, Classroom Version 4.2c.1, 1994
- NFPA National Fire Protection Association
- PIV Particle Induced Velocimetry

CHAPTER 1

1 INTRODUCTION

In this introduction, the concept of balcony spill plume is introduced and its significance in the smoke control system design is discussed. Illustrations on the need for investigations in this field are made.

1.1 GENERAL

Nowadays, there are an increasing number of multi-storey pedestrian malls being built throughout the world. The current architectural trend in shopping mall design is to artificially create an outdoor environment within the mall. The intention is to create visually and spatially an ideal external environment indoors (Saxon, 1983). To achieve this objective, the idea of the atrium which originates back in the Roman Empire is revised and blended into modern shopping mall designs. Today, atria are always designed as undivided volumes within a structure that connects between levels inside the mall.

Atria are used as focal points for the malls. In order to feature the atria, modern atrium buildings arrange stores or rooms adjacent to the atria. To appreciate the view from within the adjacent rooms, the room to atrium boundary is usually either glazed or completely open. Compared to "conventional" building, this architectural feature creates additional problems for life safety during a fire situation. As an undivided volume within the structure, the smoke, hot gases and even flames may spread from the source(s) via the atrium to other areas relatively remote from the fire source. Additionally these large shopping malls tend to contain large quantities of combustible materials and large numbers of people. With the open-plan layout nature, it creates a very unfavourable situation to protect or evacuate people in an emergency (Hansell and Morgan, 1994). A schematic diagram of a typical two-level shopping mall is shown in Figure 1.1.

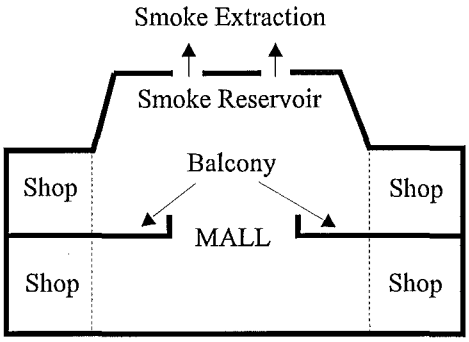

Figure 1.1 A schematic diagram of a typical two-level shopping mall.

1.2 BALCONY SPILL PLUME

As indicated in Figure 1.1, it is common to have balconies on upper floors serving as pedestrian walkways. The presence of this architectural feature introduces an additional member into the fire plume family. It is known as the *balcony spill plume.* When a fire occurs within a store of a large shopping mall, the smoke that "spills" from underneath a balcony into an atrium is referred as balcony spill plume. These plumes will entrain a large amount of air when they rise, hence producing a large quantity of smoke. Figure 1.2 shows a schematic view of a balcony spill plume within an atrium building.

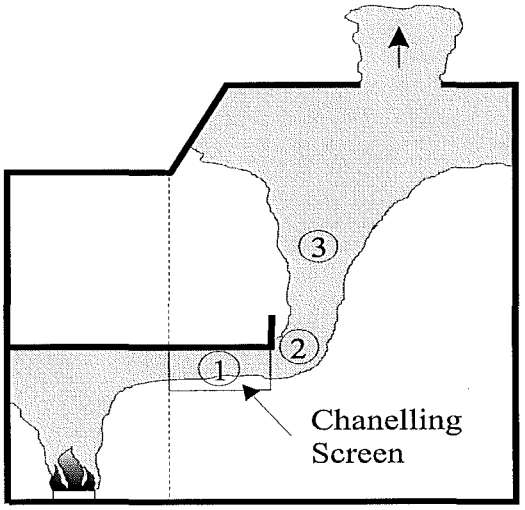

Figure 1.2 The balcony spill plume.

Balcony spill plume can be considered to consist of 3 parts as indicated in Figure 1.2.

1. The smoke rises from the fire forming a hot smoky layer in the shop and then flows under the fascia beneath the balcony. There it will spread laterally while travelling to the balcony edge, unless contained by parallel curtains running from the shop front to the balcony edge.
2. The smoke will flow around the balcony edge like an "inverted waterfall". This region is usually noted as the "rotation" or "turning" region for the balcony spill plume.
3. The smoke rises as a line plume into the hot smoky gas within the ceiling reservoir. This is shown in Figure 1.3 below.

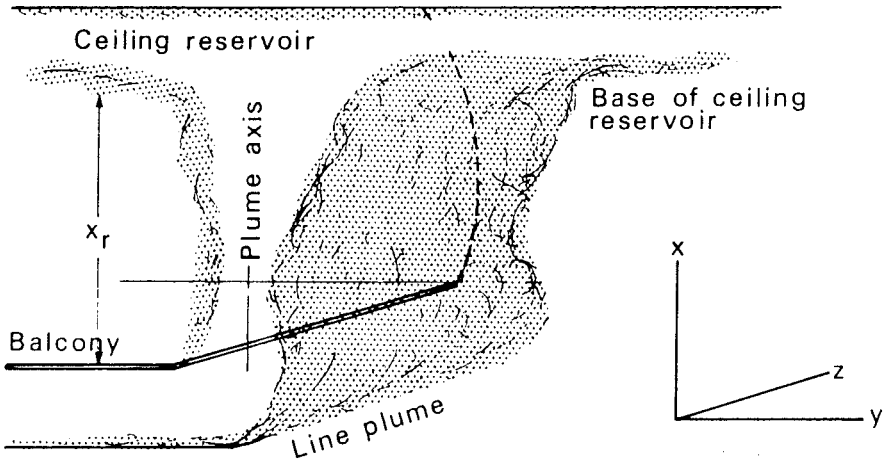

Figure 1.3[†] The line plume.

[†] Figure taken from Morgan and Marshall (1975).

1.3 SIGNIFICANCE OF BALCONY SPILL PLUME

1.3.1 Entrainment Prediction

Since the smoke plume will entrain air as it rises, the worst situation arises in the upper floor or floors of a multi-storey complex when a fire occurs on the lowest floor. A typical way to manage smoke within atrium buildings includes smoke ventilation (throughflow ventilation). This makes use of the buoyancy of the hot smoky gases produced by the fire to get the smoke up into the ceiling smoke reservoir, to be either extracted mechanically or vented naturally (Butcher and Parnell, 1979). By matching the extraction rate to the entrainment rate into the smoke reservoir, smoke can be kept in the upper reaches of the building. This would leave clean air near the floor allowing people to move freely.

Concerning the smoke management design within covered malls, Milke (1995) suggested that balcony spill plume is an important scenario to consider in the design process. Based upon the Law (1986) correlation, Milke (1995) showed that the balcony spill plume would entrain a greater amount of air than a normal axis-symmetry plume within the vertical range of up to 40 meters. Beyond this range, an axis-symmetry plume would be expected to entrain a greater amount of air than the spill plume. The results of his findings are presented in Figure 1.4. A heat release rate of 5 MW is assumed for both cases.

A survey of the literature shows that existing balcony spill plume correlations do not provide a good estimation of the entrainment rate at low height (0~5m) (Marshall et al., 1993). Also the smoke-logging effect on the upper levels has hardly been investigated. Figure 1.5 and 1.6 compare the predicted and measured entrainment rate using the experimental data by Marshall et al. (1993).

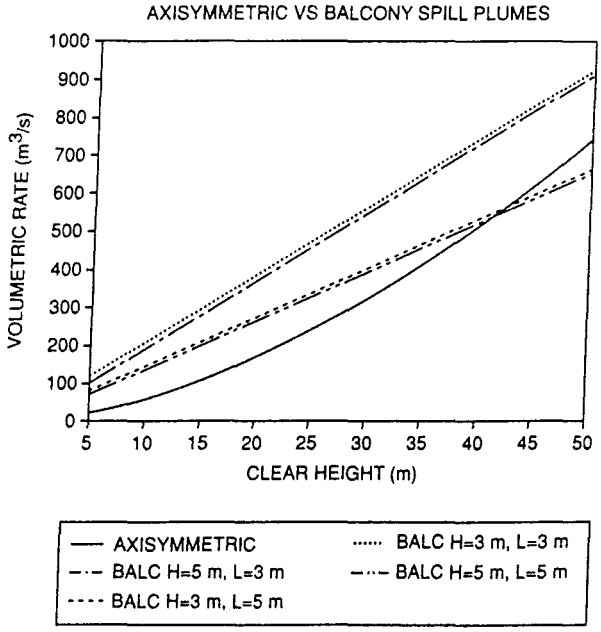

Figure 1.4[†] Comparison on the entrainment rate between balcony spill plume and axis-symmetric plume.

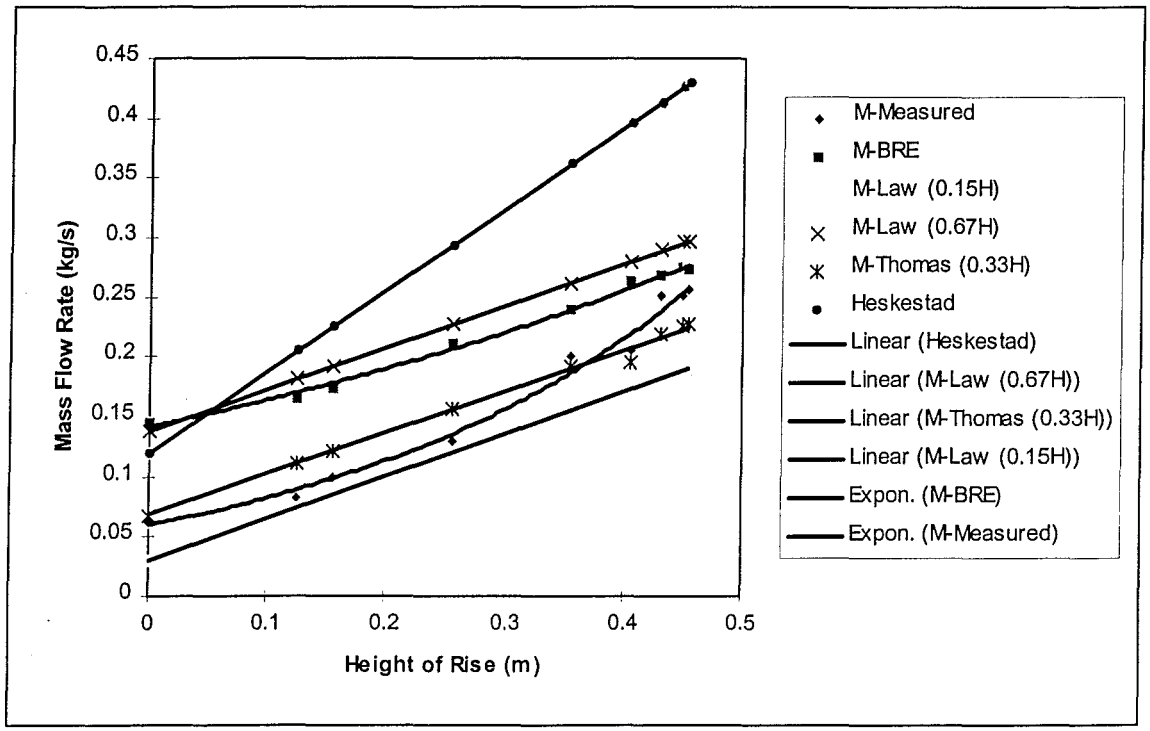

Figure 1.5 Comparison between the predicted and measured entrainment rate. (Fire size of 5.5kW without ends entrainment)

[†] Figure taken from Milke (1995).

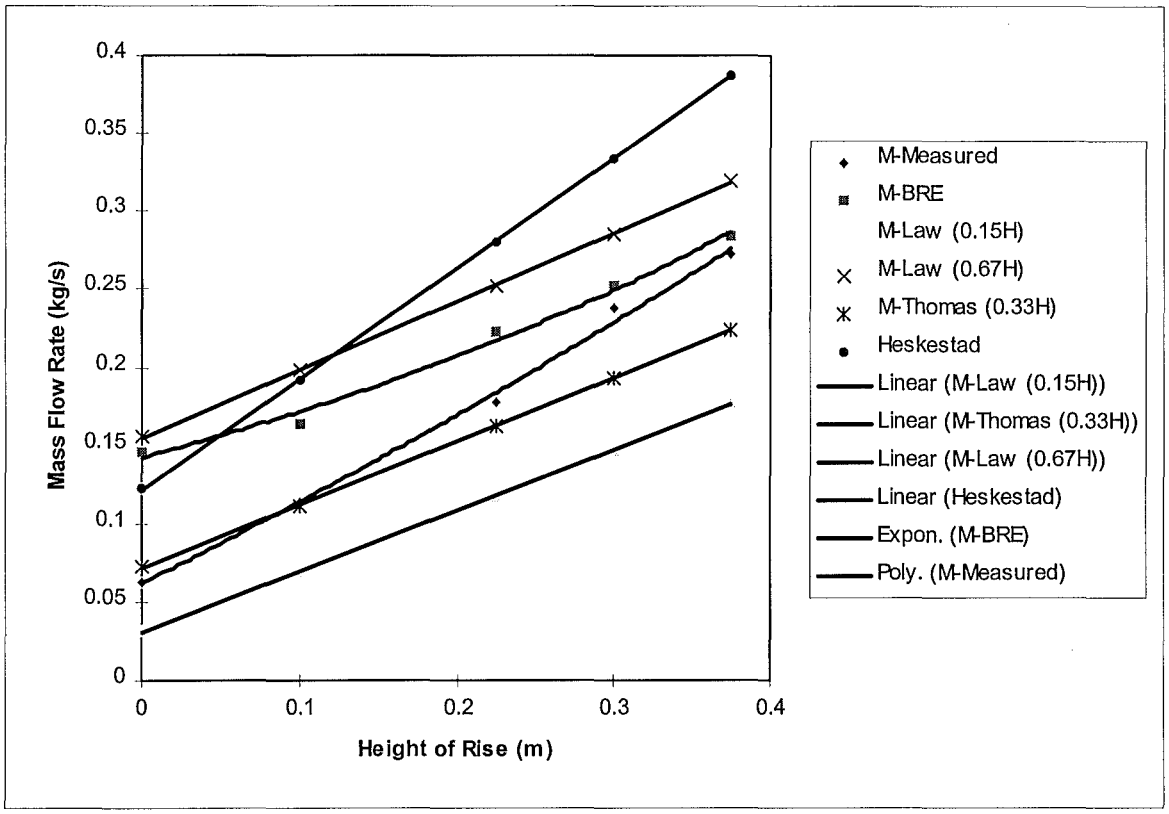

Figure 1.6 Comparison between the predicted and measured entrainment rate. (Fire size of 5.5kW with ends entrainment)

The inaccuracies in the prediction of balcony spill plume at low heights pose a concern in smoke extraction design, especially for the two-storey malls where the smoke reservoir layer may fall within this range (0~5m above the balcony edge). The smoke extraction systems may be undersized thus threatening life, or oversized leading to economic infeasibility.

1.3.2 Smoke Logging

Smoke logging of the upper balcony by the balcony spill plume has hardly been investigated. It has become an issue with the shift in priority for building design where architectural features of the building are an important issue to consider. With the complex architectural features that may possibly exist in the design of atrium buildings, any obstruction above the balconies is possible. The obstruction may be in

the form of a wider balcony stacking on top of the shorter one or as a roofing on the top floor. This is schematically shown in Figure 1.7.

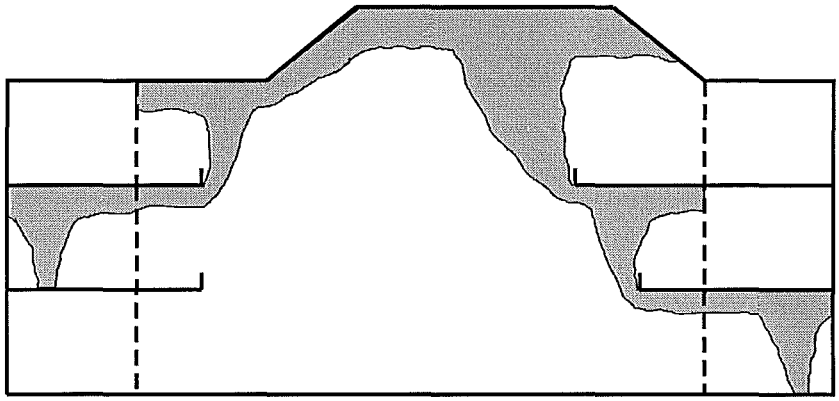

Figure 1.7 Schematic diagram of possible smoke logging above balconies.

Under performance based design, it is up to the fire engineers to design a suitable means of protection for these situations. However, there has been little work carried out of use for design engineers. Since the smoke flow pattern is unknown, fire engineers might have to take a more conservative approach in their designs.

1.4 SMOKE MANAGEMENT

As pointed out in the early section, covered atria buildings or shopping malls create problems during fire. These problems include the spread of smoke and the evacuation of people within the buildings. Robinson (1982) gave the Fire Service view point regarding these atrium buildings. He commented that if the roof covering the atrium space is left off, a lot of concerns would be diminished.

To deal with these covered atrium buildings, smoke management has to meet the design objectives required. Milke (1990) gave a few design objectives that might be cited for smoke management systems in atria:

1. Maintain a tenable environment for egress in the atrium during the evacuation period.
2. Confine the smoke in the atrium to a limited region of that space.
3. Restrict the migration of smoke from atrium into adjacent space.
4. Provide conditions in the atrium that will assist emergency response personnel in conducting search-and-rescue operations and locating and controlling the fire.
5. Contribute to the overall protection of life and reduction in property loss.

Milke (1990) pointed out that a particular design may attempt to accomplish only one of the objectives or a combination of several objectives. He stressed that the objectives need to be revised if the required smoke management system is considered to be impractical.

To formulate a design based upon engineering principles, the objectives need to be restated in measurable terms. One set of measurable terms consists of "hazard parameters" and are quoted below.

- Smoke layer depth
- Visibility through the smoke layer
- Carbon monoxide concentration
- Temperature rise in the smoke layer

The last three terms become critical when the situation involves immersing people in the smoke layer. Under most circumstances, life safety has been the priority in fire system design. For this reason, smoke layer depth becomes an important parameter in the design. While involving multi-storey building, instead of specifying the smoke layer depth, a design clear height[†] needs to be carefully selected. Maintaining a minimum design clear height above the highest walking level in the atrium relates to the life safety design objective stated above. That is, maintaining a tenable environment for egress in the atrium during the evacuation period (see Figure 1.8).

[†] Clear height is the height between the walking level to the bottom of the smoke layer interface.

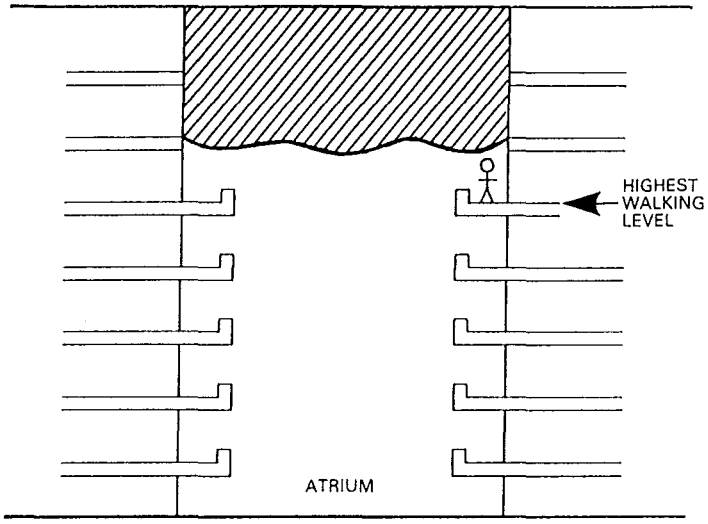

Figure 1.8[†] Clear height assigned to maintain smoke layer above highest walking level.

There are different recommendations made by BRE (UK) and NFPA (US) regarding the required clear height above the upper floor level.

NFPA 101 [1997, section 6-2.4.6] requires that in a smoke-protected place of assembly, the clear height is required to be maintained at least 6 feet (~1.85 meter) above the highest walking level.

The BRE however, recommends that for two-storey malls with small voids, the smoke layer should not be less than 3 meter above the upper floor level and preferably more than 3.5 meter (Morgan and Gardner, 1990).

To meet the criteria, a lot of options could be applied to achieve compliance. Methods including using physical barriers and airflows to limit the migration of the smoke can indirectly meet the clear height requirements as stated above. These strategies are shown in Figure 1.9. The physical barrier may range from simple fire-rated walls and windows to sophisticated automatic deploying smoke curtains.

[†] Figure taken from Milke (1990).

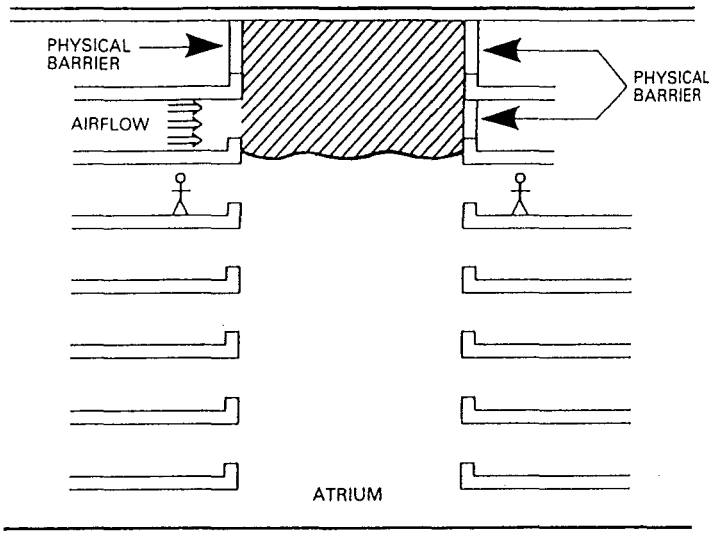

Figure 1.9[†] Smoke management strategies.

1.5 RESEARCH PURPOSE

Balcony spill plume is a very complex plume type and it is a relatively new field in fire research. The mismatch between existing correlations and real entrainment at low height, and the smoke logging effects are only two of many unsolved problems. Mathematical modelling of the balcony spill plume in order to estimate its entrainment has found to be difficult and complicated (Morgan and Marshall, 1975). The complication comes from the large number of variables involved and the changing of flow pattern along the spilling plume.

Currently, there are three basic methods that can be use to investigate the balcony spill plume. There are:

- Fire tests (Full or small scale)
- CFD (Computational Fluid Dynamics) modelling
- Salt water modelling

[†] Figure taken from Milke (1990).

Fire tests are the conventional method for investigating fire plumes. The entraining mass flow rate into the smoke layer at a certain height is the primary variable that most designers are after. This would allow them to size the required extraction systems for the buildings. For this reason, fire tests are conducted. By using the extraction hood system, the entraining mass flow rate into the rising plume can be readily measured.

However, a fire test is expensive and requires an extensive setup. This includes the preparation of the model, the placement and calibration of the thermal-couples and bi-directional velocity probes. An extraction hood setup is the main requirement for measuring the mass flow rate. With the equipment involved, any change on the geometry of the model and the position of the hood could lead to an overhaul of the entire experimental setup. Most of the data acquisition systems need to be relocated and re-calibrated. This would become an extremely time consuming and expensive task. The adjustment of the hood to various heights would also bound by the space restriction within the laboratory involved.

The flow visualisation for small scale fire tests requires additional equipment. For small scale fire tests, usually the industrial methylated spirits (IMS) of known calorific value is supplied to the burner. The heat release rate from the burner is to be scaled according to the scaling principles set out by Thomas et al. (1963). With the application of IMS fuel type, visualising the hot gas flow requires the introduction of visible fluid to the flowing hot gases. This can be done with the smoke from a commercial smoke generator, using carbon dioxide as a carrier gas (Morgan et al., 1976). The gas has to be piped into the hot gases flowing out as a buoyant gas layer under the ceiling towards the balcony edge, to allow visual observations to be made. For monitoring the finer details of the smoke behaviour, smoke from titanium chloride ventilation tubes may need to be used (Marshall and Harrison, 1996).

CFD modelling has been another useful tool for investigating fire plume. Unlike zone modelling that solves only the conservation of energy, mass and continuity equations, CFD modelling solves the set of three-dimensional, partial differential equations that govern the phenomenon of interest. This set consists, in general, of the following

equations: the continuity equation; the three momentum equations that govern the conservation of momentum per unit mass in each of the three space directions (the Navier-Stokes equations); and the conservation of energy equation. In addition, modelling includes a turbulence model to account for the sub-grid behaviour. The major drawback for this type of investigation is that it requires powerful computers and long simulation time to perform a simulation. CFD modelling on window plume had been performed using a parallel computing technique (Galae et al., 1995; Hoffmann et al., 1996). It was reported in these modellings, to simulate a full 60 seconds real time fire at a time step of 0.5 seconds requires 25 days computational running time! However, it allows the predictions of the temperature contours of the plume and the velocity flow fields. Although this method is usually used for research purpose, it has been practically applied for consulting and design purpose such as smoke flow in atrium buildings (Waters, 1989).

There have been a few of salt water modelling experiments performed relating to the fire scenario (Thomas et al. 1963; Steckler et al., 1986). The results shed new light on the investigation of smoke. The main advantages of the salt water modelling experiments are that they are clean and relatively inexpensive compared to the conventional fire test and CFD modelling.

The Fluids Mechanics Laboratory in the Civil Engineering Department at the University of Canterbury has a fresh water tank and laser apparatus. These facilities have previously been used to study buoyant plumes. The laser apparatus is used to conduct the Laser Induced Fluorescence (LIF) flow visualisation technique. This technique allows the collection of the density distribution profiles within the plume region. With the available of this apparatus, it seems appropriate to perform a feasibility study on this alternative method. The focus is to investigate any possible contribution that could be obtained from this method in studying balcony spill plume and suggest any potential substitutions to the fire test.

1.5.1 Objective Statement

The purpose of this research study on balcony spill plume is not to solve the quantitative problems associated with the balcony spill plume. It is however a qualitative study of the flow nature of the balcony spill plume at its rotational region and its smoke logging effects. It attempts to obtain experimental data to support the recent theoretical claim of small degree of entrainment into the rotational region (Miles et al., 1996; Thomas et al., 1996; Poreh et al., 1997). The study also explores the potential of using the LIF (Laser Induced Fluorescence) technique in conjunction with salt water modelling for studying the balcony spill plume.

1.6 SCOPE OF STUDY

This study was conducted in the fresh water tank in the Fluid Mechanics Laboratory. The flow density data was gathered using the Laser Induced Fluorescence (LIF) flow visualisation technique refined by Papps (1995) and Gaskin (1995). A 1/20 scale perspex model was used in the experimental study. The experiment collected a series of density profile data along the longitudinal cross sections of the plume. With the compilation of these data sets, three-dimensional pictures of the spilling plumes were mapped. These data sets allowed the determination of the nature of flow and density distributions within the plume. The study also investigated the effects on the spilling flow caused by changing the buoyancy in the spilling plume and the breadth of the balcony. This study was highly experimental orientated. The contents of this study report are outlined below.

Chapter 2 is a literature survey dealing with previous research on the balcony spill plume. The bases of the existing correlations are outlined. The current research and findings are included.

Chapter 3 presents the background of the salt water modelling technique for fire induced gas flow. It reviews the assumptions and restrictions implied in the modelling. The governing equations are presented as well.

Chapter 4 introduces the LIF (Laser Induced Fluorescence) technique used. The basic setup of the laser and data acquisition equipment are described. The dye type together with the hardware and software used on the computer for this application are reviewed.

Chapter 5 describes the model and experimental setup. A discussion on the choice to generate the spilling plume and the incoming laser direction are presented. It also outlines the entire experimental programme conducted.

Chapter 6 describes both the pre- and post experiment measurements and operations. The use of the density meter was also outlined. A description of the image data processing is also presented.

Chapter 7 presents the experimental results obtained. These results are divided into two major portions which include the smoke layer height above balcony and the flow nature of the spilling plume.

Chapter 8 contains the discussion of the results obtained. It discusses the significance of the results and compares them to those of previous workers. The potential errors in the data collected are also discussed.

Chapter 9 contains a feasibility study of salt water modelling of balcony spill plume using LIF technique. A few comments are made regarding the data and the software used. A short discussion on the limitations of the salt water modelling is also made.

Chapter 10 gives the conclusion of the study.

Chapter 11 recommends the direction for future research.

CHAPTER 2

2 BACKGROUND

This background chapter attempts to cover the basis of the derivation of existing correlations. It summarises the current research and development in the field of balcony spill plume. For full details, readers should consult the original documents listed in the Reference lists.

2.1 LITERATURE REVIEW

As the balcony spill plume has a complex flow path, conventional weak or strong plume correlations cannot be applied. Currently there are four well-known correlations available for estimating the entrainment rate of balcony spill plume. They are

- BRE spill plume model
- Thomas's spill plume correlation
- Law's spill plume correlation
- Heskestad's spill plume correlation (as in NFPA 92B- 1991 Edition)

2.1.1 Previous Development- An Overview

Plumes first attracted the interest of researchers in the mid-1900s. The first plume theories were developed by Morton, Taylor and Turner in 1956. Other researchers such as Lee and Emmons developed the line plume theories in 1961. It was not until 1975 that Morgan and Marshall from BRE Fire Research Station in UK started to investigate the behaviour of balcony spill plume. Since then, Law and Thomas have developed their own correlations based upon the data from the Morgan and Marshall experiments. Heskestad modified the correlation by Thomas and developed his own correlation. Heskestad's correlation is found to be quoted in NFPA 92B- 1991

Edition. These three correlations developed by Law, Thomas and Heskestad all take the form of a single equation for design purpose.

2.1.2 BRE Spill Plume Model

The BRE spill plume model was first proposed by Morgan and Marshall (1975) from Fire Research Station (UK). They conducted a series of 1/10 scale model experiment in their investigations on spill plume behaviour. Their experimental model took the typical dimensions for a single frontage shop within the mall as shown in Figure 2.1 below.

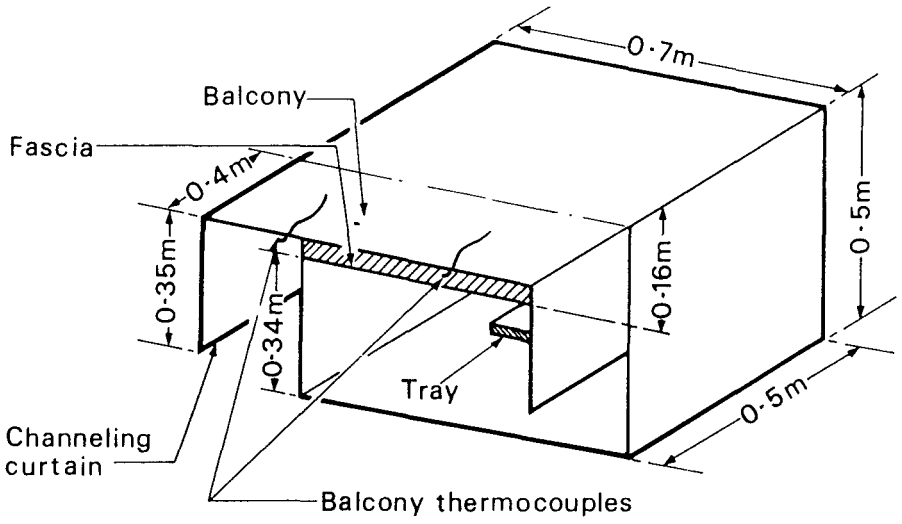

Figure 2.1† Morgan and Marshall (1975) experimental model.

They used a methylated spirit burner to simulate the fire in the compartment. The burning rate of the burner was scaled according to the scaling law used by Thomas et al. (1963). In the Morgan and Marshall (1975) experiment, the under balcony temperature rise, the temperature distribution at a height of 310mm above balcony and the entraining mass flow rate with various fire sizes were measured.

† Figure taken from Morgan and Marshall (1975).

Morgan and Marshall (1975) modelled the spill plume on the basis of Lee and Emmons (1961) line plume theory. The main assumptions that are made upon the BRE spill plume model are summarised below.

- The surrounding ambient air which the plume passes through remains at a uniform temperature. This includes the air below the smoke layer in the reservoir.
- The flow lines entering the plume are normal to the plume axis.
- The velocity and temperature profiles across the plume are in Gaussian distributions immediately after the rotation over the horizontal plane of the balcony.
- The horizontal inward air velocity to the plume is proportional to the vertical component to the characteristic stream velocity at the same height.

Since the BRE spill plume model was first proposed in the mid 1970s, input from various researchers has contributed to the development of this model. The important developments are summarised below.

Based on the horizontal flow of two-dimensional flows for non-uniform approach velocities induced by the layer's buoyancy toward an opening, Morgan (1986) derived the horizontal mass flow expression below the balcony. The expression takes the form as shown in Eq. (2.1).

$$M_w = \frac{2}{3} C_d^{3/2} \left(2 g \theta_{cw} T_1\right)^{1/2} \frac{W \rho_1}{T_{cw}} D_w^{3/2} \kappa_M \tag{2.1}$$

Morgan proposed that for a deep downstand, the discharge coefficient takes a value of 0.6, ie $C_d = 0.6$. For no downstand, the discharge coefficient is 1, ie $C_d = 1.0$. He considered this expression to be more appropriate than simply applying the energy balance for the smoke stream below the balcony as in the 1975 work. As for κ_M, it is a profile correction factor for mass flow, which Morgan recommended a value of $\kappa_M \approx 1.3$ for most practical cases.

Based on Morgan's (1986) work, Morgan and Hansell (1987) suggested the use of the mean layer temperature $\overline{\theta}_w$ as shown in Eq. (2.2).

$$\overline{\theta}_w = \frac{\kappa_Q}{\kappa_M}\theta_{cw} \tag{2.2}$$

They also suggested the use of heat flux in the gases (in horizontal flow) at the opening, Q_w as opposed to the actual fire size Q (1975) in calculating the under balcony horizontal velocity, v. Both of these parameters have their forms shown in Eq. (2.3) and (2.4) respectively.

$$Q_w = M_w c_p \overline{\theta}_w \tag{2.3}$$

$$v = 0.96\frac{C_d \kappa_M}{\kappa_Q^{1/3}}\left(\frac{gQ_w T_{cw}}{c_p \rho_1 W T_1^2}\right)^{1/3} \tag{2.4}$$

Morgan and Hansell (1987) used Eq. (2.1), the modified calculation method for under balcony mass flow, M_w and Eq. (2.2), the mean layer temperature, $\overline{\theta}_w$ and correlated with the experimental data as collected by Morgan and Marshall (1975). Applying Eq. (2.5), which is the equation for the amount of air entrained into this mass of gas as it rounds the edge of the balcony, they obtained a new entrainment constant in the rotation region α'. They found that this new constant α' has a value of 1.1 as opposed to 0.9 as found in 1975. They suggested that this larger α' value was an indication of large entrainment into the bulk rotating flow at the top edge of the opening.

$$\delta m = \frac{2}{3}\rho_1 W \alpha'\left(\frac{2g\theta_c}{T_1}\right)^{\frac{1}{2}} D_w^{\frac{3}{2}} \tag{2.5}$$

The total mass of gas flowing vertically across the horizontal plane through the outer balcony spilling edge is thus modelled as the sum of the mass flow below the balcony and the entrainment into the rotating edge. The expression is given in Eq. (2.6). This

parameter will be accounted for in calculating the Gaussian profile parameter. Figure 2.2 shows the mass flow rate at the spilling edge of the balcony.

$$M_y = \delta m + M_w \tag{2.6}$$

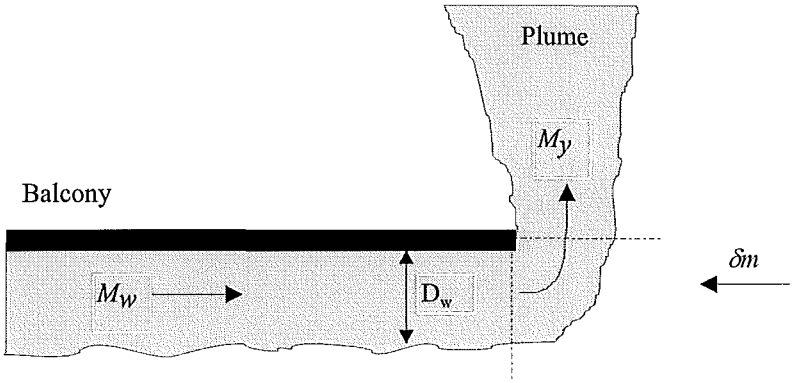

Figure 2.2 Entrainment at the rotation.

Following Lee and Emmons (1961) line plume theory, Morgan and Marshall (1975) showed that the total mass entrainment into the line plume sides (per channel width), rising through the horizontal plane at a height x takes the form as shown in Eq. (2.7). λ in this equation is an empirical thermal plume constant that takes a value of 0.9 and u, b and p' all take values appropriate to the corresponding height of rise, x.

$$m_r = \sqrt{\pi}\rho_1 u|_x b|_x \left[1 - p' \frac{\theta}{T}\bigg|_G \frac{\lambda}{\left(1+\lambda^2\right)^{1/2}} \right] \tag{2.7}$$

To account for the side-ends entrainment into the plume, a near rectangular shape had been assumed (Morgan and Marshall, 1979). Eq. (2.8) is derived and adopted for this application.

$$\delta M_r = 4\bar{b}\,\bar{u}\,\alpha x \rho_1 \tag{2.8}$$

where $\bar{b} = (b_G + b)/2$

$\bar{u} = (u_G + u)/2$

The total mass entrainment into the spill plume at height x is simply the sum of the entrainment from the sides and the ends of the plume as shown in Eq. (2.9).

$$M_r = m_r W + \delta M_r \tag{2.9}$$

Any two parameters listed below have to be known to apply the BRE spill plume model.

- mass flow/heat flux
- mass flow/mean layer temperature
- mass flow/ceiling temperature
- heat flux/mean layer temperature
- heat flux/ceiling temperature
- heat flux/layer depth
- layer depth/mean layer temperature
- layer depth/ceiling temperature

The BRE spill plume model is a very complicate mathematical model. It is not appropriate to outline every single detail and equation to be used in the calculation. For full details of the BRE spill plume calculations, readers should consult documents by Marshall and Morgan (1992) and Hansell and Morgan (1994).

2.1.3 Law Correlations (1986)

Law's correlation was developed by correlating the experimental data from Morgan and Marshall (1975). She adopted the temperature rise to heat input relationship developed by Yokoi in 1960 that takes the form as shown in Eq. (2.10).

$$\Delta T_{\max} = \frac{6.89}{z}\left(\frac{Q}{L}\right)^{2/3} \tag{2.10}$$

Law correlated the maximum temperature rise on the axis of the plume, ΔT_{max} vs Q/L and the under-balcony temperature rise, ΔT_{balc} vs Q/L. She showed that both temperature rises have the relationship as proposed by Yokoi by plotting the data on a log-log scale and obtaining a slope of 2/3.

Law then used the analogy of conservation of heat under the balcony to show that the mass flow M has relationship given in Eq. (2.11).

$$M \propto \left(QL^2\right)^{1/3} z \tag{2.11}$$

By plotting $\frac{M_r}{\left(QW^2\right)^{\frac{1}{3}}}$ against the clear height layer depth, d_1, Law demonstrated that the effective source of plume is only a small distance of 0.15H below the balcony. This is indicated in Eq. (2.12) which is the final form of Law's (1986) correlation.

$$M_r = 0.34\left(QL^2\right)^{1/3}\left(d_1 + 0.15H\right) \tag{2.12}$$

Recently, Law (1995) revised the correlation using the more recent experimental data (Hansell et al., 1993). This revised correlation is given in Eq. (2.13).

$$M_r = 0.31\left(QL^2\right)^{1/3}\left(d_1 + 0.25H\right) \tag{2.12}$$

Morgan (1987) suggested a modification of Law's (1986) correlation by incorporating the effective value d_1' rather than d_1 as in Law's original correlation. This is to account for the temperature gradient below the smoke reservoir. Upon their correlation, the effective value d_1' to d_1 takes the form shown in Eq. (2.14).

$$d_1' = h_v - 1.26d_1 \tag{2.14}$$

Morgan (1987) ended up obtaining an expression as shown in Eq. (2.15). However, this particular equation has not been extensively quoted in texts.

$$\frac{M_r}{\left(QL^2\right)^{1/3}} = 0.40d_1' + 0.061 \tag{2.15}$$

2.1.4 Thomas correlation (1987)

Like Law, Thomas used the experimental data obtained by Morgan and Marshall (1975, 1979) to develop his correlation. He proposed that the rising plume can be treated as a "far plume" rising from a line source of zero thickness some distance below the balcony.

Thomas adopted a similar procedure to Law by using Yokoi's relationship of ΔT and Q/L to determine the virtual source location, Δ. Using data from Morgan and Marshall's (1975) experiments, Thomas showed that in the rising plume region, the virtual source is 0.33m below the balcony, ie Δ=0.33m. This can be written in terms of the shop's height H as in Law's correlation. Since the shop's height used in Morgan and Marshall (1975) test model had a dimension of 0.5m, this implies that Δ=0.66H. As for the region just underneath the balcony edge, Thomas found Δ~0.16m or Δ=0.32H.

To account for the entrainment into the ends of the plume, Thomas connected a finite strip plume in a way consistent with a point source of equal strength. This was by matching the mass flow for line and point plumes and obtaining an effective L of the line plume. The relationship is shown in Eq. (2.16).

$$L = L_0 + \mu(x+2\Delta) \tag{2.16}$$

where $\mu = \left(\frac{B}{0.58}\right)^{3/2}$

From Zukoski's work, this gives B=0.21 and hence μ=0.22.

The final form of Thomas's correlation for the spill plume is shown in Eq. (2.17) below. Without ends effect, the last term is zero.

$$M_r = 0.58\rho\left(\frac{gQL^2}{\rho c_p T_1}\right)^{1/3}(x+\Delta)\left(1+\frac{0.22(x+2\Delta)}{L}\right)^{2/3} \tag{2.17}$$

2.1.5 Heskestad's correlation (NFPA 92B- Balcony Spill Plume Correlation)

Based on the semi-empirical relationships developed (Morgan and Marshall, 1979; Law, 1986; Thomas, 1987), Heskestad developed a design equation which provides a good correlation for smoke production over the full range of data from Morgan and Marshall (1979).

Heskestad's balcony spill plume equation as quoted in NFPA Section 92B (1991) document has the form shown in Eq. (2.18).

$$M_r = 0.41\left(QL^2\right)^{1/3}(x+0.3H)\left(1+\frac{0.063(x+0.6H)}{L}\right)^{2/3} \tag{2.18}$$

2.2 CURRENT RESEARCH AND ISSUES

Since the 1990s, researchers have been looking at the limitations of the BRE spill plume model as well as verifying some of the earlier theories proposed.

2.2.1 Hansell, Morgan and Marshall (1993)

Their studies of smoke movement were performed in a 1/10 scale model atrium. They looked at verifying the early theories proposed, the limitation of the BRE spill plume model and effects on the smoke flow by different balcony breadths. A brief summary of their work follows.

2.2.1.1 Discharge coefficient

From the studies of flows at the compartment opening and beneath balconies projecting beyond it, they confirmed the assumption made by Morgan (1986) that a horizontal flow approaching a flush-ceiling free edge experiences an effective coefficient of 1.0.

2.2.1.2 Effect of balcony breadth with different fire size

Hansell et al. (1993) performed some experiments to find the effect of varying balcony breath for different fire sizes. They tested three balcony breadths which had dimensions of 5m, 2.5m and 1.25m in full scale equivalent. They showed that for balconies less than 1.5m (full scale equivalent) in breadth for a large fire (5MW) or less than 1.0m for small fire (1MW), these balconies can survive without the channelling screens as lateral spread below the balcony had been observed to be minimal.

They recorded the attachment height of the rising plume above the balcony and they showed that smoke logging can be expected above a balcony having a breadth less than 2m (full scale equivalent). They suggested that if higher balconies are present, the smoke-logging effect is worsened although extensive experiments had not yet been carried out.

2.2.1.3 Visual, buoyancy derived depths and effective plume height

Hansell et al. (1993) suggested that these are qualitatively different for different geometry for smoke layers, ie smoke layers depth to their width. They suggested the aspect ratio of the atrium ($H / \sqrt{A_a}$) can significantly affect the smoke ventilation safety requirement, but could not suggest any method to be used with confidence.

2.2.1.4 Temperature limitation

Hansell et al. (1993) showed the limitation in temperature for free plumes to be adequately described by the existing Gaussian model, being:

(a) *Double sided plume*

Opening Width (full scale equivalent)	Limiting Temperature
4-5m	250°C
7m	330°C

(b) *Adhered (single sided) plume*

Opening Width (full scale equivalent)	Limiting Temperature
4m	280°C

For the adhered plume model, an effective entrainment constant of 0.077 is to be used. Users should also consult the "ghost-plume" methodology by Marshall (1986).

2.2.2 Marshall, Harrison and Morgan (1993)

Marshall et al. (1993) examined the BRE spill plume model using a 1/10 scale model for their studies. They tried to explain the mismatch between the prediction made by the BRE model and the measured mass flow rate by discussing the flow nature of the plume.

2.2.2.1 Height limitation

By matching the mass flow rate measured in the exhaust and the calculated values from BRE spill plume correlation, Marshall et al. (1993) showed that for double sided thermal line plume with ends entrainment, the BRE model is reliable for a minimum height rise of 3m (full scale equivalent). Without ends entrainment, the theoretical predictions are reliable for a minimum height of rise of between 4 to 5m.

They suggested that the unreliability of the theoretical prediction of the model to actual mass flow rate below the limiting heights, is the result of the violation of assumptions made in the theoretical model. The BRE spill plume model assumes the vertically rising gas stream to have both temperature and velocity profiles being Gaussian immediately after the rotation at the balcony edge. However, it is impossible for this to happen, as in practice a thermal line plume of gases will need to rise through a "transition region" before it becomes fully established. Hence they suggested the limiting heights are an indication of where the Gaussian profile has been fully established. Figure 2.4 shows the schematic view of the gradual formation of the vertical gas stream into a Gaussian line plume.

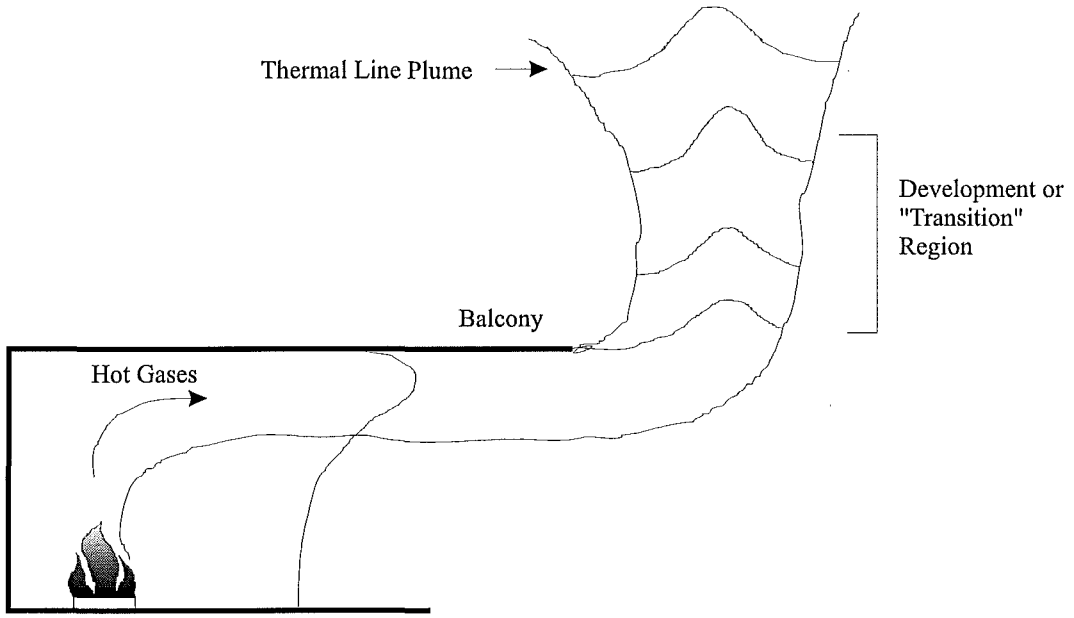

Figure 2.3 Anticipated distributions of the rising thermal line plume.

Marshall et al. (1993) also attempted to test the BRE spill plume model at small (or no) height of rise. Their findings showed that the BRE spill plume model does not correctly predict the entrainment. Their observations found that not only has the Gaussian profile not been established, the nature of the flow into the reservoir or base of smoke layer is significantly less acute in comparison with experiments which had the hoods positioned at a greater height. Figure 2.4 shows the flow pattern that they had observed.

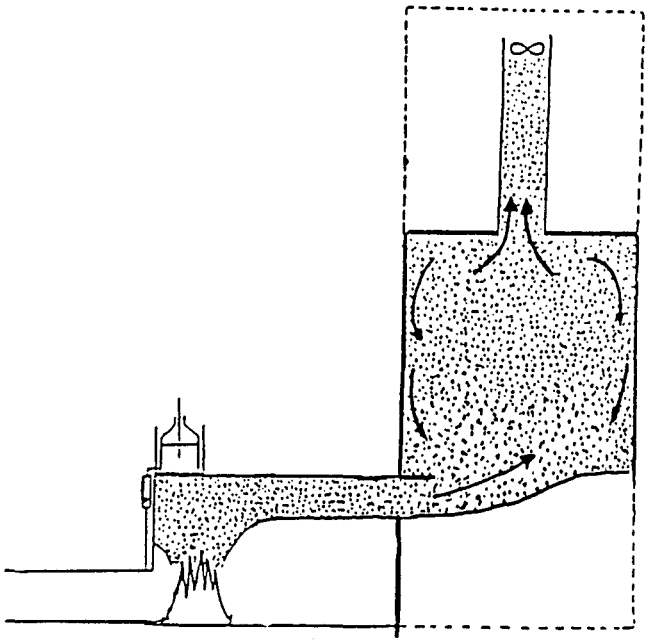

Figure 2.4[†] Balcony spill plume at low height of rise.

2.2.3 Marshall and Harrison (1996)

Marshall and Harrison used a 1/10 scale model to investigate the effect a reservoir has on the air entrainment as well as looking at the effect of counter flow at compartment opening.

2.2.3.1 Smoke reservoir

Their studies suggested that for smoke reservoirs less than 10m x 10m x 19m in height, additional air entrainment is likely as compared to larger reservoir.

2.2.3.2 Counter flow

Counter flow at a compartment opening was found to produce a 30% increase in layer depth and mass flow rate at the opening leading to 15% increase in mass entering the smoke layer. They suggested this was likely to be caused by the fire plume at the fire compartment leaning backwards due to air flow inwards and hence entraining more air.

[†] Figure taken from Marshall et al. (1993).

2.2.4 Thomas, Morgan and Marshall (1996)

Thomas et al. used recent data by Poreh et al. (1997) to produce correlations for the mass flow of a two-dimensional plume emerging normal to the straight edge of a flat horizontal surface, ie the balcony, and rising up into a uniform atmosphere (the spill plume).

They found the effective entrainment coefficient, α, to be 0.11 as opposed to 0.16 found by Lee and Emmons (1961) and used in early spill plume works (Morgan and Marshall, 1975, 1979; Marshall and Morgan, 1992; Hansell and Morgan, 1994). Their correlation is shown in Eq. (2.19) below. The correlation demonstrates a small degree of air entrainment in the turning region.

$$\frac{M'}{Q'} = 1.2\frac{M_b'}{Q'} + 0.16\frac{z}{Q'^{2/3}} + 0.0027 \tag{2.19}$$

Poreh et al. (1997) obtained a correlation as shown in Eq. (2.20) which also suggests small entrainment in the turning region.

$$\frac{M'-M_b'}{Q'} = 0.15\left(\frac{z+z_0}{Q'^{2/3}}\right) \tag{2.20}$$

2.2.5 Miles, Kumar and Cox (1996)

Miles et al. performed a CFD study on the experiments by Marshall and Harrison (1996). They showed good agreement of results between the experimental and CFD modelling. Their modelling did support the recent dimensional analysis which suggested a small degree of air entrainment into the turning region of the smoke flow from the horizontal to the vertical. A typical result from their CFD modelling is shown in Figure 2.5. The small velocity vector arrows indicated small entrainment into the turning region.

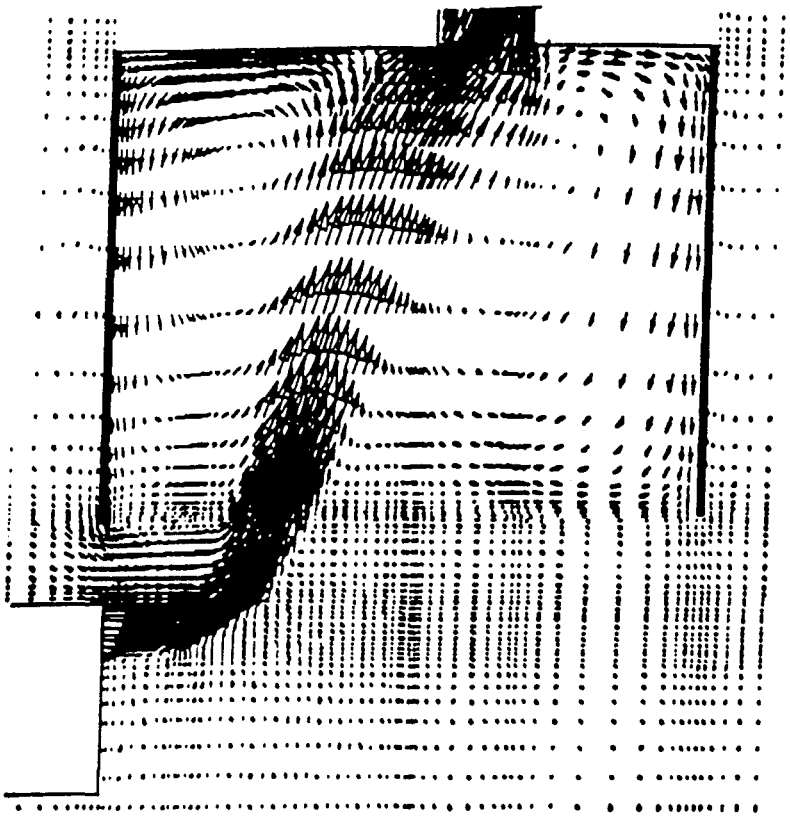

Figure 2.5[†] Predicted balcony spill plume flow pattern in a hood of 0.3m height of rise.

2.3 SUMMARY

The literature review indicated that the commonly-used correlations are developed and derived from experimental fire data. Increasing awareness of the flow nature of the spilling plume to the appropriateness of the assumptions made in the entrainment models has been established. The survey also shows that the majority of the observations and investigations on the flow nature of the spilling plume are still two-dimensional. Smoke logging on upper floor by the spilling plume has not been dealt with as much as it should be.

[†] Figure taken from Miles et al. (1996).

CHAPTER 3

3 SALT WATER MODELLING

This chapter introduces the basic ideas behind the salt water modelling technique and its scaling equations as developed by Steckler et al. (1986). The limitations of this modelling method are discussed.

3.1 INTRODUCTION

Salt water modeling technique is a useful tool to simulate fire induced flows. Thomas et al. (1963) used this technique to show the effect of roof and side vents on clearing smoke from large rooms. Tangren et al. (1978) applied this technique to study the densities and positions of hot gas layer produced by a fire in a room with a doorway or window vent. However, proper documentation was scarce until 1986, when Steckler et al. (1986) started to document this technique while they were evaluating the smoke movement for a multicompartment multideck naval combat ship for the US Navy.

Salt water modeling is a hydraulic analogue technique. The major advantages offered by this modelling technique are:

- Provision of a clean environment for measurement with excellent visualisation;
- Models most of the characteristic of the flow.

3.2 BASIC IDEAS

The main idea behind salt water modeling of a real fire scenario is to preserve the same driving phenomena between the two situations- the buoyancy. In salt water modeling,

turbulent buoyant salt water moving in fresh water is used to substitute for turbulent buoyant hot gas moving in cold gas.

Under these two processes, the driving phenomena are identical- buoyancy forces resulting from density differences. Both are dependent on the gravitational acceleration. Considering the density differences between these plumes to their surroundings, backward analogies could be observed. In salt water modeling, a denser fluid is used to simulate the rising plume as in real fire scenario. To conserve the same driving mechanism between the two cases, that is the buoyancy resulting from the density differences, the entire model geometry needs to be inverted. By doing so, the salt water plume would be driven by the gravitational forces. This would eventually create effects similar to the hot rising plume driven by the buoyancy forces.

Since salt water is used to simulate the plume, the concentration of the saline solution can be regarded as the heat energy in the gases heated by the fire. Heat energy is usually associated with temperature. From the gas behaviour, it is well known that the densities of the gases are dependent on their associated temperature. Under the hydraulic analogy, the concentration of the salt water is responsible for the density difference. In the reverse analogy, a high concentration of the saline solution can be regarded as a high gas temperature in the fire situation.

3.3 GOVERNING EQUATIONS

Baum and Rehm (1984) derived the non-dimensional governing equations for the flow of inviscid thermally non-conducting gas within an enclosure heated by a source. By assuming that this source, which is representative of a fire, to be sufficiently weak relative to the size of enclosure, they demonstrated the validity of the application of the Boussinesq approximation to the flow outside the source region. This means that the approximate equations of motion can be reduced to the Boussinesq equations, which describe the large scale buoyant convective motion of an inviscid thermally non-conducting gas within an enclosure.

By preserving the same driving phenomena in both the salt water plume and the fire plume, Baum and Rehm (1984) suggested these two processes can be related through the non-dimensional Boussinesq equations when viscous and heat transfer effects are small.

Steckler et al. (1986) presented the governing theory for salt water modelling of fire induced gas flows. The scaling equations are written in terms of non-dimensional variables for relating both the hydraulic and fire situations. The ideas behind these equations are such that the two situations can be related if the non-dimensional variables in both cases have the same value. Hence results from a salt water experiment can be used to calculate its non-dimensional variables for a particular situation; the non-dimensional variables can be solved, in terms of fire variables, to predict the behaviour of gases in the equivalent fire situation.

The non-dimensional governing equations, taken from Steckler et al. (1986) are presented below. Eqs. (3.1) to (3.3) are the main governing equations in their general forms.

The conservation of mass.

$$\nabla^* \cdot \bar{u}^* = 0 \tag{3.1}$$

The conservation of momentum.

$$\frac{d\bar{u}^*}{dt^*} + \nabla^* \tilde{p}^* - \theta^* \tilde{k} = \left(\frac{1}{\mathrm{Re}}\right) \nabla^{*2} \bar{u}^* \tag{3.2}$$

The conservation of energy

$$\frac{d\theta^*}{dt^*} = GQ^* + \left(\frac{1}{\mathrm{Re}\,P}\right) \nabla^{*2} \theta^* \tag{3.3}$$

The above three equations have their non-dimensional variables expressed in terms of length scale H, the enclosure height; a length scale L, the spatial extent of source; a velocity scale U and a density (or temperature) perturbation scale ζ. Steckler et al. chose to include both U and ζ to make the convective and buoyancy terms in the momentum equation of the same order. Both the U and ζ are defined below.

The governing equations are shown below. The variables on the left hand side correspond to the parameters as in a fire (hot gases) scenario. As for the variables on the right hand side, they are the parameters in the salt water scenario that are considered to be appropriate to compare with their corresponding fire parameters. Figure 3.1 schematically defines the variables used for each case.

$$H\nabla = \nabla^* = h\nabla \tag{3.4}$$

Non-Dimensional Position

$$\frac{\bar{x}_g}{H} = \bar{x}^* = \frac{\bar{x}_s}{h} \tag{3.5}$$

Non-Dimensional Time

$$\frac{t_g U_g}{H} = t^* = \frac{t_s U_s}{h} \tag{3.6}$$

Non-Dimensional Velocity

$$\frac{\bar{u}}{U_g} = \bar{u}^* = \frac{\bar{u}}{U_s} \tag{3.7}$$

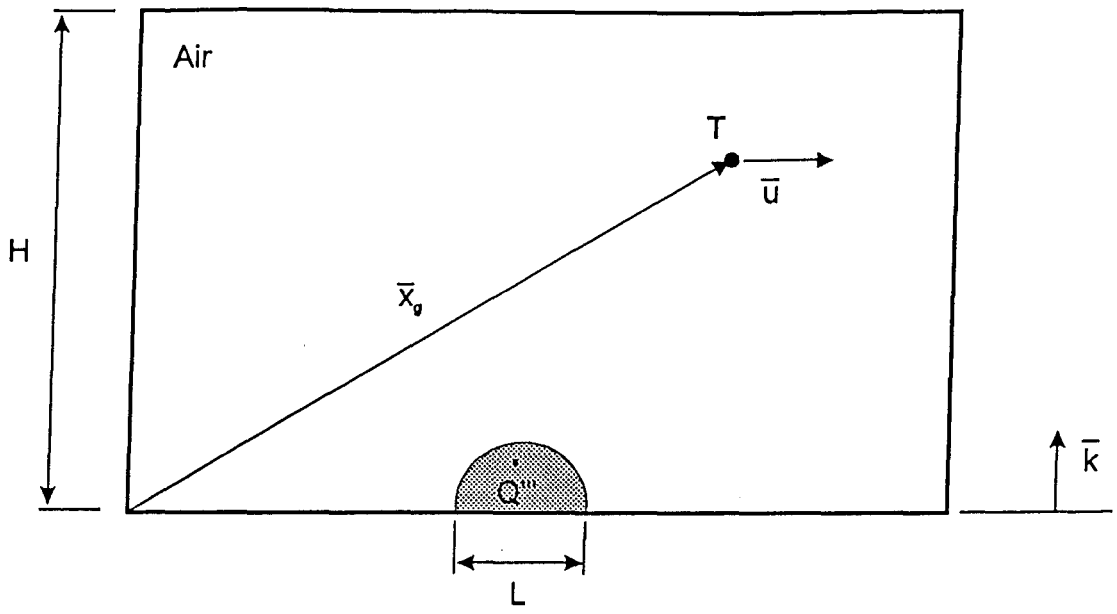

(a) *FIRE*

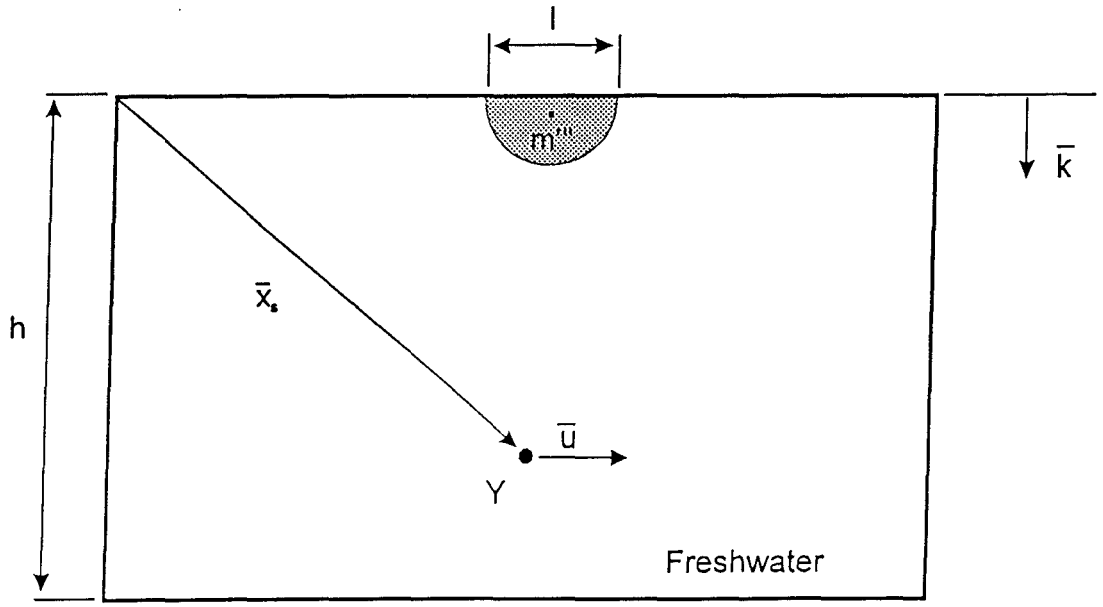

(b) *SALT WATER MODELING*

Figure 3.1[†] Schematic of variables used in salt water modelling calculations.

[†] Figure taken from Clement (1996).

Non-Dimensional Pressure Perturbation

$$\frac{\tilde{p}}{\rho_0 U_g^2} = \tilde{p}^* = \frac{\tilde{p}}{\rho_0 U_s^2} \tag{3.8}$$

Non-Dimensional Temperature

$$\frac{(T - T_0)}{T_0 \zeta} = \theta^* = \frac{Y}{\zeta} \tag{3.9}$$

Non-Dimensional Heat Input

$$\frac{\dot{Q}'''}{\left(\frac{\dot{Q}_0}{L^3}\right)} = 1 = Q^* = 1 = \frac{\dot{m}'''}{\left(\frac{\dot{m}_0}{l^3}\right)} \tag{3.10}$$

Velocity Scale

$$\left(\frac{\dot{Q}_0 g}{\rho_0 c_p T_0 H}\right)^{\frac{1}{3}} = U = \left(\frac{\dot{m}_0 g}{\rho_0 h}\right)^{\frac{1}{3}} \tag{3.11}$$

Density (or Temperature) Perturbation Scale

$$\frac{U_g^2}{gH} = \zeta = \frac{U_s^2}{gh} \tag{3.12}$$

Viscous and Heat Conduction Effects

$$\frac{\mu c_p}{k} = \mathrm{Pr} = P = Sc = \frac{\mu}{\rho_0 D} \tag{3.13}$$

Reynolds Number Matching

$$\frac{\rho_0 U_g H}{\mu} = \mathrm{Re} = \frac{\rho_0 U_s h}{\mu} \tag{3.14}$$

Compartment Size Scaling

$$\left(\frac{H}{L}\right)^3 = G = \left(\frac{h}{l}\right)^3 \tag{3.15}$$

3.4 LIMITATIONS

It should be noted that salt water modelling can only approximate the real fire scenario. There exists certain limitations such as heat transfer deficiency and practical difficulties in preserving the identical non-dimensional variables such as G, Re and P according to Eqs. (3.13-3.15). The current salt water modelling technique is also bounded by the assumption made in deriving the non-dimensional Boussinesq equation.

Certain important assumptions and approximations made during salt water modeling are briefly described below.

3.4.1 Boussinesq Approximation

During the derivation of the non-dimensional governing equations, Baum and Rehm (1984) made the following assumptions.

1. Heat addition to the surrounding space is slow;
2. The pressure over a large region surrounding the source is almost uniform in space during heating;
3. No restriction upon the magnitude of the density (or temperature) variation during heating;

4. The magnitude of the temperature variation, the density variation and the flow velocities are induced by the heat source, ie buoyancy effects;
5. Static density variation from its mean value is small;
6. The density variations produced by the heat source are small.

3.4.2 Heat Transfer

Salt water was used to simulate the fire plume. However no heat transfer effect to the surrounding boundaries can be simulated in the modelling, as this would otherwise imply mass transfer of salt into the model surfaces. The result of this is that the buoyancy is maintained longer than in the real fire situation. Hence salt water modelling can be considered as a fire scenario at an adiabatic environment.

3.4.3 Plume Reynolds Number

Typical turbulent fire plumes have Re number of the order of 10^5 (as defined by Eq. 3.14). In the reduced scale salt water experiments, this value is difficult to achieve due to the length reduction and source restriction. Turbulent plumes with Re numbers in the order of $\sim 10^4$ do exist (Steckler et al., 1986) and this is considered as a much more achievable value from salt water experiments. Steckler et al. (1986) reported that when $Re \geq \sim 10^4$, the inconsistencies between the Prantl number, Pr for air and Schmidt number, Sc for salt water in fresh water become unimportant. Also beyond this Re value, the molecular transport terms in Eq. (3.2) and Eq. (3.3) become negligible in relation to other terms.

3.4.4 Plume Momentum

Under normal circumstances, the turbulent hot gas plume from a real fire contains no initial momentum flux as it is purely driven by buoyancy. This is basically due to the higher temperature in the rising plume than the surrounding. As for salt water, it must be injected with some initial momentum such that its flow rate is large enough to create a turbulent plume ($Re \sim 10^4$), hence satisfying the Reynolds number criteria as discussed before.

Compromise has to be made such that the salt water is able to simulate a turbulent plume (Re criteria), and initial momentum effects do not dominate the buoyancy effect over the large portion of the plume height.

To evaluate the effect of initial momentum, Steckler et al. (1986) followed Tangren et al.'s (1978) method by considering the ratio F of initial momentum flux to buoyancy flux at height z above the source.

$$F = \frac{\rho U_0^2}{2(\rho - \rho_0)gz} \tag{3.16}$$

At some distance z = z', the initial momentum effect becomes small and buoyancy forces dominate. Hence a purely buoyant plume is approximated beyond z'.

3.4.5 Plume Mass Flux

In a real fire situation, the fire plume has a mass flux which is larger than the initial mass flux issuing from the source. Hence it is highly desirable that the same relative size of mass flux ratio is conserved.

3.4.6 Source Geometry

The scaling of the source geometry criteria as defined in Eq. (3.15) cannot be met precisely. This is because a real fire is a volumetric heat source with poorly defined spatial extent. In practice, salt cannot be released in a precise scaled volume corresponding to the full scale situation. Steckler et al. (1986) suggested that this condition can be partially met by considering L as the base diameter of the full scale fire and l = (h/H)*L as the base diameter of the salt water source.

3.4.7 Boundary Conditions

As indicated before, salt water modeling can be related to the real fire scenario when the viscous and heat transfer effects are small. This is not quite the case for flows close to the boundaries. Near the boundaries, the Re number of salt water flow does not match that of the hot gas flow, as drag effects having a weak function of Re are not precisely simulated. Also, no heat transfer is accounted near the boundary which would otherwise require the mass transfer of salt into the model's surfaces.

For the experiments involved, certain modifications were made in generating the spilling plume. This will be further discussed in Chapter 5.

3.5 SUMMARY

The scaling equations are derived based upon a plume behaviour. With the assumptions made during the derivation of these scaling equations, the applications of these equations in scaling for real fire results are still quite crude. The major difficulties associated in the reduced scale experiments are to satisfy the contradictory momentum and Reynolds number criteria. Other limitations or criteria that one should be aware of during the salt water experiments are the source geometry and boundary conditions.

CHAPTER 4

4 FLOW VISUALISATION TECHNIQUE

The Laser Induced Fluorescence (LIF) technique was used to visualise the balcony spill plume generated for this study. It allowed the acquisition of both qualitative and quantitative measurements on the concentration of the spilling plume. With this density concentration data, certain insights into the spilling flow could be explored.

4.1 LASER INDUCED FLUORESCENCE (LIF) TECHNIQUE

The LIF technique achieves good flow visualisation by illuminating the spilling plume with dye. To properly illuminate the plume of interest, a laser source and a special dye are required. A fixed amount of dye was mixed with the spilling saline solution that generated the spill plume flow for this study. Illumination was achieved when the laser light excited the dye in the flow. The dye was excited because its excitation wavelength corresponded to the laser light wavelength. The illumination brightness of the plume depends on the concentration of the dye at the particular region. At the initial injecting region, the brightness was high as entrainment was minimal. Further away from the injection point, the brightness decreased due to the dilution within the plume.

Using the LIF technique, the density differences across the cross sections of a buoyant plume to its surrounding could be measured. This density manipulation depends on the relative brightness between the buoyant plume to its initial injecting brightness. To convert the brightness data to density data, both the densities of the ambient fluid and the saline solution need to be measured. The conversion is achieved by applying Eq. (4.1).

$$\rho(x,y,z) = \rho_{ambient} + \left|\rho_{plume} - \rho_{ambient}\right| \cdot Ratio(x,y,z) \qquad (4.1)$$

where

ρ (x,y,z)	=	density of the plume at location (x,y,z)
$\rho_{ambient}$	=	density of the surrounding ambient fluid
ρ_{plume}	=	initial density of the plume before injection
Ratio (x,y,z)	=	Ratio between the net brightness in the flow to initial brightness of the plume before experiment in the calibration cell.

In order to pick up the brightness data from the experiment, a set of image capture equipment was used. It included a digital camera, a video cassette recorder, an IBM-compatible PC with frame-grabber board and a Sony Trinitron colour video monitor. The equipment will be described later in this chapter. In this research project, the equipment settings followed the recommendation made by Papps (1995) and Gaskin (1995) and are briefly described below.

4.2 LASER SHEET AND EQUIPMENT

The LIF technique required a laser source to excite the dye mixed within the spilling solution. The laser source needed to be a constant intensity light source and to have a wavelength corresponded to the excitation wavelength of the dye used. With the use of the digital camera, the relative brightness of the spilling plume could be picked up and processed to obtain the quantitative concentration measurements.

In this experimental programme, the Coherent Innova 70-5 argon ion laser was used. Operating in a single line mode, it produced light at a wavelength of 514.5 nm. This wavelength corresponded to the excitation wavelength of Rhodamine type dyes used in the experiment. During the operation, the laser was set on light power mode. At this operating mode, the light power of the laser self-regulated itself to a maximum power variation of ±0.5% of the set power level according to Gaskin (1995). A laser power

level of 2.0W was used in the study, which was slightly below the maximum power level achievable of 2.4W.

In order to obtain the density profiles across the longitudinal cross section of the generated balcony spill plume, the plume needed to be sectioned with a planar sheet of laser light. For the setup in the laboratory, the planar sheet of laser light was generated by a rotating octagonal mirror, a Lincoln Laser Company rotating mirror, model M-660-010-LVW0B. When the mirror rotated, each mirror face of the polygon reflected the laser beam onto an arc mirror. The reflection of the arc mirror generated the planar laser sheet required. The schematic layout is shown in Figure 4.1.

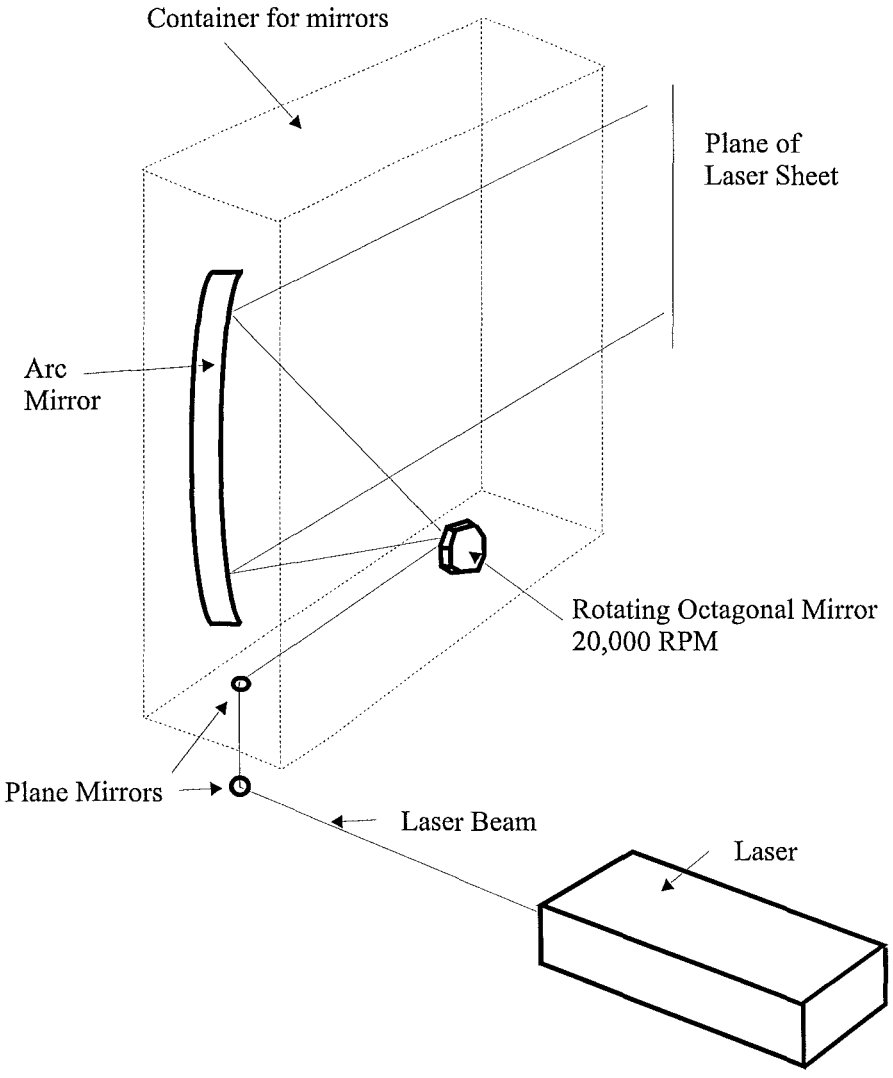

Figure 4.1 Laser sheet created with rotating mirror.

The rotational speed of the mirror was 20,000 RPM. Gaskin (1995) reported that by running the rotating mirror at this speed, it lay within the middle of an interference free frequency band.

4.3 RHODAMINE DYE

The LIF technique achieved the flow visualisation effects by exciting the fluorescent dye in the injected buoyant plume. As indicated before, the dye's excitation wavelength had to correspond to the wavelength of the laser light that went past it to become fluorescent. With the particular laser source used, Rhodamine dye was found to be appropriate for the application. In the experiments, Rhodamine 6G fluorescent dye was used. This dye produced an orange fluorescent light with a peak wavelength of 560 nm.

This particular type of dye produced a relatively high fluorescent at low concentration. Gaskin (1995) reported that the lower the concentrations of the dye, the less attenuation of power in the laser sheet as it passed through the dyed fluid. Her results are shown in the Figure 4.2 below.

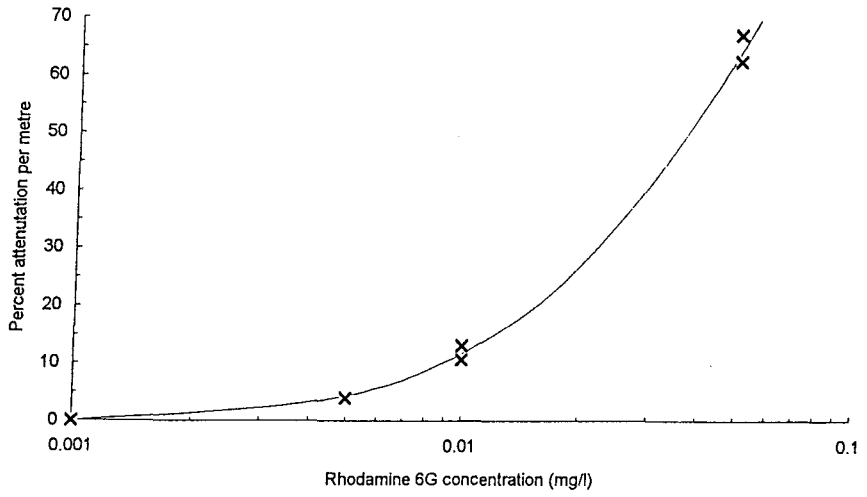

Figure 4.2[†] Attenuation of laser light as it passes through a fluorescent solution.

[†] Figure copied from Gaskin (1995).

A dye concentration of 0.05 milligram per litre was recommended by Gaskin (1995) and was used for all the experiments conducted in this study. By using this concentration, good visualisation and minimal attenuation of the laser light were expected.

4.4 IMAGE CAPTURE EQUIPMENT

A Pulnix CCD black and white digital camera, model TM765E with Image Intensifier was used to capture the fluorescent flow image generated from the excitation of dye by the laser light. A Schott glass filter, glass type OG530 high pass optical filter was mounted in front of the camera lens. This was to filter out the scattered laser light and light of wavelength less than 530 nm. The lens used for the camera setting had a focal length of 25mm. This particular focal length allowed the entire balcony spill plume flow to be captured. Figure 4.3 shows the basic arrangement of the image capture equipment in used.

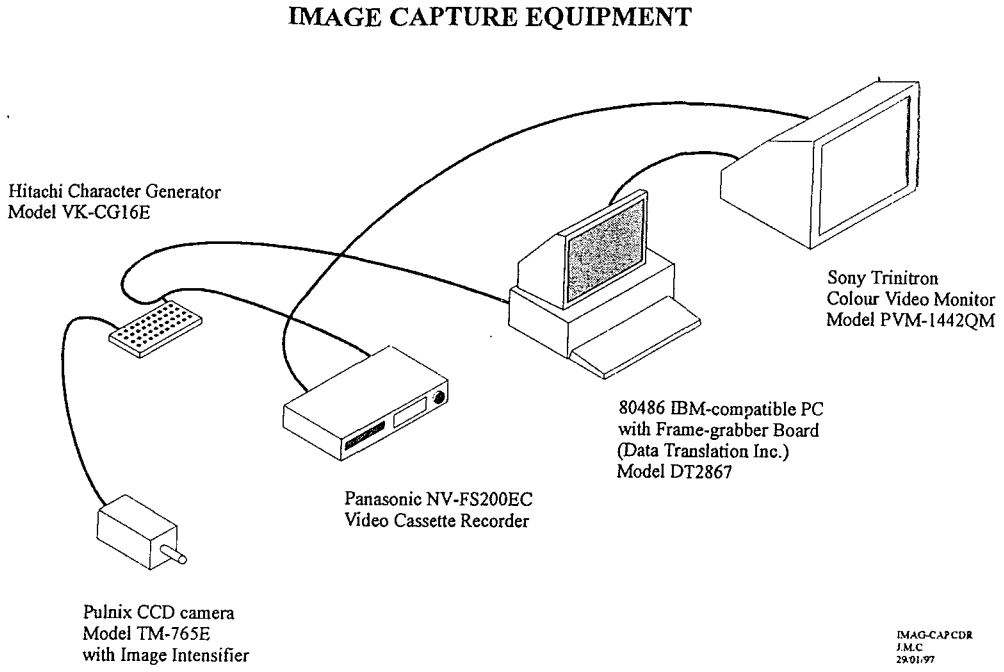

Figure.4.3[†] Basic arrangement of the image capture equipment.

[†] Figure obtained from Clement (1997).

During operation, the camera sent the PAL type video signal to the video recorder where it was recorded onto a master grade video cassette (VHS). The images were recorded at a frequency of 25 Hz and covered an area of 512 pixel wide and 440 pixel high per image. The images stored on the video tape were later retrieved by the frame-grabber hardware on the computer.

4.5 HARDWARE AND SOFTWARE ON COMPUTER

The frame-grabber board used was from Data Translation Incorporated, model DT2867. The board had the ability to allow real time averaging of up to 10 seconds and could capture a series of instantaneous images at a frequency of 0.5 Hz. For the experiments in this research program, the image capturing frequency of 25 Hz was used following the recommendation by Gaskin (1995) and Papps (1995).

The software that supported the frame-grabber board was the Global Lab Image-Version 2 (1992) software from Data Translation Incorporated. This software was Windows based and was used to manipulate the captured images with the frame-grabber board. It had basic image processing capabilities; for instance the Arithmetic tool allowed the adding and subtracting of images, and the Draw tool for the addition of boundaries and other functions. The images were stored on the hard drive and were retrieved and analysed at a later stage.

The frame-grabber digitised the video signal voltages such that the images were stored as a set of light intensity values. Since the images were stored on the 393,216 pixels in a 768 by 512 array, the intensity at each pixel was recorded as a grey-scale integer between 0 (black) and 255 (white).

During operation, an input look up table (ILUT) developed by Papps (1995) was activated. Papps found that the camera used did not response linearly to a linearly varying light source. The ILUT was able to map each of the 256 in-coming intensity levels to levels required for a linear intensity response by the camera. The reference

voltage and the offset voltage of the frame-grabber were set to the recommended value of 1024 mV and -60 mV respectively. This was to achieve low background light levels such that it measured less than 10 grey scales.

4.6 SUMMARY

The Laser Induced Fluorescence (LIF) flow visualisation technique used in this study follows the recommendations by Papps (1995) and Gaskin (1995). Both Papps and Gaskin had looked at this technique in a thorough fashion. Hence reasonably good data was anticipated.

CHAPTER 5

5 EXPERIMENTAL SETUP

This chapter discusses the choices taken for setting up the experiments. It also discusses certain problems and uncertainties that were encountered during the experimental programme.

5.1 SIMULATION OF BALCONY SPILL PLUME

5.1.1 Physical model

The physical model used to simulate a shop connected to an atrium during the experiments was made of perspex sheets. Its basic appearance is shown in Figure 5.1. For detail dimensions, please refer to the engineering drawings in Appendix A.

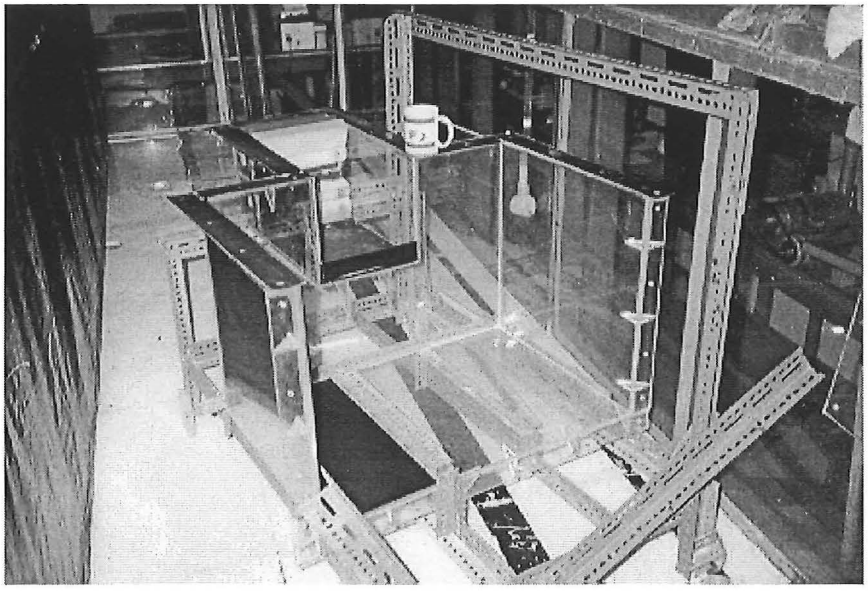

Figure 5.1 Perspex model used.

The model was placed in the upside down position. This was because a salt water layer in ambient fresh water was used to simulate the hot smoke layer in ambient cool air during salt water experiments. To preserve the same driving mechanism-buoyancy, salt water was allowed to spill through the ambient fresh water in a downward direction acting under gravitational forces. This would eventually create similar effects to the hot smoke plume rising through the ambient cool air; a reverse analogy to the real fire scenario. The model was a 1/20 scale model having geometry that simulated the conditions such as 1) roofing above the balcony or 2) the presence of an upper balcony. This is illustrated in Figure 5.2.

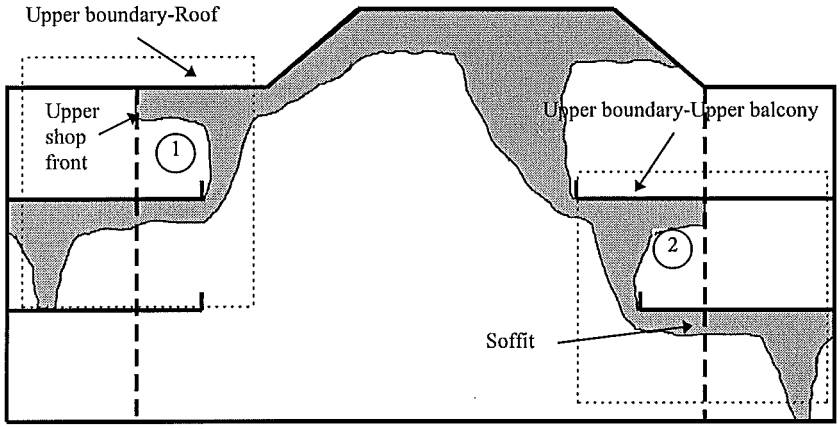

Figure 5.2 Conditions simulated.

The model had a fire compartment representing a typical single shop of dimensions 5m in height, 5m in width and 7m in depth at full scale equivalent. It was connected to a bigger compartment representing part of the atrium's space beyond the fire compartment. This space had a basic dimension of 10m in height, 15m in width and 10m in depth at full scale equivalent. Wraight (1973) suggested that when a fire broke out within a shop having a glass window front, it could be assumed that the glass front would break, hence the model had a full compartment width opening. As for the adjacent and upper shops, they would be unaffected by the fire, based upon the assumption that fire barriers between shops would be installed under normal circumstances. For this reason, these shops were simulated by flat pieces of perspex sheets to represent their intact glass window fronts.

Two balconies each with a different breadth (125mm and 250mm in model scale) was introduced successively during the experiments. Both of these balconies had channelling screens attached to them. Channelling screens are commonly used to restrict the lateral spread of smoke and hence the amount of smoke generated. The requirement of channelling screens and their basic dimensions were documented by Hansell and Morgan (1994). In this model, channelling curtains having a depth of 75mm in model dimension were used representing curtains of 1.5m depth. A downstand fascia (soffit) of 40mm was introduced on the shop front so as to realistically model the common shop front layout with actual fascia of 800mm.

5.1.2 Generation of Smoke Layer

To generate the smoke layer within the fire compartment, a counter action pumping method was chosen instead of the injection of free plume. Figure 5.3 shows two alternative ways of generating the "smoke layer" using the saline solution within the model.

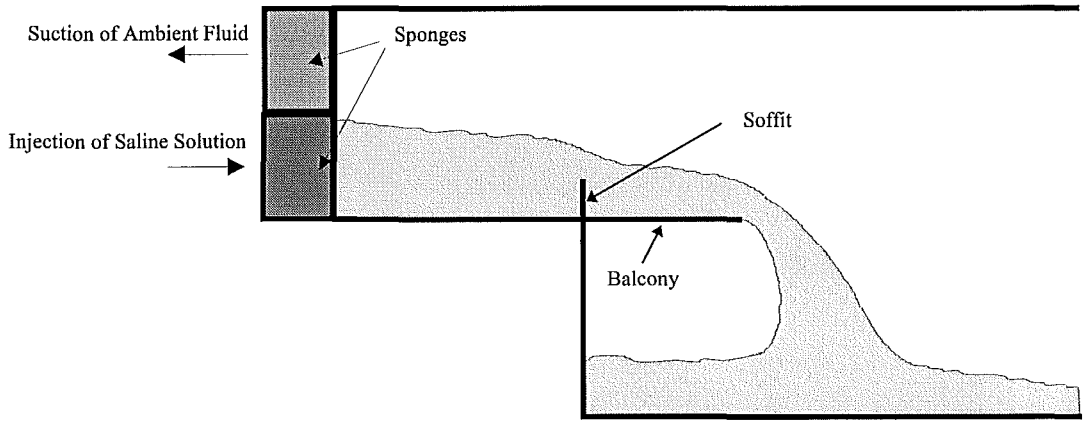

(a) Counter action pumping method

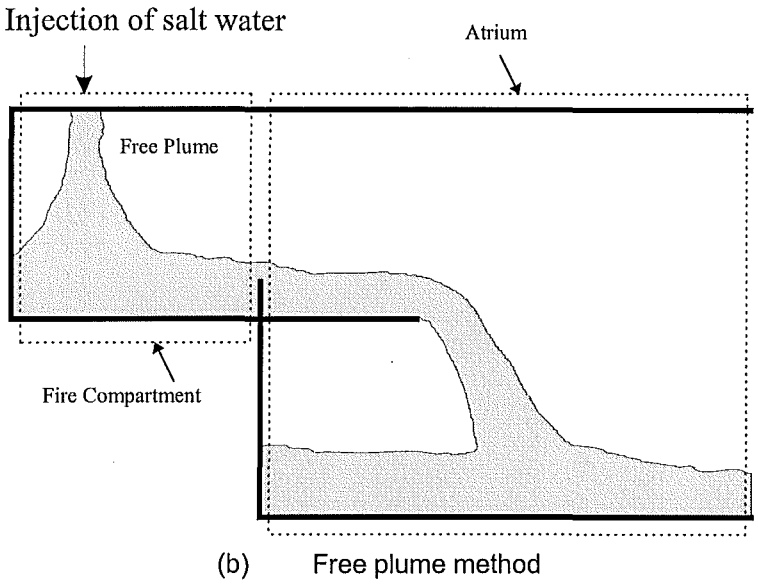

Figure 5.3 Two alternative methods to generate the smoke layer within compartment.

The two alternative methods include (a) the counter action pumping method and (b) the free plume method. Although the injection of salt water as a free plume within the compartment is visually good as it takes the shape of the real fire plume, the control of it is very difficult.

The approach taken in this study was to simulate the saline layer, hence the smoke layer in the fire case, within the fire compartment as realistically and theoretically as possible. This would allow data of saline flow downstream, ie the balcony spill plume, to be taken with greater confidence both qualitatively and quantitatively.

The major difficulty involved with the free plume method was the injection rate of the salt water plume. This injection rate is a critical factor. A higher injection rate would result in the formation of a salt water jet rather than the required plume.

When a jet was formed, the Froude Number $Fr = \frac{u^2}{gD_f}$, would have a value greater than 1. This is an indication of a momentum driven jet plume. In this situation, the prediction of the entrainment into the rising jet plume would be difficult. Drysdale (1986) pointed out that jet flames consist of 3 possible types depending on the jet

velocities. These types include laminar diffusion flames, transition region flames and fully developed turbulent flames. These three types of flame all have a different length of establishment.

It might sound trivial to introduce the salt water at low velocity to avoid the formation of a jet. However, because momentum is usually associated at the injection point, certain jet characteristics cannot be avoided, especially using mechanical devices in controlling the injection. With the low model height in the fire compartment, it is not entirely certain whether the establishment length of the injected salt water would exceed the model's height or not. Under these circumstances, little confidence could be put upon the saline plume layer generated. Figure 5.4 shows the possible situation.

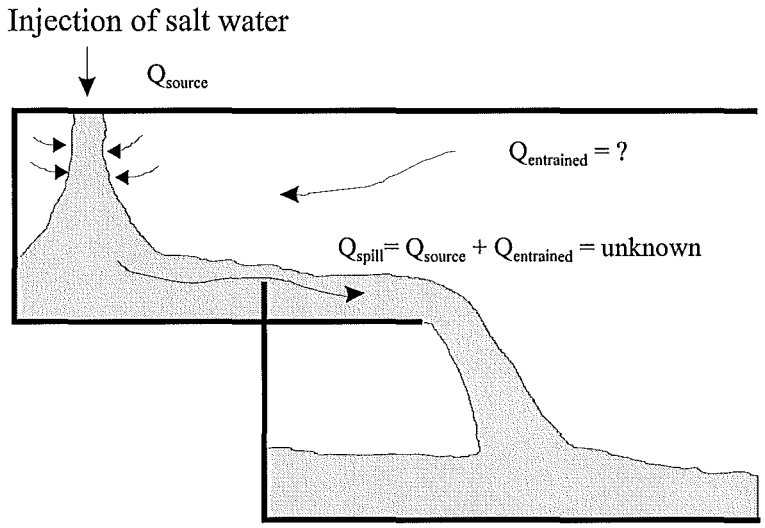

Figure 5.4 Unknown entrainment quantity as in free plume method.

To avoid these problems, the counter action pumping method shown in Figure 5.3 (a) was chosen and used for all the experiments conducted. Under this method, a better control over the flow was achieved and hence the simulation of the smoke layer from the fire compartment. Figure 5.5 illustrates the situation.

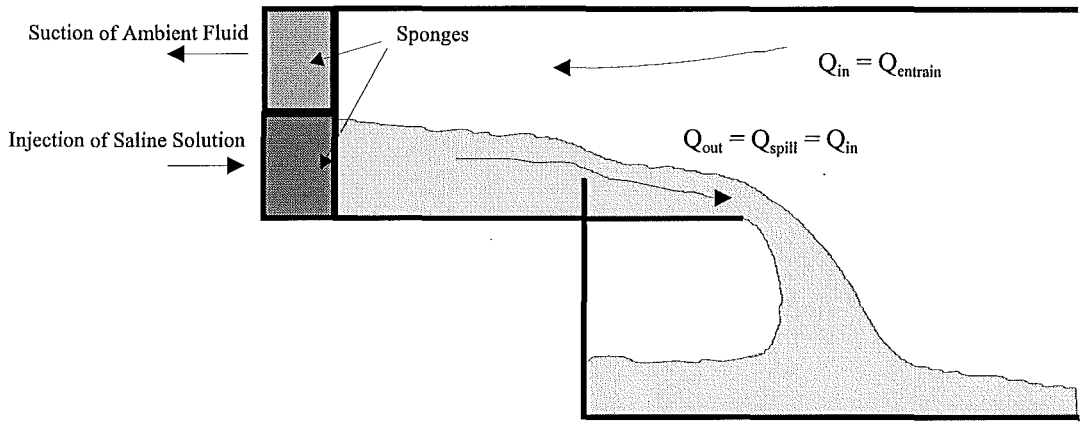

Figure 5.5 Controllable flow rate on the spilling plume.

As shown in Figure 5.5 above, there were two ports at the far end of the fire compartment. The upper port was a suction port for ambient fluid whereas the lower one was the saline solution injection port. Both ports were bounded by sponges to smooth out the flow and avoid any turbulence jet that might occur.

The suction of the ambient fluid was created by a hydraulic pump. The suction amount was monitored and controlled through a rotameter. The saline solution was injected from the header tanks via an electrical booster pump. The amount of the injected fluid was controlled through the valve on the pump and monitored on an electro-magnetic digital flow meter.

The ability to control both the injecting and suction flow rates offered the opportunity to quantitatively simulate the counter flows at the doorway of the fire compartment. Matching both the suction and injection flow rates, a quantitatively correct saline counter flow at the *plane of vent opening* was achieved. This was based upon the assumption that the mixing between the layers within the fire compartment was negligible.

In the real fire case, it is mass that is conserved rather than volume as modelled in the experiments described. Figure 5.6 shows the schematic view of the real fire case in the compartment.

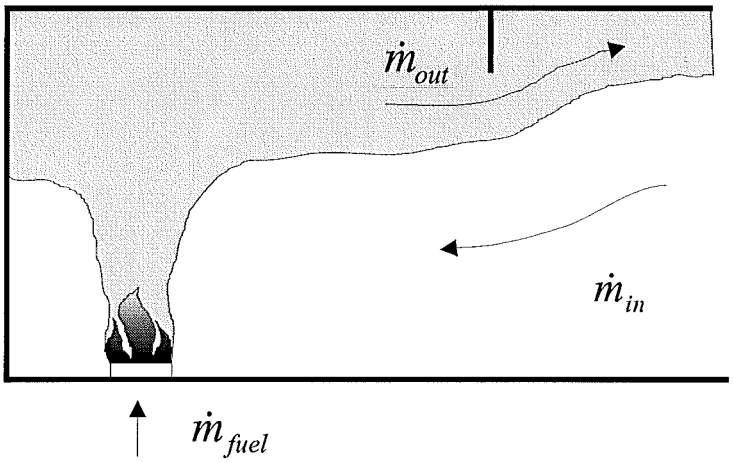

Figure 5.6 Real compartment fire scenario.

For the fire induced gas within an enclosure, the mass balance at the opening vent can be written in the form given in Eq. (5.1).

$$\dot{m}_{out} = \dot{m}_{in} + \dot{m}_{fuel} \tag{5.1}$$

Rockett (1976) suggested typical $\dot{m}_{fuel}$ normally had a value of $\dot{m}_{in}/15$ which can be treated as negligible. Hence Eq. (5.1) can be reduced to the form as in Eq. (5.2).

$$\dot{m}_{out} \approx \dot{m}_{in} \tag{5.2}$$

Applying the continuity equation at the plane of the vent opening, written in terms of volumetric flow rate, Eq. (5.2) could be re-written to give Eq. (5.3).

$$\dot{Q}_{out} \cdot \rho_{out} = \dot{Q}_{in} \cdot \rho_{in} \tag{5.3}$$

Rearranging Eq. (5.3) gives Eq. (5.4).

$$\dot{Q}_{out} = \dot{Q}_{in} \frac{\rho_{in}}{\rho_{out}} \tag{5.4}$$

In the case of salt water modelling, ideally the injection and suction flow rates had to be adjusted corresponding to the density ratio between the spilling saline solution and the ambient fresh water. However, the saline solutions used in the experiments (0.5% and 1.0% by weight) did not have large density differences between the ambient fluid. Also, the accuracy of the flow adjustment through the rotameter and the pump was bounded by the stability of the equipment. This was especially true for the injection flow rate. The control of flow through the pump valve proved to be difficult to achieve the preciseness desired. The fluctuation on the injection flow rate had been observed to be approximately ±1.5%. This uncertainty was also observed to be time dependent. As time passed, the reduced hydraulic head of the spilling fluid in the header tanks could lower the proposed injection flow rate of 16.25 litre per minute. Also bearing in mind that the derivation of the flow equation ignored the contribution from the fuel and itself imposed certain uncertainties within the derived equation. Hence by matching both the suction and injection flow rates, the flow was considered to be of reasonably good accuracy, at least within the practicality and preciseness able to be achieved on the equipment available.

5.2 LASER SETTINGS

With the planar laser sheet generated by the rotating mirror, there was a question regarding the best direction for this laser sheet to section the spilling plume. Clement (1997) found that incoming direction of the laser light might have an effect on the accuracy of the results.

The initial proposed setup was to allow the laser sheet to come from the top of the spilling plume via an angled mirror. This would minimise the attenuation of the laser light per distance travelled through the ambient water. However, this setting did create some unexpected problems. The problem encountered was the possible "shadowing" effect on the flow. Since the spilling saline solution had a density slightly greater than the ambient fluid, the two fluids eventually created an interface while flowing along each other. By introducing the laser light from the top of the spilling plume, the laser

light passed through the flatter saline surfaces with minimal refraction. However, at the rotational region of the spilling plume, the angle of the saline surface to the incoming laser light was steeper. With this angle being greater than a "critical angle", the laser light would be deflected off instead of passing through the flow as intended. This might cause the shadowing in the plume region.

As the LIF technique relied on the excitation of the dye by the laser light, the loss of laser light over the "shadowed" plume region would result in the loss of detail over that area. Clement (1997) found that this was a problem in his vent flow works as his vent flow results could not be repeated. This shadowing effect is schematically shown in Figure 5.7.

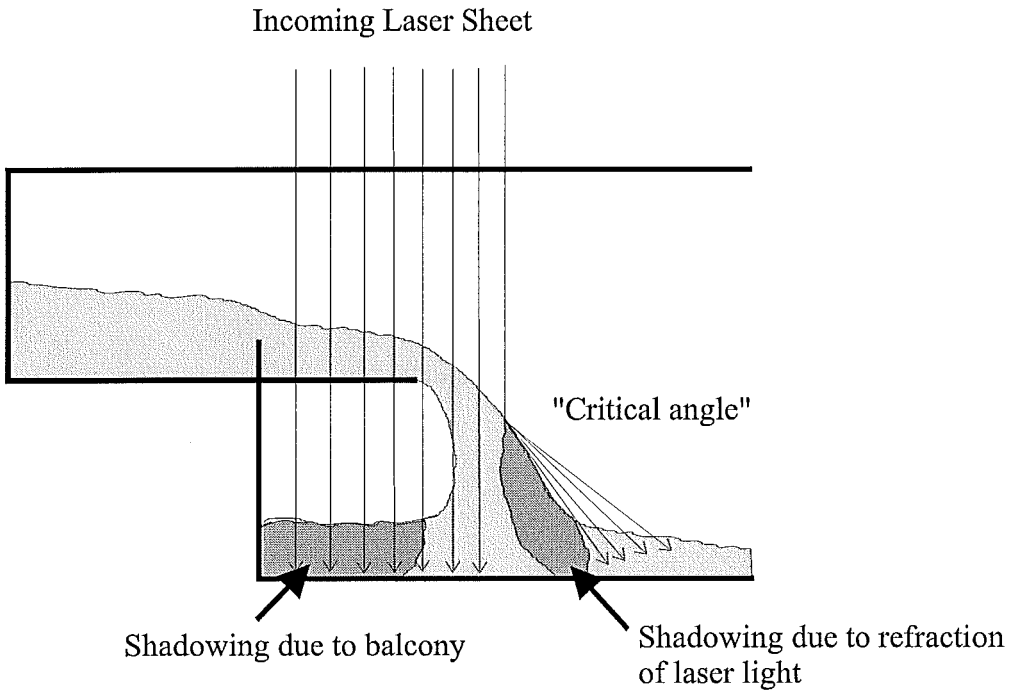

Figure 5.7 Shadowing effects resulting from incoming laser light from the top of the model.

The other potential problem that would be encountered in this setup was the possible attenuation of the laser light intensity through the perspex made balcony that had a thickness of 6mm in thickness. Although there were no documented results to support the possibility of perspex sheet absorbing the laser light, for precaution sake it was to be avoided if possible.

To get around these potential problems, the proposed laser setup was adjusted. This modification allowed the laser sheet to come from the front site of the spilling plume rather than the top. Although there might be some possible shadowing effect on the flow near the balcony as shown in Figure 5.8, the main portion of the spilling plume was relatively undisturbed. This was thought to be a sensible compromise with the retention of quality results on the main emphasis, ie the spilling plume.

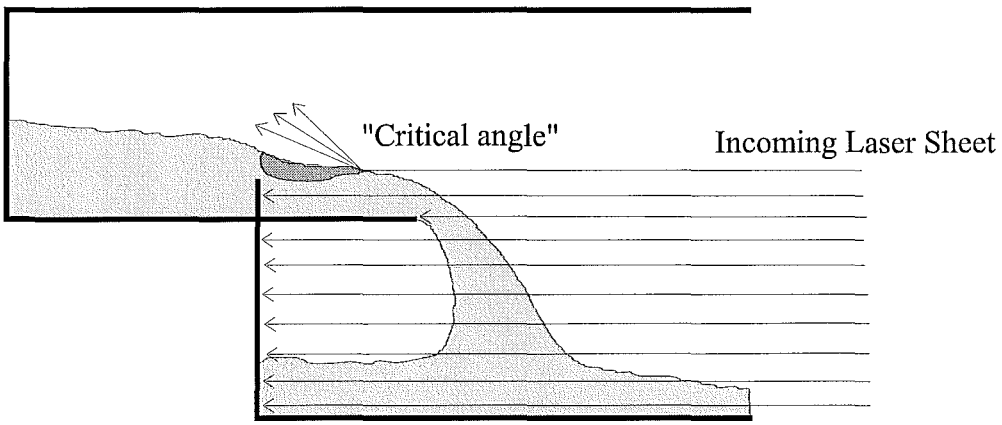

Figure 5.8 The setup used in the entire experimental program.

5.3 EXPERIMENTAL PROGRAMME

In this experimental study of balcony spill plume, four experiment series were conducted. Each experimental series had a different setting and consisted of a number of longitudinal sections measured across the model. The details of these experimental series are outlined in Table 5.1.

Table 5.1 List of experimental programme.

Experimental Series	Experiment Settings	Sections† Investigated
SP-B01	Short balcony (125mm) with 0.5% saline solution	centre, 100mm, 200mm, 300mm
SP-B02	Short balcony (125mm) with 1.0% saline solution	centre, 50mm, 100mm, 150mm, 200mm, 250mm, 300mm, 350mm
SP-C01	Long balcony (250mm) with 0.5% saline solution	centre, 50mm, 100mm, 150mm, 200mm, 250mm, 300mm, 350mm
SP-C02	Long balcony (250mm) with 1.0% saline solution	centre, 50mm, 100mm, 150mm, 200mm, 250mm, 300mm, 350mm

All of these experimental series had the same injection and suction flow rates of 16.25 litre per minute. The experimental procedures were conducted in the identical manner for each section in every experimental series. These procedures are briefly described in the next chapter.

5.4 SUMMARY

The model used was made of perspex. It was a 1/20 scale model in an attempt to simulate the conditions where the balconies have upper overlapping boundaries. The saline layer that represented the smoke layer in the real fire scenario was generated using the counter action pumping method. The method would allow the matching of the volumetric flow rates between the suction ambient and injection saline fluids. Having the ability to control these flow rates, a quantitatively correct counter flow at the plane of vent opening was achieved. The laser sheet was designed to come from the front of the model. By doing this, potential shadowing problems were minimised.

† The distance values given are the distances measured from the centre of the model.

CHAPTER 6

6 PREPARATIONS AND OPERATIONS

This chapter outlines the pre-experimental preparations necessary and the operations involved while running the experiments. Post-experimental measurements are also described.

6.1 PRE-EXPERIMENT: PREPARATION

Before running any experiments, there were certain things that needed to be prepared. These included the preparation of saline solution, model and equipment setting. The details of the procedures taken during the preparation works are outlined in the following sections.

6.1.1 Saline Solution

Saline solution was an essential ingredient for the experimental work. The saline solution was mixed up in the header tanks as shown in Figure 6.1. The amount of fresh water into the header tanks for mixing purpose was obtained from the water main and its quantity monitored by a KENT flow meter. After the required quantity of water was stored, an appropriate amount[†] of salt was weighed on an electronic scale and then poured into the header tanks. To achieve proper mixing, both the stirrer and circulating pump on the header tanks were switched on. An appropriate amount[‡] of Rhodamine 6G dye was added at the same time. Their quantities were measured using pipette tubes.

[†] The amount of the salt added depended on the concentration of the saline solution needed. For 0.5% and 1.0% solutions, they were mixed in accordance to the density of 5.0 g/l and 10.1 g/l. However, the exact densities for this saline solutions were later measured using the PARR density meter.

[‡] The quantities of the Rhodamine dye added to the mixtures were calculated in order to have a concentration of 0.05 mg/l.

The stirrer and the circulation pump were run for approximately 2-3 hours. The saline solution was then left overnight allowing the dye to uniformly diffuse throughout the entire solution. Before running an experiment, both the stirrer and the circulating pump were again run for approximately 1-2 hours to prevent any pre-stratification possible within the overnight saline solution.

6.1.2 Model and Calibration-Cell

The model was made of perspex sheets and took the basic shape as indicated in Figure 5.1 above. The camera was located outside the ambient tank and shot the flow images through the glass window of the ambient tank and perspex wall of the model. In order to film good quality flow images, both of these surfaces needed to be cleaned. This applied to the calibration cell[†] as well. The perspective locations between the camera, the model, the laser sheet and the ambient tank are schematically shown in Figure 6.2.

The inside of the glass filming window, and the perspex walls for both model and calibration cell were smeared with Finish® Rinse-Aid solution. This prevented the formation of air bubbles on these surfaces which might interfere with the filming of the flow images. The outside of the filming window was kept clean by the use of normal soap water. Nevertheless, the glass window on the ambient tank where the incoming laser light passed through before reaching the model was smeared and cleaned with appropriate agents.

[†] The calibration cell was a clear cell of 1.0m high by 0.7m x 0.1m in dimensions. It was made of perspex sheet and was used to contain the initial spilling fluid. This was for calibrating the initial brightness of the spilling fluid for density measurement.

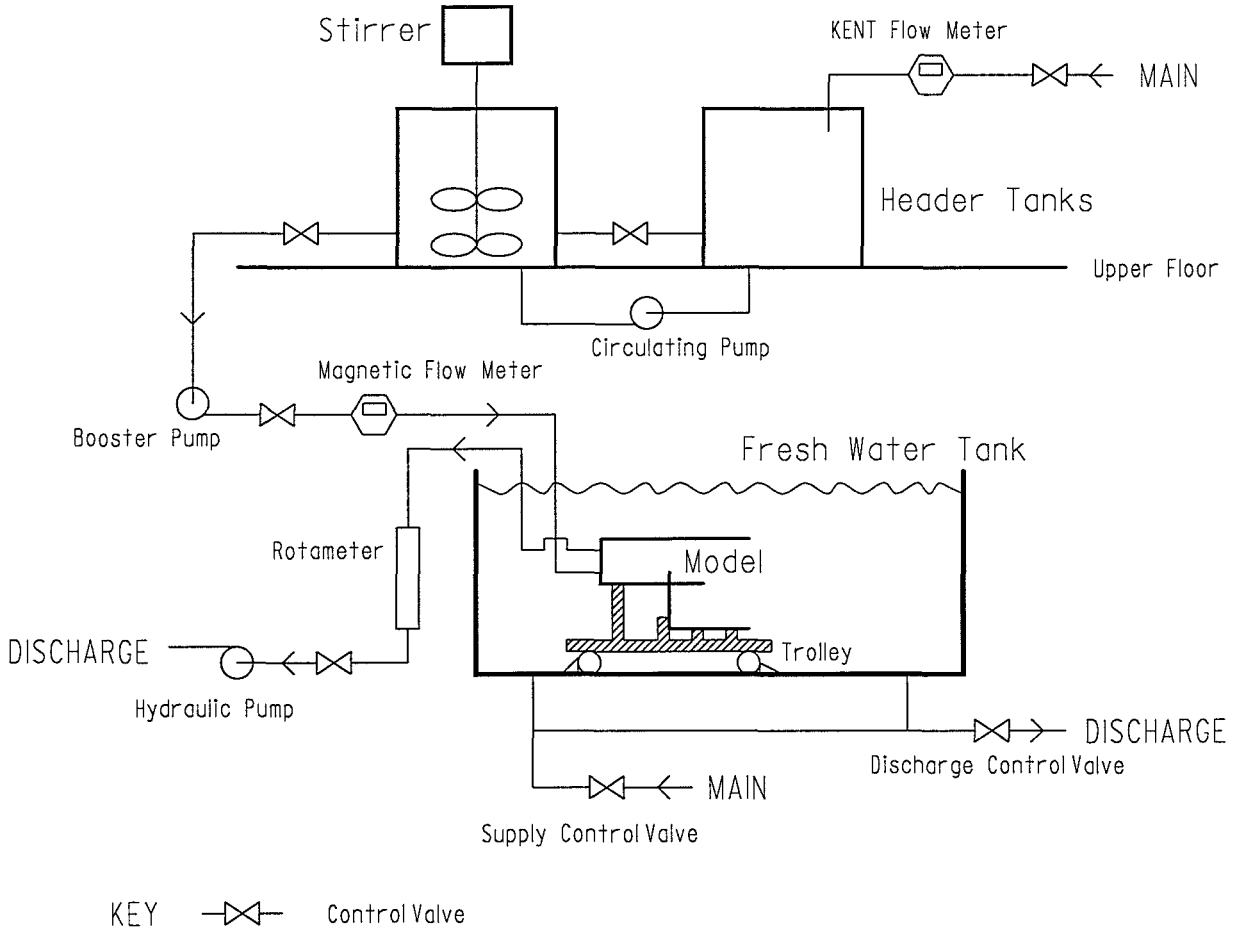

Figure 6.1 The schematic layout of the equipment and devices used in the experiments.

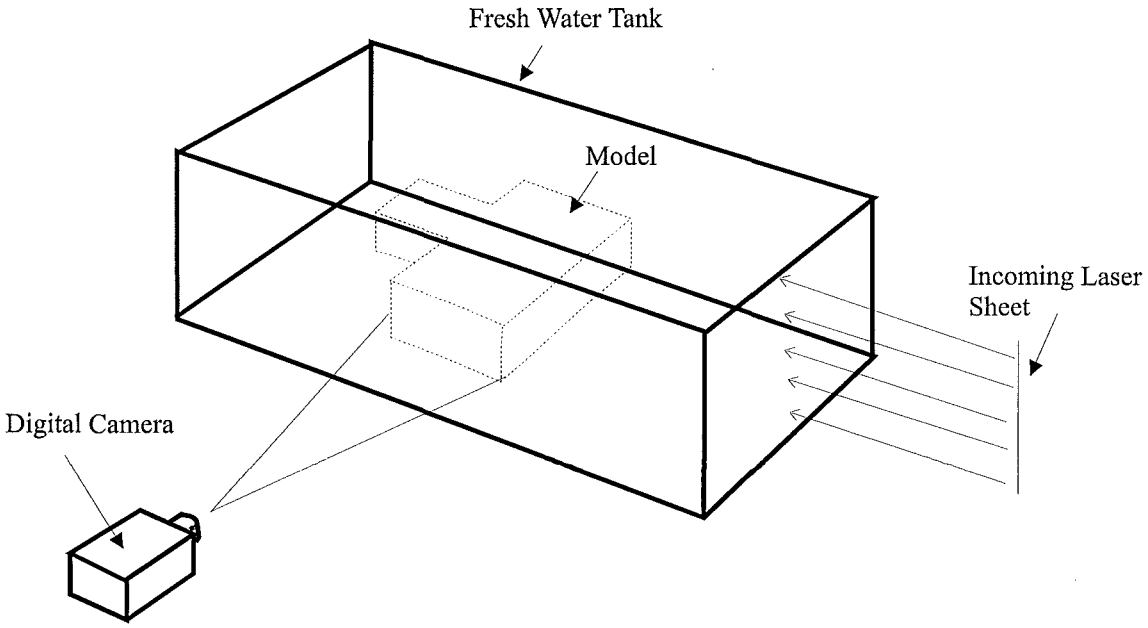

Figure 6.2 Perspective layout between camera, model and laser sheet.

6.1.3 Filling the Ambient Tank and Calibration Cell

With the surfaces smeared with Rinse Aid solution, both the ambient tank and calibration cell were ready to be filled with fresh water and the prepared saline solution respectively. However, before any filling, approximately 10 litre of the saline solution was flushed into a bucket. This was to avoid the adhered Rhodamine dye from previous runs being passed into the calibration cell, thus giving a wrong calibration of the dye. As indicated in Figure 6.1, the saline solution was piped from the constant head tanks to the injection port via a vinyl piping. According to Gaskin (1995), an amount of dye, varying with the flow rate of up to 10% of the original concentration was absorbed onto the vinyl. Flushing allowed the dye concentration to stabilise at the prepared concentration.

Both the ambient tank and the calibration cell were then filled simultaneously after flushing the vinyl pipe. The fresh water was filled to a level approximately 2-3 inches above the top of the model to totally submerge the model. The calibration cell was filled up to the same level as the fresh water.

6.1.4 Warm-up of Equipment

The laser and the camera were warmed up before starting any experiment, as recommended by Papps (1995). The laser was warmed up for at least 2 hours under maximum light power mode and the camera for at least 1 hour. This assured that both items of equipment were operating at their stable conditions.

6.1.5 Sampling

The temperatures and samples for both ambient fluid and saline solution were to be taken for density measurement purpose. The plan for the experimental operation was to totally discharge the ambient fresh water in the fresh water tank after recording 4 separate sections of the spilling fluid for each experimental series. This was to prevent any contamination in the fresh water tank that might affect the density results obtained. The temperatures and samples for both ambient fluid and saline solution were taken before and after the 4 sections performed. The temperatures were measured using a mercury thermometer. Temperature readings for the ambient fluid were taken within the fresh water tank and saline solution taken from the vinyl piping with booster pump on. The samples were contained in containers and were analysed for their precise densities using a DMA 60 PARR Density Meter available in the Chemical and Processing Engineering Department, at the University of Canterbury.

6.1.6 Camera Settings

The Pulnix digital camera was used to capture the flow images. It needed to be focussed in line with the laser sheet before commencing any filming. To focus the camera, the model, which rested on a trolley, was moved in front of the camera. The model was aligned such that its centre was in line with the incoming laser sheet. A metal sheet grid was placed vertically within the centre of the model and in line with the laser light. The focus of the camera was adjusted accordingly to the grid.

The aperture of the camera that controlled the brightness of the filmed images was adjusted. The calibration cell in the fresh water tank was moved in front of the camera. On the Global Lab® Image software, the reference voltage and the offset voltage were

set to a value of 1024 mV and -60 mV respectively. This allowed low background light levels and generally less than 10 grey scale. With the calibration cell in front of the camera, the camera's aperture was adjusted. The adjustment on the aperture was to get the dye as bright as possible in the filmed image but without over-exposing it. By having a larger aperture setting, greater dilution details on the spilling plume could be picked up by the camera than otherwise. The adjustment on the aperture setting was monitored using the Profile and Histogram tools on the Global Lab® Image software.

6.2 EXPERIMENT OPERATIONS

After the warm up of the laser and the adjustment of the camera, the experiment could then be started. Under the experimental program as given in Section 5.3, for each experimental series, a set of density profile data each on appropriate longitudinal sections of the spilling plume was collected. For all the experimental series except SP-B01, the spilling plume was divided into eight sections starting from its centre. Each section was spaced 50 mm apart from one another. To take the flow images at each section, the model was slid across the trolley guided by an aligning bar behind the model. The markings on the front of the model allowed each section to be properly located in line with the incoming laser sheet.

6.2.1 Calibration-Cell and Grid Shot

After the aperture on the camera was set, the laser light power level was tuned to 2.0W. With the Global Lab® Image software operating in Live mode, the image of the calibration cell was taken at the frequency of 25 Hz and recorded onto a master grade video cassette for 20 seconds. The calibration cell was then moved away and its background in the ambient fresh water tank was recorded for 20 seconds. Both of these shots were taken with all the background lighting switched off.

The model was brought in front of the camera by the trolley running on a fixed rail in the tank. The position of the trolley was adjusted such that the entire flow generated was within the view of the camera. The trolley was then fixed in place with the

blockages on its wheel and the model was aligned such that its centre was in line with the incoming laser sheet. The metal sheet grid was inserted again to check the focus of the camera. The image of the model with the grid was recorded for 20 seconds. The grid image was later used in the image processing stage to identify the boundaries and positions.

6.2.2 Flows Shot

After taking the grid shot, the grid was removed and a background shot of the model was recorded for 20 seconds. Both the injection and suction ports at the model were connected with appropriate piping. In order to generate the flow required, the hydraulic suction pump was activated first. The rotameter was set to a reading of 18 which corresponded to a flow rate of 16.25 litre per minute. The calibration of the rotameter was in accordance to that documented by Clement (1997).

The control valve on the header tanks was turned on and the booster pump was started and adjusted to obtain the same flow rate as in the suction pump, a flow rate of 16.25 litre per minute. This injection flow rate was monitored through the electro-magnetic flow meter connected. All lighting inside the laser room was switched off. A time period of approximately 3-4 minutes was allowed for the flows to become fully established and stabilised. This included the flow within the fire compartment and the spilling plume. The laser power level was checked to ensure that it stayed on the required 2.0W setting. A routine check on the suction and injection flow rates was made as well. With everything satisfactory, the flow was recorded for 5 minutes onto the video tape.

After the flow images were taken, both the booster and hydraulic pumps were switched off. The header tank's control valve and the rotameter valve were also turned off.

The ambient fresh water tank was then drained of approximately 10% of its volume through its own drainage system. The main intention of the draining was to get ride of any saline solution that might accumulate under the tank. The tank was filled up again

with fresh water. The model was shifted to the new position, ie next section. The background shot of the model at new position was taken and the same procedure was repeated.

Samples for both the ambient fluid and spilling solution were taken just before the test run of the fourth section. At the end of capturing the flow image at the fourth section, the ambient tank was totally discharged. This was to prevent contamination of the ambient fluid by the saline solution. The ambient tank was then refilled with fresh water and experiments for the next four sections continued. Again samples were taken before and after the four sections performed.

6.3 POST-EXPERIMENT: DENSITY MEASUREMENT

6.3.1 Density Meter

Both ambient and spilling fluids' samples were taken during the experiment. These samples were analysed using a density meter to obtain their precise density values. The density meter used was a DMA 60 Density Meter that was located at the Chemical and Processing Engineering Department's Plasma Laboratory. The density meter measures the precise densities of fluid samples at corresponding temperatures.

The density meter consisted of a remote DMA602H cell, into which the fluid sample was injected. The temperature of the cell was regulated through a constant temperature water bath. A digital thermometer was connected to the cell to monitor its temperature. A DMA processing unit was used to give the density count on the injected samples. The counts were used in Eq. (6.1) to calculate the corresponding densities. Figure 6.3 is a photo of the density meter used.

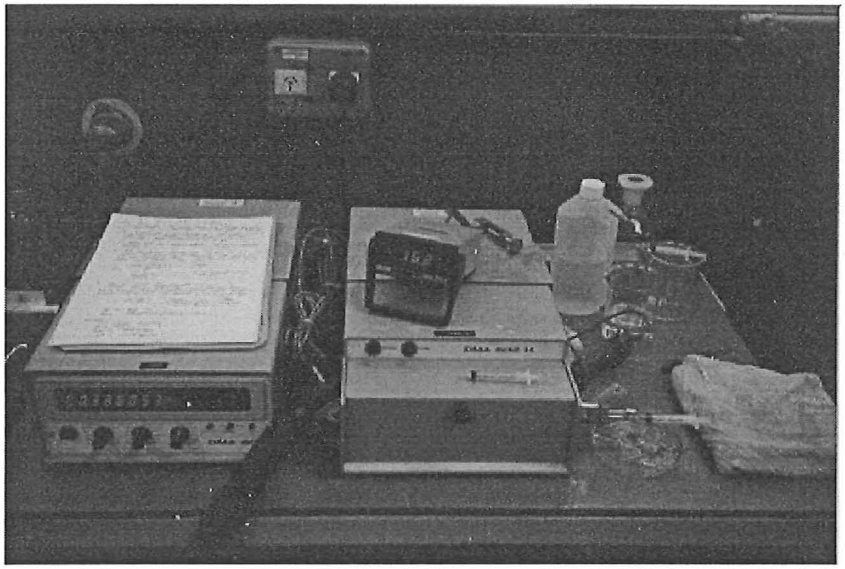

Figure 6.3 The layout of the PARR density meter.

6.3.2 Density Manipulation

In the density measurement exercise, apart from the experimental samples, two other types of fluid samples were measured. These were air samples and distilled water samples. The use of these samples were for calibration purposes, as they provided both the upper and lower bounds in their reference counts. These counts were then used to calibrated the samples obtained from the salt water experiments.

The density of the air sample is given by Eq. (6.1).

$$\rho_a\left(\frac{kg}{m^3}\right) = \frac{1.2930}{1+0.00367\theta_a(^\circ C)} * \frac{P_{atm}(mb)}{1013.25} \tag{6.1}$$

where θ_a = air temperature in the cell (°C)

P_{atm} = atmospheric pressure (mb)

The density of each sample is determined from Eq. (6.2).

$$\rho_{sample} = \rho_w + \left(\frac{\rho_w - \rho_a}{T_w^2 - T_a^2}\right) * \left(T_{sample}^2 - T_w^2\right) \tag{6.2}$$

where ρ_{sample} = density of the sample

ρ_w = density of the distilled water sample

ρ_a = density of the air sample

T_{sample} = count for the sample

T_w = count for the distilled water sample

T_a = count for the air sample

6.3.3 Density Meter Operation Procedures

The density meter was an electrical appliance. To operate it, the power to the DMA processing unit, water bath and its circulating pump was switched on. An offset temperature setting was set on the water bath to achieve the desired temperature on the cell. Usually the offset temperature was approximately 5°C. The oscillation counter on the processing unit was set to 1k and cell-1 setting.

Before any measurement was conducted, the sampling cell needed to be cleaned. It was first rinsed with distilled water and then acetone. With the small air pump available on the remote cell, the cell was blown with air to evaporate any residual acetone remaining within the cell. A time period of approximately 5 minutes was allowed for the cell to come to thermal equilibrium with the water bath.

The cell temperature was checked to be at the same temperature as measured when the samples were taken. Air samples were injected into the sampling cell by a syringe. The count was recorded from the reading in the processing unit. The atmospheric pressure was measured using a mercury barometer located within the Mechanical Engineering Gas Turbine Laboratory. After the air samples, the distilled water and

then the experimental samples were measured. Three counts were taken for each of these fluids to avoid possible errors.

The densities of the samples were manipulated from Eq. (6.2). The densities of distilled water and air were obtained from standard tables and Eq. (6.1) respectively. The densities measured and used for the evaluation of the density profiles within the spilling plumes are presented in Table 6.1.

Table 6.1 Density values for experimental series.

Experimental Series	Ambient Density (kg/m^3)	Saline Density (kg/m^3)
SP-B01	999.13	1002.28
SP-B02	999.47	1006.2
SP-C01	999.08	1002.07
SP-C02	999.16	1005.94

6.4 POST-EXPERIMENT: IMAGE DATA PROCESSING

The flow images were captured during the experimental series and were recorded on the video tape. These images were later retrieved from the video tape and processed to obtained the data required. The phase of image processing was divided into two major parts. The first part was the flow image plots given in Appendix B, and the second part was the detail density distributions and contour plots given in Appendix C.

6.4.1 Flow Image Plots

The flow images were images grabbed directly from the video tape through the frame-grabber installed. A flow image of 100 seconds real time average was to be plotted for every section in every experimental series. The idea of having the flow image was to investigate the flow nature of the fully established balcony spill plume. The 100 seconds average flow images were considered to have compiled most of the flow features by the spilling plume generated. Since the frame-grabber could only manage

to grab a flow image of 10 seconds real time average, ten 10 seconds images were taken for averaging purpose. Before averaging these ten images, each was zeroed by subtracting from the background image. This allowed the flow image to have a net brightness as a result of the flow.

In order to obtain the dilution on the plume as in the plots given in Appendix B, the 100 seconds averaged image was calibrated with the net calibration cell image. This net cell image was the result of zeroing the initial calibration cell image from its background image. Dividing the net calibration cell image by the 100 seconds averaged flow image gave the dilution ratio.

Papps (1995) pointed out that Global Lab Image (Glab) software (1992) stored brightness data in integer form. Hence any manipulation with the brightness data in Glab would involve a built in truncation error, for instance a brightness ratio of 2.01 to 2.99 would be stored as 2. To counter this problem, he multiplied the ratio by a factor of 2 in his buoyant jet works. However, multiplication by a factor of 2 to the ratio was thought to be a crude solution to the truncation error. Hence in this spill plume work, a multiplication factor of 10 was used. This meant that for the initial ratio value of 0.1 and 1.0 were to be increased to 1 and 10 respectively. Compared to the untreated version that would store the whole range of 0.1 to 1.0 as value 1, significant details of the plume were retained.

Multiplying the ratio value by a huge factor might improve the accuracy of the flow image plots generated. However, a compromise occurred with the restriction in the grey scale available, ie 0 (black) and 255 (white). Multiplying the dilution ratio by a factor of 10 imposed a restriction to show the maximum dilution of 25 times on the image plot. This dilution range from 0 to 25 was considered good enough to represent the balcony spill plume.

After the multiplication, this manipulated flow image had its grey scale inverted. This allowed the image to be converted to a 256 colour image. The multiplication and inversion process were performed using the script files written by Papps (1995). The

conversion process from grey to colour image was performed in CorelPaint. A key palette for the multiplication factor of 10 was built and inserted along side in the flow images presented.

6.4.2 Density distributions and contour plots

The data for density distributions and contour plots given in the results section and appendices were manually collected from the ten 10 seconds average flow images. This was done in Glab using its Profile-Log function tool. By retrieving this log data and averaging the value in a spreadsheet, the truncation problem was eliminated. More discussion of this will be given later in the Discussion chapter. Profiles were taken along the x-axis, starting from the onset of the spilling plume at the balcony edge. These brightness profiles were collected at an interval of 12.5mm along the y-axis, in the direction of buoyancy forces. Profile sampling was carried out over the ten 10 seconds images to obtain the distribution and contour data. The data were then averaged to give an average flow of 100 seconds real time average.

As for the under balcony layer flow, the brightness profiles were taken along the y-axis and sampled at a 50mm interval along the balcony length in the x-axis. The brightness data on the net calibration cell image were taken accordingly along the pixels as sampled in the flow images. Having these brightness data in hand, the density data were manipulated in the spreadsheet using the Eq. (4.1) presented.

CHAPTER 7

7 EXPERIMENTAL RESULTS

In this chapter, the experimental results are presented. These results include the clear heights above the balcony with different balcony settings, the trajectory, the physical plume shape and the flow behaviours of the balcony spill plume.

7.1 CLEAR HEIGHT ABOVE BALOCNY

The clear heights above the balcony with different settings are tabulated in Table 7.1. They were measured from the flow images of 100 seconds real time average taken during the experiments. These images are presented in Appendix B. The square grids drawn on the images have a regular spacing of 25 mm both vertically and horizontally and the contrasts on the images represent the dilution on the spilling plume. The outmost contour line is an indication of dilution of 25 times the original spilling concentration. Hence the clear height tabulated can be considered as the smoke level with 4% of its original concentration from the fire compartment.

Table 7.1 Measured clear layer height on upper floor.

Experiment Series	Clear layer height at upper floor at corresponding sections. (mm)				Average clear layer height (mm)	Full scale equivalent (m)
	Centre	100mm	200mm	300mm		
SP-B01	119	119	124	124	122	2.44
SP-B02	119	124	144	144	133	2.66
SP-C01	150	144	150	144	147	2.94
SP-C02[†]	-	-	-	-	-	-

[†] Data not included due to the loss of brightness. Please refer to data errors section in Discussion chapter.

In the context of a fire scenario, the tabulated results show that spilling fluid with greater buoyancy would result a greater clear height. This suggested that the buoyancy of the smoke did play a role in determining the clear height. It was also observed that the shorter the balcony, the smaller the clear height above the balcony on the upper floor. This indicated that the clear height on the upper floor was dependant upon the geometry involved. More specifically, the clear height depended on the distance between the bounding surfaces on the upper floor that acted as shop fronts and the spilling edge. However, it should be noted that the clear layer heights tabulated in Table 7.1 above are based on the assumption that an infinite smoke reservoir was placed beyond the roofing of the upper floor. This was the analogue of discharging the spilling saline solution freely into the ambient tank as in the experimental setup.

7.2 FLOW NATURE OF THE BALCONY SPILL PLUME

The flow nature of the spilling plume was visualised using the LIF flow visualisation technique as described in the previous chapter. The directional coordinates convention used in the analysis is given in Figure 7.1.

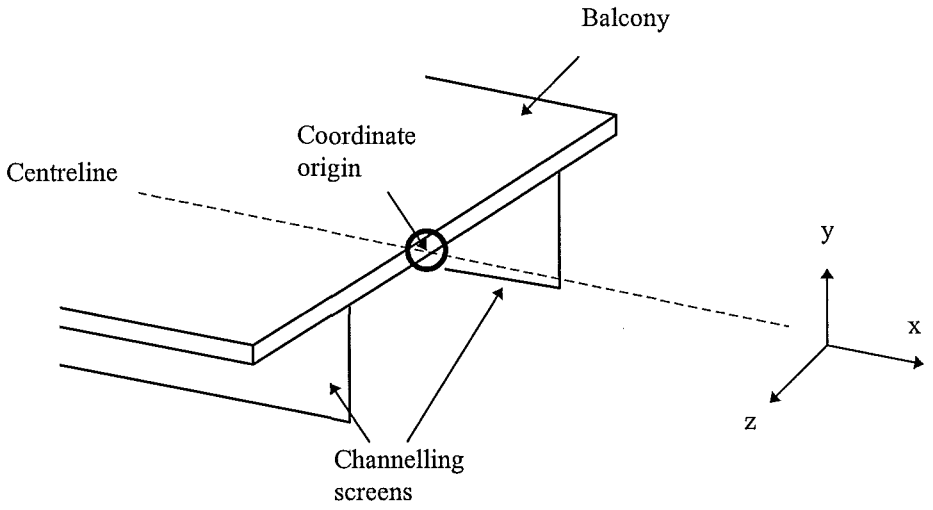

Figure 7.1 The definition for the directional coordinates convention used.

Where:

x- is in the direction parallel to the projecting balcony;

y- is vertically perpendicular to the balcony in the direction of buoyancy force;

z- is in the longitudinal direction to the breadth of the balcony.

These coordinates had their origins located at the under-face of the balcony edge as indicated in Figure 7.1.

It should be noted that the flow results are presented with the inversion of the salt water spilling direction. This would give the typical smoke flow as anticipated in the fire scenario. This is done by inverting the local y coordinates as in the salt water experiments.

7.2.1 Flow Trajectory

In this study, the flow trajectory of the spilling plume was investigated. The flow trajectory for the spilling plume is basically a curve drawn through the local concentration maxima on the centre section flow images plotted in the x-y plane. The corresponding flow parameters for the experiment are shown in Table 7.2 and results shown in Figure 7.2 and Figure 7.3.

Table 7.2 Flow parameters for experiments

Experiment Series	Froude Number†	Reynolds Number†	Layer height at balcony edge, h' (mm)	Aspect ratio‡ of layer at balcony edge W/h'
SP-B01	0.692	1666	36	7
SP-B02	0.705	1720	27.5	9
SP-C01	0.792	1705	38	6.5
SP-C02	0.834	1757	27	9.25

† These non-dimensional numbers were evaluated at the fire compartment opening. For variables and equations used in the evaluation, please refer to Appendix D.

‡ The aspect ratio is to be further discussed in Discussion (Chapter 8).

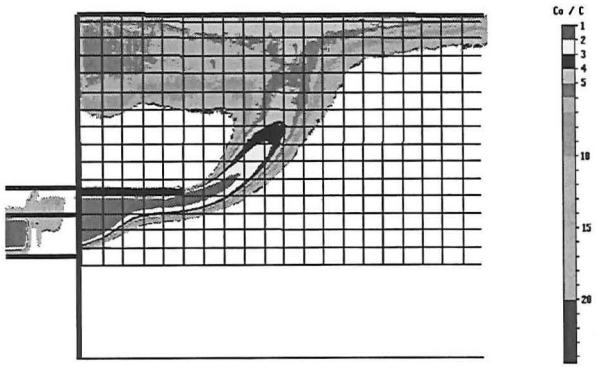

(a) SP-B01

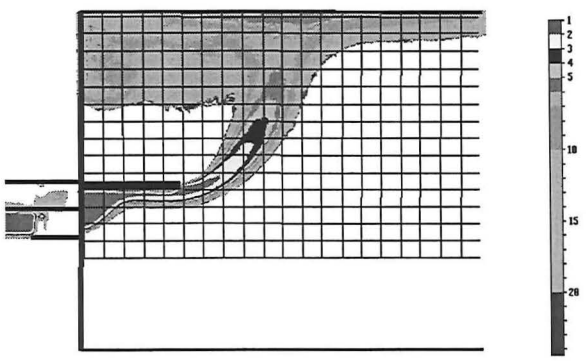

(b) SP-B02

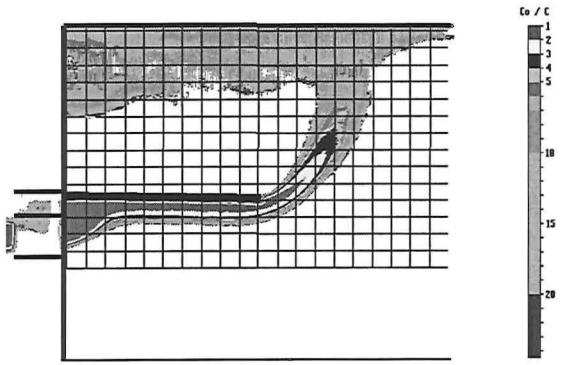

(c) SP-C01

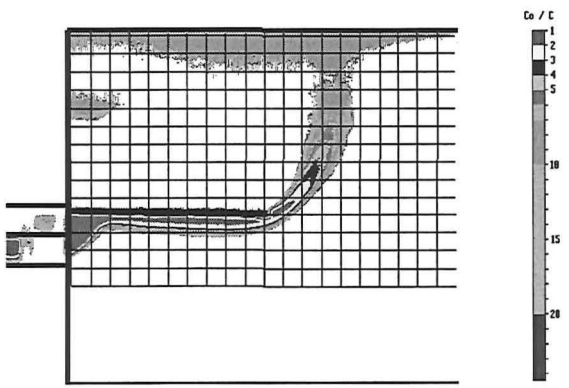

(d) SP-C02

Figure 7.2 Centre section flow image plots for experimental series SP-B01, SP-B02, SP-C01 and SP-C02.

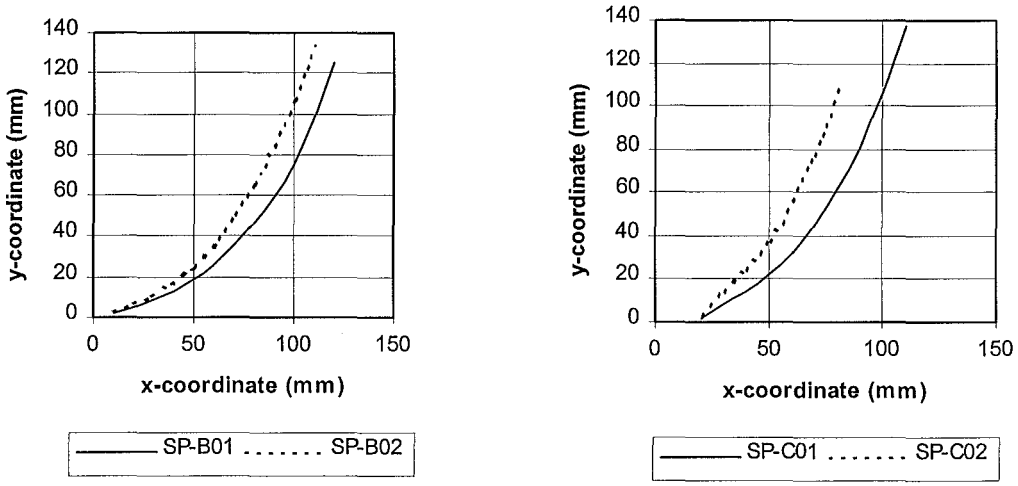

(a) Short balcony setting (125mm)

(b) Long balcony setting (250mm)

Figure 7.3 The experimental flow trajectory plots in x-y (mm) plane beyond balcony edge.

From the trajectory plots shown in Figure 7.3, the results show that the trajectories of the spilling plume have some dependence on the "aspect ratio" of the approaching flow at the balcony edge. This could be observed as SP-B02 and SP-C02 had steeper trajectories than SP-B01 and SP-C01 respectively. Both of these two sets of comparators have a ratio of approximately 3:2 in their corresponding aspect ratios evaluated at balcony edges. Apart from having larger aspect ratios, both SP-B02 and SP-C02 involved denser spilling fluids. In the fire scenario, this was not entirely surprising as one would anticipate that hotter air would possess greater buoyancy. These buoyancy forces would take immediate effect when the horizontal smoke layer passed the balcony edge dominating the horizontal momentum. This would eventually restrict the throw of the rising plume.

7.2.2 Physical Shape of Spill Plume

In this study, the physical shape of the spilling plume was studied. This investigation was able to be carried out with the possession of data across the plume sections, ie along the z-axis. Under this investigation, the major interest was on the development of the shape for the spilling plumes with rising height.

To reveal these developments, the spilling plumes had their density contours mapped in horizontal sections, ie x-z planes, at various heights of rise. The mapping of these contours were performed using *Matlab® for Windows* software, a Classroom Version 4.2c.1 (1994) available in the School of Engineering at the University of Canterbury.

Figure 7.4 and 7.5 depict the density contours in horizontal sections through the spilling plumes for all four experimental series conducted. These figures presented are for illustration purposes. For greater details and contour plots for other experimental series, please refer to Appendix C in this report.

From the x-z contour plots as shown in Figures 7.4 and 7.5, it was found that the plumes had a different development and behaviour when different spilling concentrations and balcony settings were involved.

The first observation from these contour plots reveals that these spilling plumes would not retain their initial distinctive elliptical plume shape throughout their rise. It followed that spilling plumes with lower concentrations (0.5% salt by weight in this case) could have been distorted into kidney-like shapes much faster than plumes with higher concentrations (1.0% salt by weight). The shorter balcony setting was also found to give this faster distortion compared with the longer balcony setting.

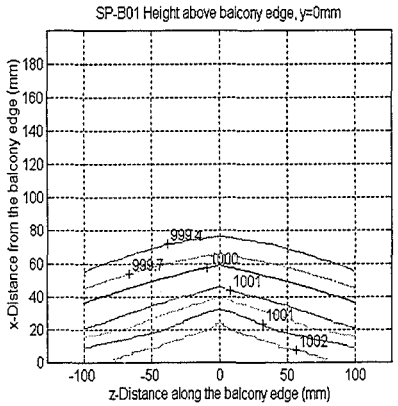

(a) SP-B01 (y=0mm)

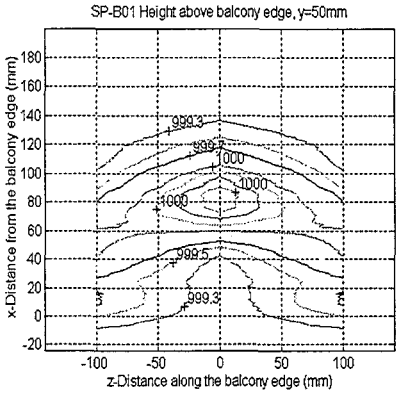

(b) SP-B01 (y=50mm)

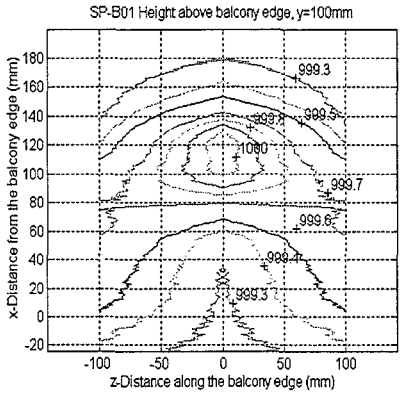

(c) SP-B01 (y=100mm)

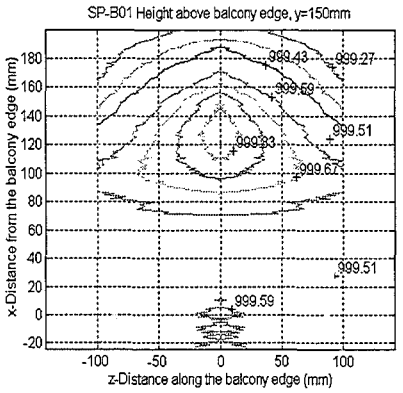

(d) SP-B01 (y=150mm)

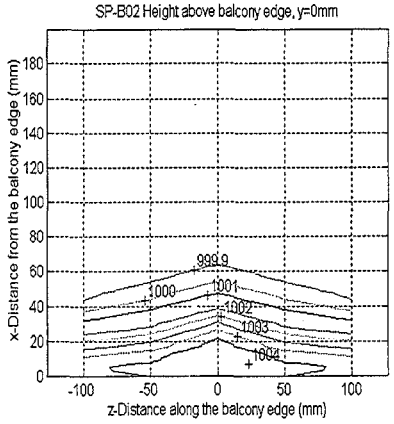

(e) SP-B02 (y=0mm)

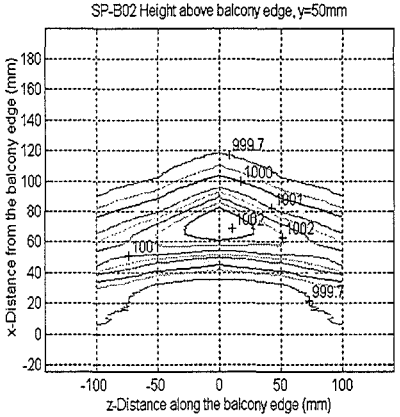

(f) SP-B02 (y=50mm)

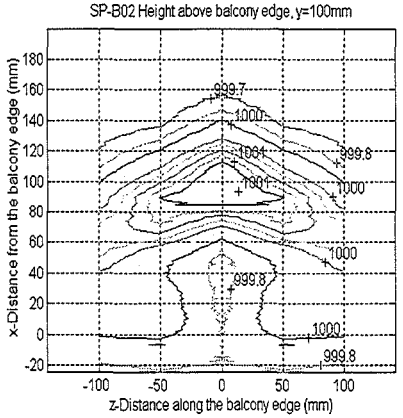

(g) SP-B02 (y=100mm)

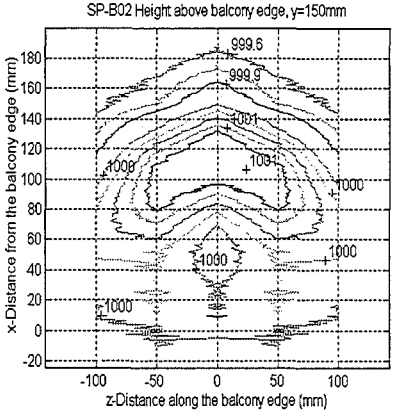

(h) SP-B02 (y=150mm)

Figure 7.4 X-Z contour plots for experimental series SP-B01 and SP-B02.

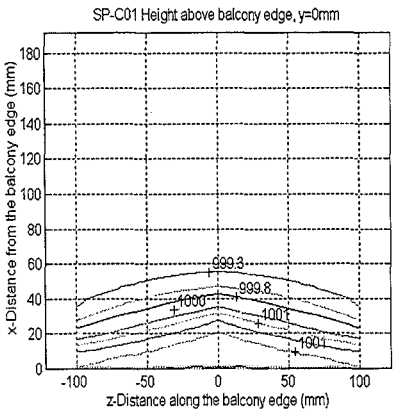

(a) SP-C01 (y=0mm)

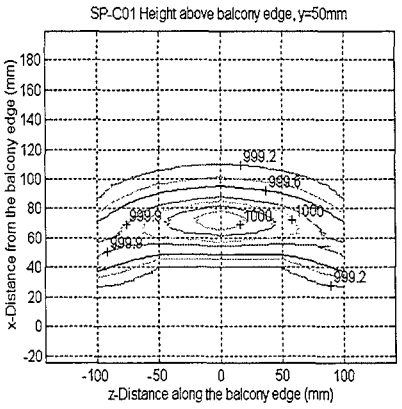

(b) SP-C01 (y=50mm)

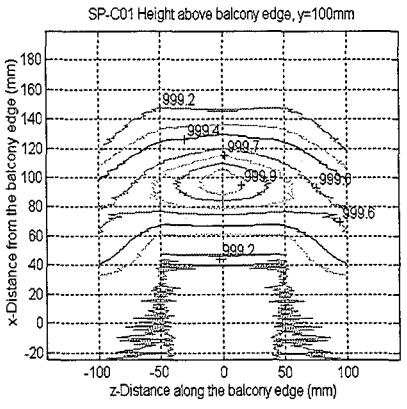

(c) SP-C01 (y=100mm)

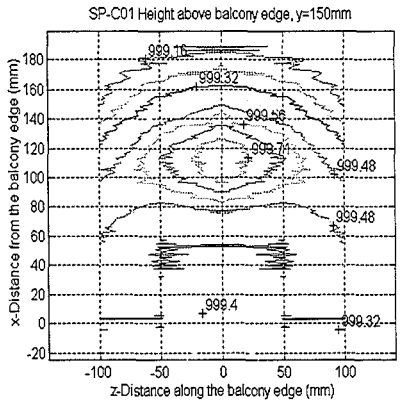

(d) SP-C01 (y=150mm)

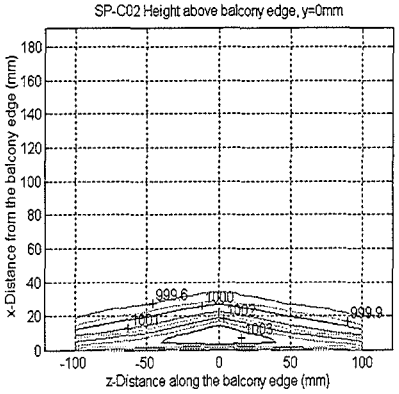

(e) SP-C02 (y=0mm)

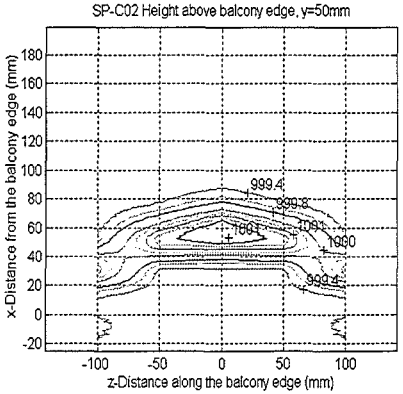

(f) SP-C02 (y=50mm)

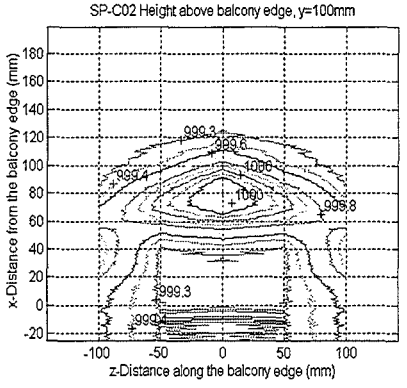

(g) SP-C02 (y=100mm)

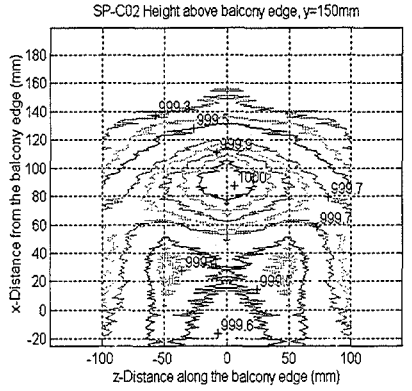

(h) SP-C02 (y=150mm)

Figure 7.5 X-Z contour plots for experimental series SP-C01 and SP-C02.

By plotting the three-dimensional density surface on the x-z coordinates, an interesting aspect regarding the density distribution was revealed. The three-dimensional density surface plot suggested that not only did density have a distribution along the x-direction as has usually been considered, it also had a distribution along the z-direction. To illustrate this, Figure 7.6 is the density distribution for experiment SP-B02 at a height of 50mm.

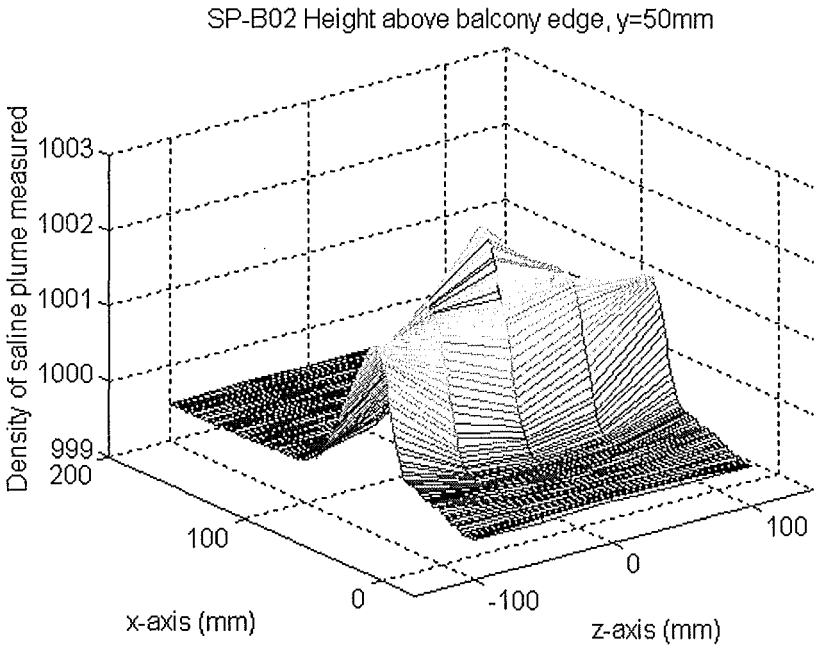

Figure 7.6 The three-dimensional density plot for experiment SP-B02 at the height of 50mm.

Since the density parameter in salt water modelling is the analogue to the temperature in the fire case, this suggests that the temperature of the spill plume has distributions along both x and z axes. Of course, these distributions will vary with different height of rise. Appendix C gives three dimensional density distributions on x-z coordinates for all the experiments performed.

It should be noted that the contour plots at height of 150mm given in the figures should not be regarded as a free plume for this model setting. This was because part of the plume that was beyond the 150mm height of rise was found to be inside the local deepening zone of the smoke layer.

7.2.3 Entrainment at Rotation Region

Figures 7.7 and 7.8 show the density distribution for the centre section of the spilling plume for experiment SP-B01. Figure 7.7 is the x-y contour plot similar to the flow image plot in Appendix B, but with density data rather than dilution data. Figure 7.8 is the three-dimensional density distribution plot on x-y coordinates. Similar plots for other experiments are shown in Appendix E.

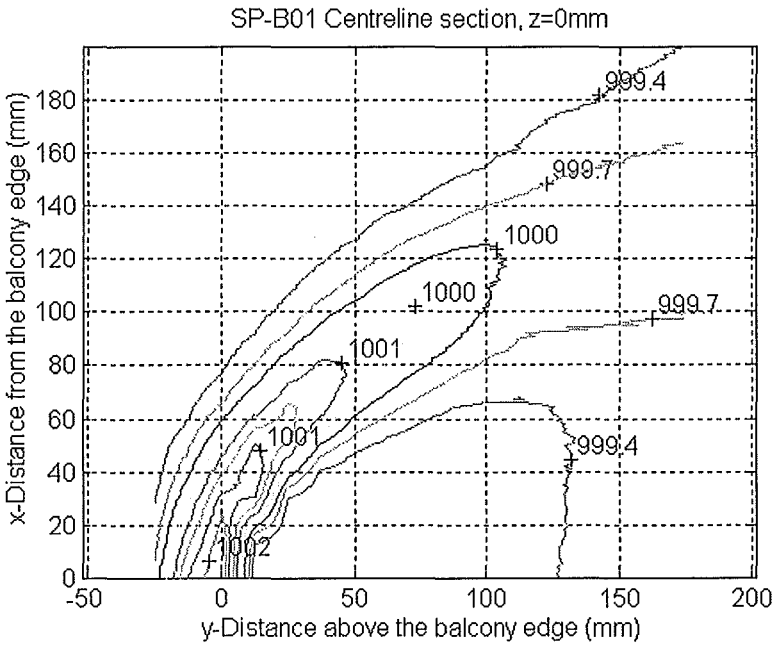

Figure 7.7 The x-y contour plot for centre section of the spilling plume in experimental series SP-B01.

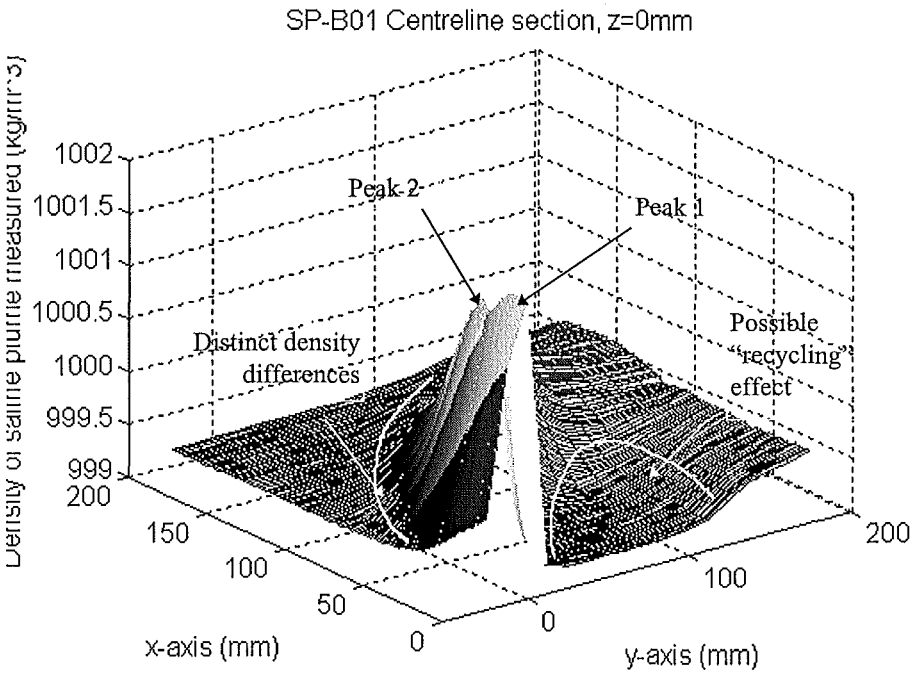

Figure 7.8 The 3-D density distribution plot for centre section of the spilling plume in experimental series SP-B01.

Figures 7.7 and 7.8 reveal an important result in the entrainment at the rotation region; a topic which has been subject to controversy through the years (Miles et al., 1996). From Figure 7.8, the two density peaks indicated in the figure as peak 1 and peak 2 can be observed. These peaks are located at and just beyond the rotation region respectively. Both density peaks have similar density values and have extremely steep surfaces. The important feature to note in this plot is the flat surface near the rotation region indicated in Figure 7.8. The significant aspect of this flat surface beside the density peaks on the three-dimensional plot is an indication of distinctive density difference (or gradient) in respect to x-y coordinates. This distinct density difference on the rotation region suggested the dilution at this area is minimal, thus low entrainment. This could also be observed from the contour plot in Figure 7.7, where the density contours stay fairly much intact while going around the rotation region. This low entrainment phenomenon was found in all of the experiments performed.

7.2.4 Gaussian distribution in x-y plane

A Gaussian distribution was certainly not achieved immediately after the turn of the spilling plume as assumed in the BRE spill plume model. An extremely distorted density distribution profile at the turn was found. It had its density peak close to the balcony edge and decreased from there. It was certainly non-Gaussian at the onset of rotation. Figure 7.9 schematically compares the typical density distribution found at the turn to a typical Gaussian distribution.

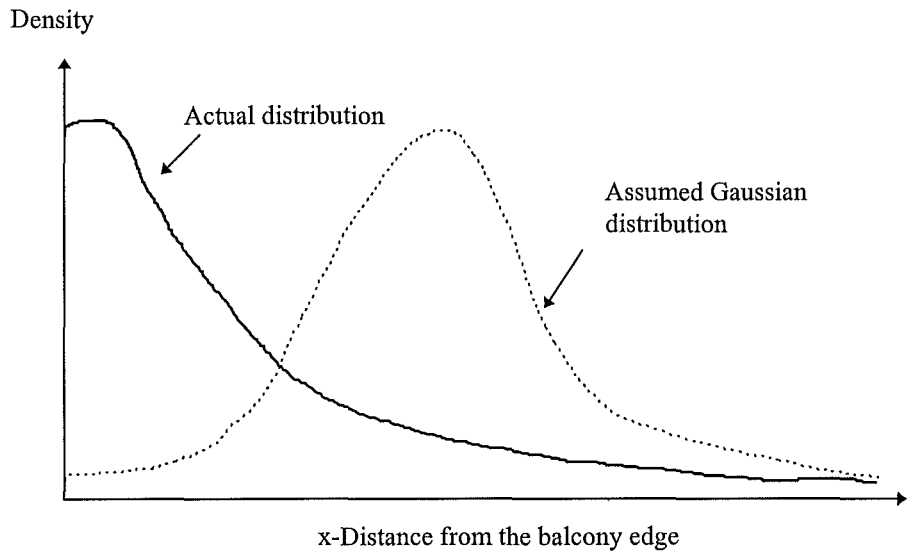

Figure 7.9 Schematic comparison between typical density distribution of spilling plume found at the turn to a typical Gaussian distribution.

In this experimental study however, the height of rise required to achieve full Gaussian distribution could not be found. This was due to the height restriction in the model and the existence of a back wall above the balcony that caused the back feeding of spilling fluid into the plume. Since the plume had been disturbed, it made the evaluation of the Gaussian distribution on the plume inappropriate.

7.2.5 The presence of soffit

In all the experiments conducted, a soffit was placed at the opening of the fire compartment. The saline flow from the fire compartment would have to flow past the soffit (fascia) before flowing onto the balcony. Figures 7.10 and 7.11 are the density

contour plots for the two different spilling fluids (0.5% and 1.0% salt by weight) flowing under the long balcony setting.

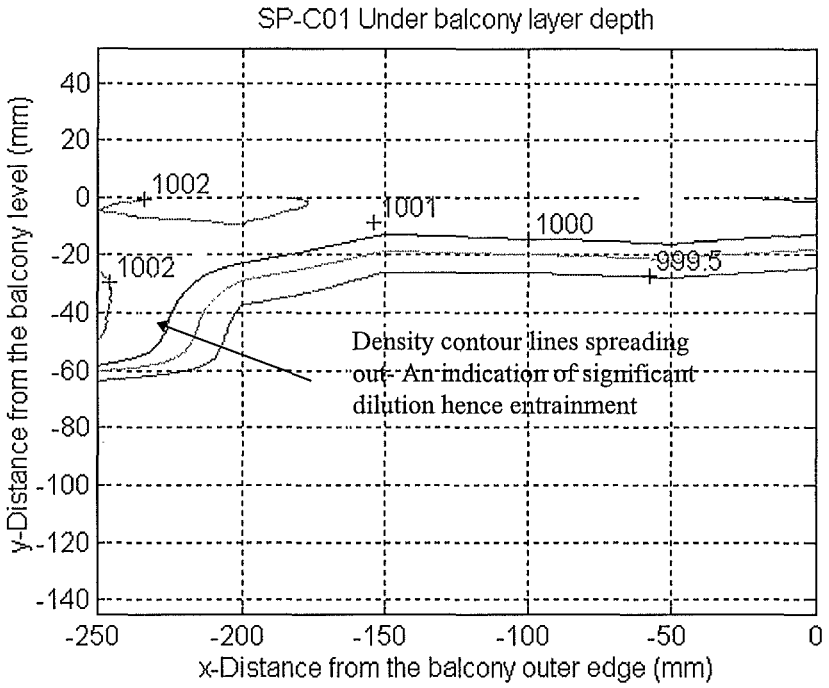

Figure 7.10 Density contour plot of under balcony layer for experimental series SP-C01 (0.5% saline solution).

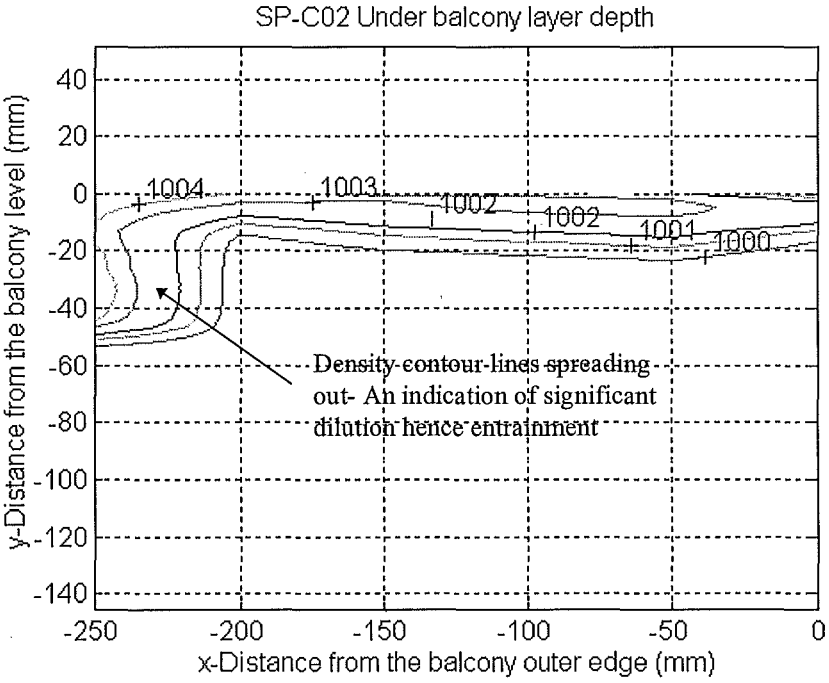

Figure 7.11 Density contour plot of under balcony layer for experimental series SP-C02 (1.0% saline solution).

Both of these contour plots show the spreading of flow density contour lines immediately after passing the fire compartment's opening (or soffit). The spread of the density contour lines is a strong indication of significant entrainment at that region which had caused the dilution of the saline layers. Beyond this entrainment region, the density contour lines along the balcony are flat and stable. This observed behaviour suggested that a significant entrainment into the saline (smoke) layer could be expected with the presence of a soffit at the fire compartment's opening.

7.3 COMMENTS ON EXPERIMENTAL RESULTS

With the nature of the salt water modelling, direct measurement of entraining mass flow rate into the spilling plumes as in fire tests using the extraction hood system cannot be achieved. It becomes unpractical to take the extraction hood idea into the tank. A lot of problems would arise such as contamination of ambient fluid, the accuracy of pumping the salt water layer from the hood inside the fresh water tank and potential plug-holing problems. The Reynolds number effect on the drag at the boundaries of the hood and the heat transfer effect are also problems. However, the extraction hood measuring method was not the only method for obtaining the entraining mass flow. There are other advanced techniques that could be used with salt water experiments such as the Particle Induced Velocimetry (PIV) technique (see Section 9.4) and hydrogen bubbles technique. These two techniques could be used to obtain the velocity of the entraining fluids into the plume and the flow velocity within the plume respectively. With these velocity data, integration over the entire plume to obtain the overall entraining mass flow is possible. In this study, only the Laser Induced Fluorescence (LIF) technique was used for investigation, and this technique would only allow the acquisition of the density data within the plume region. Without any velocity data, the quantitative study of the entrainment cannot be made. For these reasons, the experiments and hence the results focussed on the flowing features of the spilling plume than the entraining mass flow rate.

CHAPTER 8

8 DISCUSSION

8.1 SMOKE LOGGING-CLEAR HEIGHT ABOVE BALCONY

The experimental results suggested that smoke logging on the upper floor could be expected with the presence of a boundary above the balcony spilling edge. These results showed that the smoke logging depended on the dimension of the balcony setting. It was found that shorter balcony enhanced the smoke logging effect on the upper floor and hence resulted in a shallower clear height. This was due to the local deepening effect caused by the formation of the standing pool.

8.1.1 Drop Structure Analogy

The smoke logging on the upper floor was thought to be the consequence of the formation of a *standing pool*, resulting from the presence of the bounding surfaces acting as the shop fronts on the upper floor. An open channel drop structure analogy is used to explain this effect. Figure 8.1 shows the typical flow situation at the base of a free overfall in a drop structure. In fire engineering, the flow may be considered as the hot gases spilling past the balcony edge up onto the ceiling of the upper floor or the base of the longer overlapping balcony.

Discussing the flow nature of the open channel drop structure in terms of water flow, the figure shows that the jet of water from the free overfall strikes the horizontal surface at an angle. The majority of the discharge flows to the right with the remainder flowing to the left. Although the velocity in each stream changes in direction, the magnitude is retained. The water flowing towards the left (with the bounding surface) begins to fill the standing pool beneath the nappe of the jet, causing a local deepening at that region. A clockwise rotation was also generated in the pool.

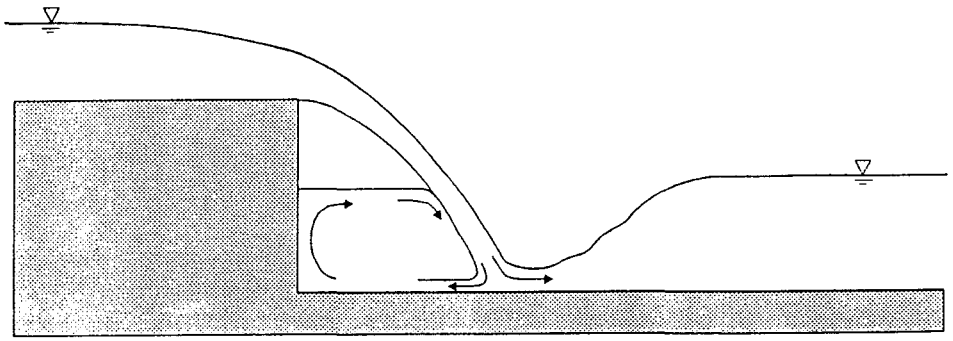

Figure 8.1[†] Typical flow situation at the base of a free overfall in a open channel drop structure.

Applying this concept to the fire scenario, it suggests that the local deepening effect observed during the experiments was caused by the formation of the standing pool. When the radial smoke flowed along the ceiling of the upper floor and hit the bounding surfaces acting as shop fronts, these bounding surfaces retarded the approaching flow. The kinetic energy of the approaching flow was converted to buoyant potential energy against the barrier as the flow was brought to a halt (Morgan and Gardner, 1990) and then possibly followed by a relatively small back flow. This results in a local deepening effect in the smoke layer similar to the formation of the standing pool with a clockwise rotation motion as described in the drop structure analogy. The results suggested that at the short balcony setting, the local deepening effect, hence smoke logging on upper floor, was much more severe than at the long balcony setting. This observation was understandable. For the short balcony, the space behind the spilling plume was smaller than the long balcony. As the spilling plumes were generated at the same flow rate, this smaller space would be "filled" up faster. This resulted in a deeper smoke layer above the balcony than would be produced otherwise.

It should be noted that the clear layer heights above the balcony presented were non-conservative. This is because the salt water modelling method is unable to simulate heat transfer, hence greater buoyancy. However, the density (temperature) parameter for the smoke layer would be conservative since no heat loss was accounted for.

[†] Figure taken from Clement (1996).

8.1.2 Application of Clear Height Results

In full scale equivalent, the results suggested that all the clear layer heights for the settings tested were recorded to have values greater than 2 meter. These values appear to comply with the recommendation made in NFPA 101 [1997, section 6-2.4.6] which requires that in a smoke-protected place of assembly, the clear height is required to be maintained at least 6 feet (~1.85 meter) above the highest walking level. However, these clear heights measured from the salt water experiments violate the recommendation made by the BRE (Morgan et al. 1990) which requires a clear height of at least 3 meter. This suggests that any overlapping boundary above the balcony's spilling edge is not a favourable geometry for the building.

Regarding the design fire for shopping mall, a 12 meter perimeter of 5 MW sprinkler controlled fire is recommended for a smoke ventilation system in a sprinklered shopping centre (Morgan and Gardner, 1990). As for the equivalent fire size being modelled in the salt water experiments, this question remained unanswered at this stage. This was because the counter flow method was used for generating the saline layer. Since the scaling equations by Steckler et al. (1986) were derived from the plume, it was inappropriate to apply these scaling equations for predicting the equivalent fire size modelled in the salt water experiments (see section 8.8). Due to this deficiency, it is not certain whether the smoke layer depths measured represent the actual consequences from the 5MW design fire.

For this reason, these clear height results collected should not be used as design reference for any design process at this stage. Further research is required to fully answer this question. Hence at the stage, a more conservative approach should still be used, by avoiding any overlapping boundary above the balcony's edge if possible. However, if this type of feature is to be retained, certain protective measures should be implemented, such as the use of a physical barrier on the upper floor or airflow to prevent the smoke-logging on the upper floor. This would help to meet the clear height recommendation and facilitate the evacuation process.

8.2 TRAJECTORY

Yokoi (1960) performed a series of small scale experiments for the study of window fire plumes. Yokoi noted that the behaviour of thermal plumes rising out of the windows had a strong dependence on the window configuration. It was found that in general, when the window is short compared to its height, the plume ejects itself considerably further before it rotates and buoyancy carries it upward. However, when the window is wide compared to its height, the thermal plume rising out of it rotates rapidly and attaches to the outside surface of the building. Similar results were found (Galae et al., 1995) using CFD modelling of window plumes.

In the results section, the aspect ratios for the four plumes involved were taken right at the balcony edges. They represented the layers' characteristics at the spilling edges. Following Yokoi's (1960) window plume studies, Yokoi defined a geometric parameter, *n*, which was the ratio of twice the width of the opening, 2W, to the height of opening, H. He used this defined aspect ratio as the parameter to investigate the trajectory of the plume formed at the window. Zukoski (1995) suggested that, because the flow of hot gas in Yokoi's experiments was controlled by a room completely involved in fire, the depth of the outflow D at the opening was about half the opening height. Hence, *n* is approximately the ratio of W/D and this is the form of the aspect ratio being applied for the spilling plumes right at the balcony edges.

The results showed that a steeper trajectory could be anticipated when the flow had a greater aspect ratio at the spilling balcony edge. This was in line with what Yokoi had found. However, no rigid conclusion could be made with only four data sets. There was also an underlying aspect of the dependence between the inside compartment's fire size to the under-balcony smoke layer's depth. Looking at the fire data from smoke flow experiments (Hansell et al., 1993), results suggested that the under-balcony smoke layer's depth was dependent on the fire size involved within the fire compartment. With a larger fire size, a greater amount of air would be entrained into the fire plume inside the fire compartment, and a deeper under-balcony smoke layer would be formed as a consequence. This suggested that the fire size might be a good

parameter to describe the behaviour for trajectory by the balcony spill plume. However, further research and tests need to be carried out to support this suggestion or to prove otherwise. The relationship between the trajectory to the layer's aspect ratio at the balcony edge was still fragile.

8.3 SIGNIFICANT OF X-Z CONTOUR PLOT

8.3.1 Distortion of plume shape

Analysing the x-z contour plots suggested that there were three possible factors that were responsible for distorting the initial plume's shape throughout the rise. These factors are listed below.

- the non-uniform velocity profiles across the balcony spilling edge;
- the entraining fluid into the spilling plumes and
- the buoyancy of the plumes.

Although the velocity profiles across the balcony spilling edge have not been measured, the flow image plots in Appendix B do suggest that the velocity profiles of the flow are unlikely to be uniform. From the flow image plots, it could be observed that the plume sections that were closer to the centre had a greater or further throw than those closer to the channelling screens. As indicated in the salt water modelling chapter, this modelling technique could not quite simulate the hot gas flow when drag effects had a weak function of Re (Steckler et al., 1986). With the presence of the channelling screens, it was suspected that the drag effect of the flow was significant hence slowing down the flows close to these boundaries. Even in CFD modelling of window plumes, these non-uniform velocity profiles were observed (Hoffmann et al., 1996).

The entrainment into the spilling plume was affected by the outer boundaries of the model involved. Since the model used had the shape of a box, for ambient fluid to be entrained into the back side of the plume, it needed to take a complicated flow path. It

was suspected that the entraining fluid into the spilling plume had to come from the front opening and then turned from the sides before being entrained into the back side of the plume. The possible flow nature of the entrainment fluid to the spilling plume is schematically sketched in Figure 8.2.

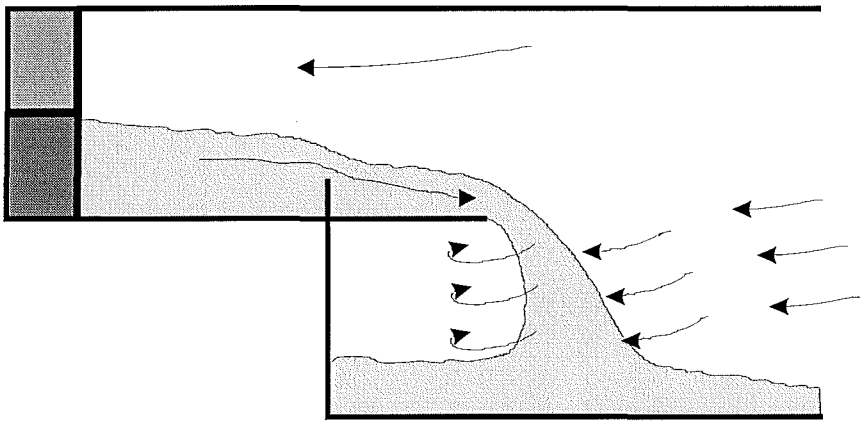

Figure 8.2 Schematic sketch of entraining fluid flow.

With this nature of the entraining fluid flow combined with slower flows close to the sides, the spilling plumes were likely to be twisted from the sides and forced into kidney-like shapes. Until a certain height, the twisted sides might be forced to merge.

The physical geometry of the balcony was found to have an influence on the nature of the entrainment fluid flow. The contour plots presented show that even at low height of rise, plumes spilling from the short balcony setting had their initial shape heavily distorted. This could be seen by comparing the two contour plots for different balcony settings as in Figure 7.4 (b) and Figure 7.5 (b). This greater distortion of plume shape in the short balcony setting was believed to be a consequence of the smaller space behind the plume. This small space did not seem to have enough ambient fluid to support the entrainment into the backside of the plume. To achieve the entrainment, ambient fluid from the front opening was introduced into the induced plume through the possible flow path as shown in Figure 8.2. Comparing this to the long balcony setting, there was greater space available behind the spilling plume and hence greater volume of ambient fluid to support the entrainment. Although greater in volume, it

might still need more of the ambient fluid from the front opening to keep the balance of the flow. However a smaller flow rate from the front opening was anticipated due to the larger "reservoir" involved. The smaller flow rate from the entrainment fluid was thought to be the key in causing less distortion to the initial elliptical plume shape.

Nevertheless, the buoyancy of the spilling plume played a role in the development of the plume shape. It is well known that cooler smoke has less buoyancy than hotter smoke. A similar situation was observed in the experiments performed. As shown in the contour plots, the 0.5% saline plumes had greater dispersion compared to 1.0% saline plume (see Figure 7.4 (b) and (f)). The reason for this was thought to be the smaller buoyancy force involved. Figure 8.3 is a schematic force vector sketch between the buoyancy forces of the spilling plume and the induced momentum forces from the entrainment fluid.

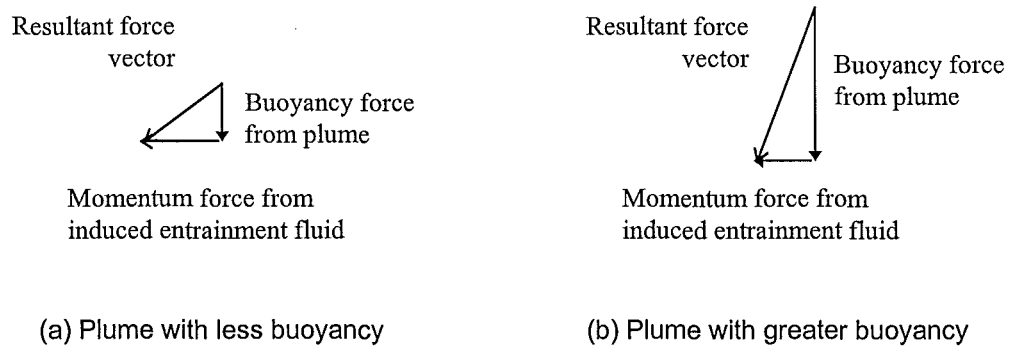

Figure 8.3 Schematic force vector sketch.

From Figure 8.3, it can be seen that for the same momentum force from the induced fluid, a plume with a smaller buoyancy force would have a relatively larger distortion in its resultant force vector. For this reason, lower density plumes and plume at greater height (ie with entrainment reducing the initial density) were more vulnerable to the entraining fluid flow hence their shape.

Hence, the distortion of the plume was considered to be the resultant of the combination effects between the non-uniform velocity profiles across the balcony

spilling edge, the entraining fluid into the spilling plumes and the buoyancy of the plumes.

8.3.2 Effects on the space behind the spilling plume

Part of the interest in the trajectory work was to observe any possible reattachment behaviour of the back wall of the balcony. For the four experiments performed, no sign of reattachment of the plumes to the back wall was observed. However the x-z plan data contour plots did shed some light in looking at the reattachment problems. Figure 8.4 shows a schematic diagram of development of the plume shape observed from the data gained.

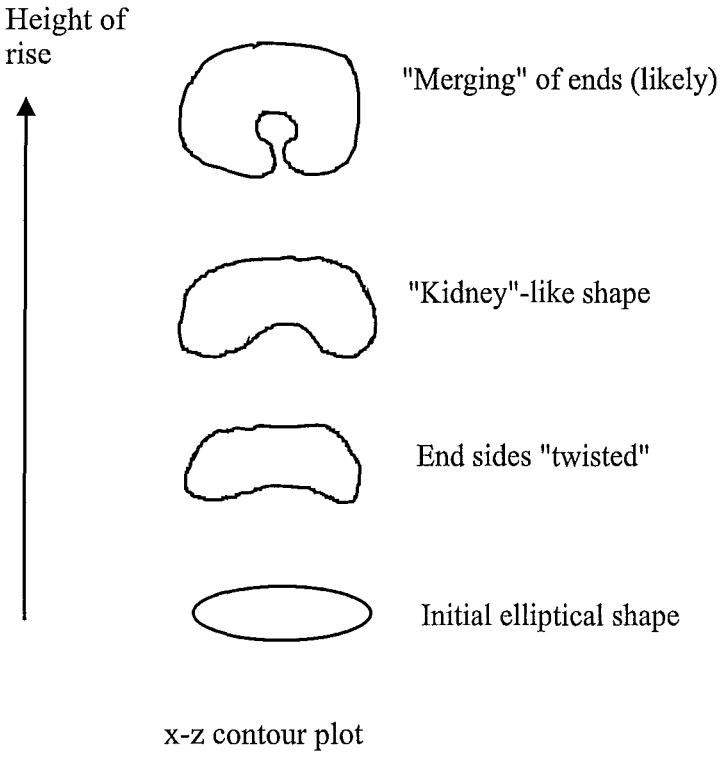

Figure 8.4 Schematic diagram on the development of plume observed in the experiment performed.

Zukoski (1995) commented that reattachment of the plume to a vertical surface above the opening can occur even in the three-dimensional situation, such as the setting in the experiment involved. He pointed out that the basic mechanism for causing reattachment of the plume to the back wall is the decrease in the static pressure at the

region between the wall and the rising plume. This pressure drop occurs when the supply ambient fluid cannot keep up with the entrainment at this region. This low-pressure region causes the plume to be dragged back toward the wall and reattachment occurs. This is known as the Coanda effect.

This comment was pretty much in line with the distortion of plume shape that was observed in the present experiments. As discussed before, the plume shape was distorted partly due to the inflow of ambient fluid feeding in from the sides of the model to the back of the plume. This inflow was stimulated from the entrainment to the plume thus the lower pressure region. Since the plume's width increases with the height of rise, the space between plume and wall decreases. This results in an even lower pressure region at the greater height. Hence more inflow is expected to be entrained into that area and as a consequence, greater distortion of the plume shape.

However, even with the short balcony setting, the region between the plume and the back wall was not small enough to cause a substantial pressure drop and thus the Coanda effect. Hansell et al. (1993) did some work looking at the possible reattachment of the smoke plume to the upper wall. They found that reattachment was likely to occur for a balcony with a breadth of 1.25m in full scale length. Comparing this full scale length (1.25m) of balcony to the one used in the experiment (2.5m), their results made a lot of sense. In their setup, they would have a space two times smaller than the one used in this salt water study, and with this small region between the rising plume and wall, a substantial Coanda effect could be produced.

It was also noticed that both Figures 7.7 and 7.8 indicate possible "recycling" of the spilling fluid. Figure 8.5 is a schematic sketch of the possible effect.

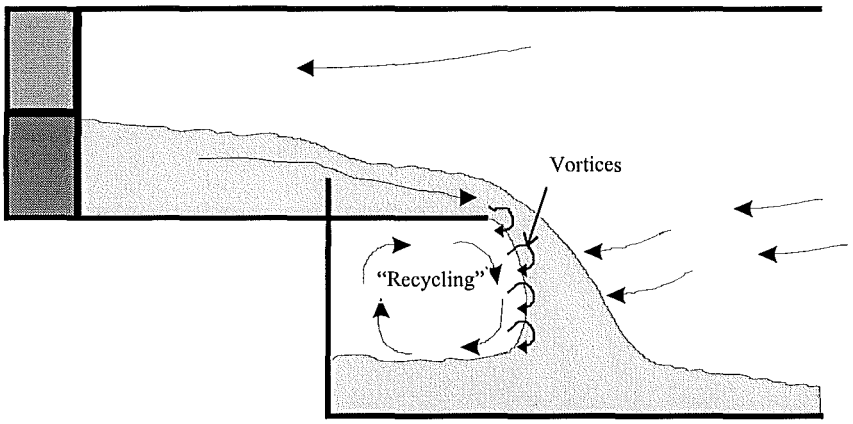

Figure 8.5 The schematic sketch of the possible "recycling" action above balcony.

This effect could be observed from the continuous flow images captured by the camera during the experiments. Vortices rotating in a clockwise direction had been observed as well. This is not a favour effect from an evacuation point of view, as smoke may be dragged back onto the evacuation path thus hindering the evacuation process. This effect was observed to be less severe for the long balcony setting.

8.3.3 Comments on the fire tests setup

In the previous discussion, it was pointed out that the distortion in the plume shape was partly due to the entraining fluid flow into the backside of the spilling plume. This particular flow nature was thought to be caused by the restriction of model geometry involved. As the model used had its sides and back sealed up with perspex sheets, ambient entraining fluid could only be introduced from the front opening of the model. The introduction of the side restrictions in this model might not seem appropriate to represent a real shopping mall. There was also a question about the appropriateness of introducing a back wall as an upper storey shop front. It was noted that no back wall was introduced in most of the fire tests carried out. Figure 8.6 shows the typical setup in most of the fire test performed to investigate the balcony spill plume. This type of setup allows the fresh air to enter the rear of the plume freely.

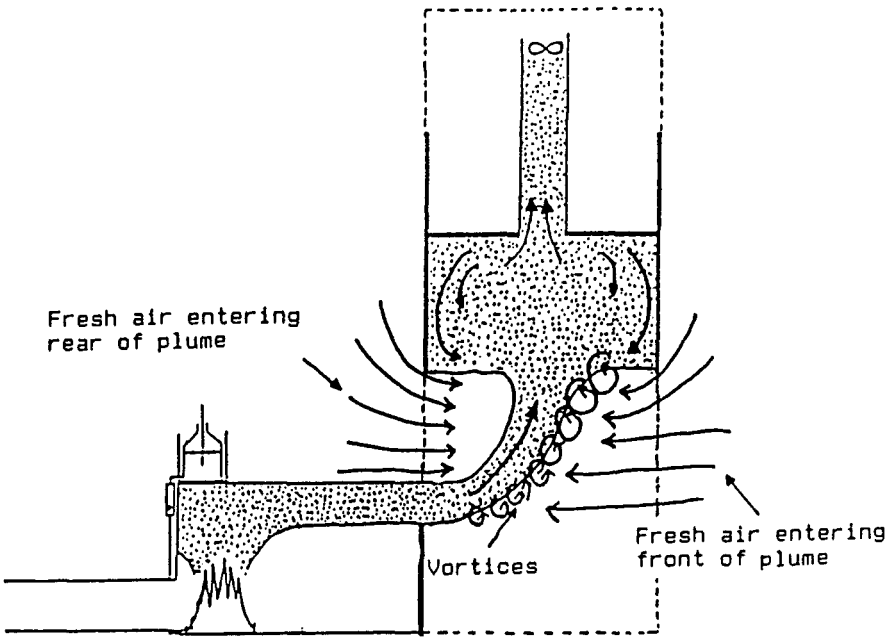

Figure 8.6[†] Typical fire test setup used to investigate the balcony spill plume.

This type of setup would be sufficient to represent the spilling plume along a relatively long balcony where the space behind the plume is large. However, for a shorter balcony setting it might not be appropriate to ignore the back wall above the balcony. This back wall would restrict the air flow into the plume at that region and possibly alter the flow nature of the entraining air into the spilling plume. The actual consequence of the presence of the back wall to the entrainment rate is unknown. It was thought that this effect would severely affect the outcome of the spilling plume for a short balcony setting and at a low height of rise, a typical geometry for a two-storey mall. However, this comment could not be justified at this stage with the lack of data available.

8.4 ENTRAINMENT AT ROTATION REGION

The salt water experiment did produce constructive results regarding the entrainment into the rotation region. Of all the experiment conducted, the results strongly

[†] Figure taken from Marshall et al (1993)

suggested minimal entrainment into the rotating region. This was indicated by distinct density difference on the three dimensional density plot as shown in Figure 7.8

This result might sound contradictory to the findings of Morgan and Marshall (1975) in their early spill plume work. They had empirically correlated an entrainment constant, α', for the flow rotating around a horizontal edge using fire data from their 1/10 scale experiments. They found that α' took a value of 0.9 compared to entrainment constant for a line plume, α, which had a value of 0.16. This α' was later updated by Morgan and Hansell (1987) in their atria study and modified to a value of 1.1. Morgan and Marshall suggested that greater vorticity was anticipated for gas stream rotating around the corner than in the rising plume. The high α' value was hence treated as a "justification" for high entrainment at the rotation region.

Considering the approach taken by Morgan and Marshall (1975) in developing their spill plume model, their high entrainment constant on the rotation region was bounded to the assumption that they had made. Morgan and Marshall based their original analysis upon the weak line plume theory developed by Lee and Emmons (1961). They used this theory to describe the degree of air entrained into the plume, and they assumed the plume to originate from a virtual source at the balcony level. This meant that this source had to absorb all the properties of air entrainment into the region between the horizontal, under-balcony layer and the vertical plume. Their analysis thus assumed a self-similar vertical flow with a entrainment constant α, of 0.16 and Gaussian velocity and profile. Under this approach, in order to fit their data, a very high degree of air entrainment into the rotation region had to be assumed, a value of α'=1.1 as shown above.

The small entrainment found in this study however was in line with the current research findings on this topic. As described in the literature review chapter, the non-dimensional analysis performed by Thomas et al. (1996) and Poreh et al. (1997) both suggested small entrainment into the rotating region. A similar result was obtained through CFD modelling by Miles et al. (1996). The present experimental results thus

verified the non-experimental findings and confirmed the belief of a small degree of entrainment into the rotation region of the spilling plume.

8.5 DENSITY DISTRIBUTION ALONG Z-AXIS

The findings of this investigation were fairly substantial as they posed a challenge to the line plume theory as developed by Lee and Emmons(1961) and adopted by Morgan and Marshall (1975) in their spill plume model. One of the assumption made in the line plume theory is that the finite length of the line has to be long enough to eventually eliminate the possible distribution along the z-axis. With a small variation on the distribution along the z-axis, it could be well regarded as uniformly distributed along the line. However for the case where the shop has a narrow front, ie "short line plume", the validity of the assumption in the theory and the application of the model would be seriously challenged. A greater calculation error was anticipated due to the violation of the assumption.

These results provide certain supportive evidence to the discussion made by Hansell et al. (1993) on the temperature restriction on balcony spill plume model. They showed the limitation in temperature for double sided free plumes to be adequately described by the existing Gaussian model being dependent on the opening width involved. Beyond the limiting temperature, the model becomes unreliable. The limitations are tabulated in Table 8.1 below.

Table 8.1 Limitation on double sided plume for BRE spill plume model.

Opening Width (full scale equivalent)	Limiting Temperature
4-5m	250°C
7m	330°C

From Table 8.1, it can be seen that for a smaller opening width, the smaller the limiting temperature. Relating to the salt water results, the temperature limitations are

thought to be sensible. For higher temperature involved, the temperature distribution along the z-axis could not be regarded as a near uniform distribution. This would eventually violate the line plume theory and loss of accuracy is thus anticipated. By having a smaller limiting temperature on a small opening width, this would keep the model within the bound of assumption to a certain degree. It should be noted that the temperature distribution along the z-axis might be one of many factors that affect the limiting temperatures and other factors need to be investigated.

8.6 UNDER BALCONY LAYER FLOW

Morgan and Hansell (1987) in the discussion of the entrainment due to a balcony pointed out that there was additional entrainment of air into the gases while flowing pass any soffit presented at the opening. Figure 8.7 below is extracted from Morgan and Hansell's (1987) article which schematically shows the additional entrainment involved.

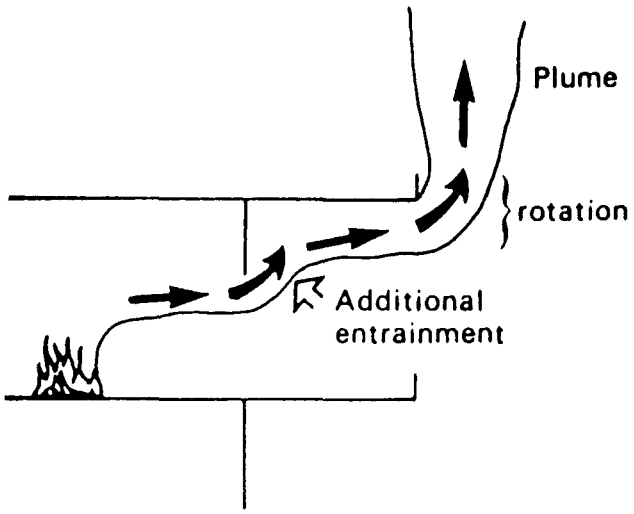

Figure 8.7[†] Schematic diagram showing the additional entrainment due to the presence of soffit at the fire compartment opening.

[†] Figure taken from Morgan and Hansell (1987).

They suggested that this entrainment was due to the turbulence close to the region of impingement on the balcony. They claimed that there would be no additional entrainment in the absence of a soffit.

The results obtained did show that significant entrainment had occurred as the flow turned around the soffit onto the balcony, a common behaviour of a rearward facing step flow. These results supported Morgan and Hansell's (1987) claim that there would be additional entrainment in the presence of a soffit. In their article, they pointed out that this additional entrainment into the under-balcony smoke layer should be accounted for while using the spill plume model. They referred to Marshall's (1984) works on this topic and suggested that the under-balcony mass flow rate, M_W at the opening (calculated using the method described in the spill plume model), should be doubled for this combination of soffit and horizontal projection. This would give a new modified mass flow rate at the outer edge.

Marshall (1984) had shown that this additional entrainment, when expressed as a percentage of the mass flow leaving the compartment, varies from 73% (±19%) for a 7m wide compartment opening and 7m channelling screen spacing (ie 7m outer edge) to about 150% for a 14m wide outer edge and the same compartment opening. Regarding this aspect, the flow image plots for the long balcony setting did show that the dilution ratio at the balcony edge was roughly between 2 and 3. In this respect, the result did show reasonable agreement with what Marshall had obtained. Having stated that, it was not entirely appropriate to compare these results as Marshall (1984) suggested that the degree of entrainment varies with the precise geometry involved. However significant entrainment into the flow by soffit was convincing.

8.7 POTENTIAL ERRORS ON DATA COLLECTED

It should be noted that data for experimental series SP-C01 and SP-C02 encountered some errors at the height beyond 150mm from balcony level. It had been observed that there was a dark band occurring on this region during the experiments involved.

Figure 8.8 below shows the dark band on the calibration cell for experimental series SP-C02.

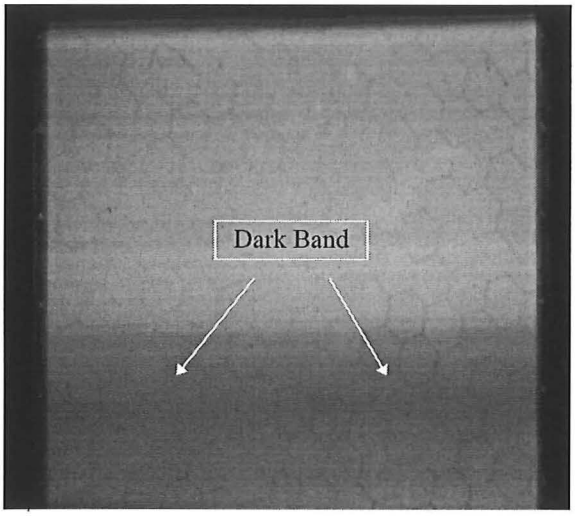

Figure 8.8 Calibration cell image for experimental series SP-C02.

The LIF technique used was highly dependent on brightness ratio data to accurately predict the corresponding density distributions within the plume. The low brightness simply meant a loss of accuracy in the data collected as this reduced the sensitivity for the camera to pick up brightness changes within that region. Apart from that, the high dilution region of the plume was simply missed out. However, the data around the balcony level were considered to be good as they had good brightness. As for experimental series SP-B01 and SP-B02, no dark band problem was observed. Hence, these data were treated as reliable.

Regarding this dark band problem, it was later found that this was caused by the slipping of a reflection mirror in the laser setup. The slip in the reflecting mirror resulted in a loss of alignment of the incoming laser to the rotating mirror. This was the cause of the dark band. However, the cure for this problem was only found after the entire experimental programme was finished.

8.8 CONVERSION OF SALT WATER RESULTS

8.8.1 Equivalent Fire Size

Regarding the conversion from the salt water experiment to the equivalent fire scenario, unfortunately this was unsuccessful. The major reason for the unsuccessful conversion was the different experimental setup involved. As described before, the experiment performed had the saline solution injected as a layer rather than a plume. Since the scaling equations by Steckler et al. (1986) were derived upon the plume, this made the conversion inappropriate. Hence this left the question of the equivalent fire size that generated the equivalent smoke flow from the fire compartment and onward unanswered.

Under this experimental setup, there was also a question about the placement of the fire plume within the fire compartment. It might appear that there were several fire sizes on different placements which would generate smoke layers having identical Froude numbers at the opening as obtained in the salt water experiment. A proposal for investigating this topic using zone modelling has been made, however no investigation has been carried out yet.

8.8.2 Further comment on the scaling equations

From the previous discussion of the salt water scaling equations, one could see the crudeness in the Reynolds number matching. Steckler et al (1986) reported that in their reduced scale salt water experiments, their plumes had Reynolds numbers in the order of $\sim 10^4$ compared to the real turbulent fire having Re of $\sim 10^5$. They claimed that turbulent plumes do exist for Re down to $\sim 10^4$. Hence an allowance on Re had to be made while evaluating the velocity scale for the hot gases when using Eq.(3.14). For this reason, the Reynolds number does not seem to be a good flow parameter to be used as the "link" between the salt water and real fire scenario. Regarding the experimental setup applied in this spill plume study, the Froude number at the fire compartment opening was considered as another possible alternative flow parameter to

be use as the "link". However further work is needed to justify this idea or proven otherwise.

8.8.3 Comment on drag effect

Regarding the possible intensifying drag effects by the channelling screens, nothing much could be done to eliminate this problem as it was a nature of the salt water modelling. Although the drag effect might cause possible disturbances to the saline plume generated, this was the compromise that one had to make while using this modelling technique. However, it is left for future researchers to determine the operating specifications for the salt water modelling to minimise drag effects. A possible way of quantifying this might be to compare the trajectories on different sections with CFD results. This again would depend on the "link" between the salt water modelling to the real fire scenario which has yet to be established.

8.8.4 Final comment

Although the scaling of salt water results to fire results could not be performed, the method for injecting the saline layer was still considered to be the preferable option. This was because the injection of plume would further complicate the situation while trying to meet the source geometry criterion and the contradiction between the momentum and Reynolds number criteria. Using the injection of the saline layer allows the situation to be simplified. The problems associated with source geometry, momentum and turbulent criteria by the injecting plume were eliminated. Hence, it was anticipated that better and more accurate scaling equations might be derived upon this setup. Again, further research on this area is needed.

CHAPTER 9

9 FEASIBILITY STUDY OF SALT WATER MODELLING USING LIF TECHNIQUE

In this chapter, the value of using LIF technique is discussed and potential errors that were likely to be encountered are presented.

9.1 REPEATIBILITY

Repeatibility is an important issue with regard to generating the spilling plume and to the data recorded using the LIF method. The repeatibility of using the LIF technique to record density data from salt water plume had been performed by Papps (1995) and Gaskin (1995). They had suggested specifications on the dye concentration used, the speed of the laser rotating mirror and the dark background behind the plume to achieve good and repeatable results. In this experimental study, the equipment operations and dye preparation followed the recommendations made. The dark background of the plume was achieved by placing a black powder-coated metal sheet behind the spilling plume. Since these criteria had been followed, good data were expected.

However, the repeatability in generating an exactly identical spilling plume was thought to be difficult. First, it depended on the preciseness of mixing the saline solution to achieve identical density. Secondly, the injection of saline flow rate was bounded by the mechanical devices involved. The saline flow rate into the model was controlled through the control valve on the booster pump. Fluctuation of the injection flow rates had been observed during the experiments. Also, since the saline solution was stored on the header tank on the second floor, a pressure drop in these tanks during experimental runs would cause a decrease in injection rate. To compensate for this head loss, the control valve on the booster pump needed to be opened a little bit more. Indeed, routine patrol and monitoring of the injection rate via the electro-magnetic

flow meter ensuring the saline was injected at the required rate had been done in all the experimental series.

Figure 9.1 below compares the density profiles obtained from two separate experimental series SP-C02 and SP-D01, both with the same long balcony setting (250mm) with 1.0% initial saline solution. Similar profiles can be observed. Although there were slight differences in initial saline and ambient fluid densities (both dependent on the temperatures) between these two comparatives, given the randomness involved in the flows, the repeatability was convincing.

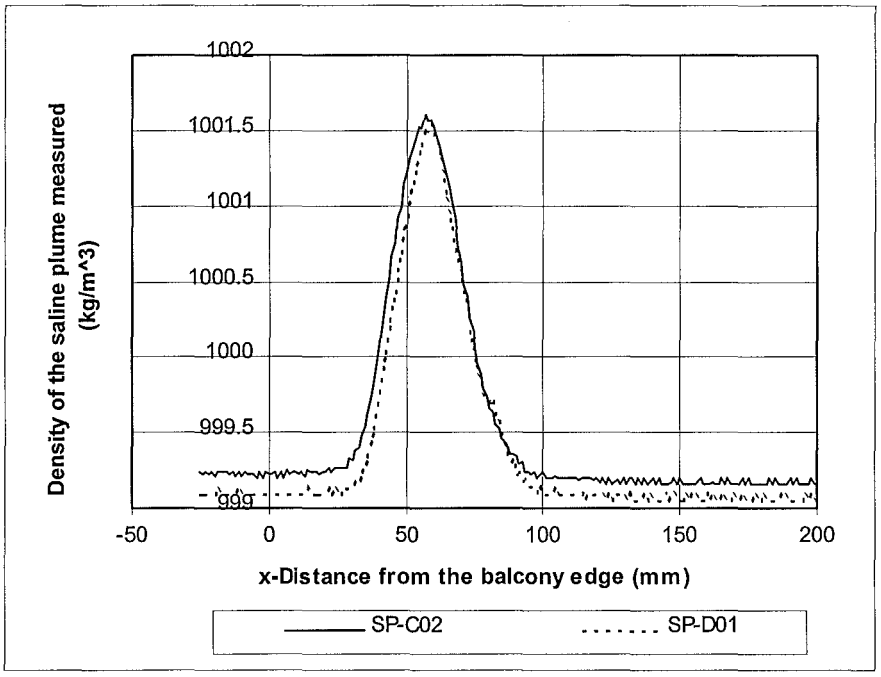

Figure 9.1 Comparison of profiles taken at y=50mm between experimental series SP-C02 and SP-D01.

9.2 DATA ACQUIRED

Using the LIF technique allows detail density data within the plume region to be collected. It allows good visualisation on the flow nature of the plume. With the detail density data collected, a lot of the flow issues associated with the balcony spill plumes could be investigated. This in the salt water modelling point of view is excellent as

density data from salt water testing is analogous to the temperature data in the real fire scenario. However, this still relies on the conversion equations to be developed before the full potential of the density data collected using LIF technique can be fully utilised and justified.

9.3 COMMENT ON GLOBAL LAB IMAGE SOFTWARE

Global Lab Image (Glab) (1992) software had been used to produce the flow image plots as shown in Appendix A. As indicated before, the frame-grabber board could only manage to produce an image with maximum 10 seconds real time average. In this spill plume study, since the major interest was on the fully established plume rather than on instantaneous development of plume, a flow image of 100 seconds real time average was needed. This type of flow image would compile most of the flow characteristics of the fully established plume.

To obtain these 100 seconds real time average flow images, the Arithmetic tool in Glab software was used. The "Xfer" command was used to multiply a gain factor of 0.1 onto the ten images each of 10 seconds real time average. Summing these ten images with modified brightness gain would give flow image of 100 seconds real time average as given in Eq. (9.2). This is illustrated below.

$$F_{100\ \text{sec average}} = (F1_{10\ \text{sec av}} + F2_{10\ \text{sec av}} + \ldots + F10_{10\ \text{sec av}}) / 10 \qquad (9.1)$$

or

$$F_{100\ \text{sec average}} = 0.1*F1_{10\ \text{sec av}} + 0.1*F2_{10\ \text{sec av}} + \ldots + 0.1*F10_{10\ \text{sec av}} \qquad (9.2)$$

Papps (1995) pointed out that the major drawback of using the Arithmetic tool in Glab was the truncation that was built in with the software. This meant that the software only handled integers rather than real numbers. For example, an average brightness value of 2.01 to 2.99 would be stored as 2. This was unavoidable on the flow image plots. However with the multiplication of 10 as described before (see Section 6.4.1), certain accuracy was retained.

A better accuracy on the brightness data hence density data could be retained by a *manual averaging* method. This is by taking the brightness data profiles from each of the 10 images on the same pixels and averaging them in a spreadsheet. By doing this, the integer brightness data from the images would be stored as their original values. Averaging them in spreadsheet would allow the averaged brightness data be stored as real numbers rather than integers as in the Glab. This method is basically in the form as in Eq. (9.1) with the manipulations performed in the spreadsheet. This would improve the accuracy in predicting the corresponding density profiles significantly. These procedures were performed to get accurate density results for plotting all the contours as in the results section and appendices. Figure 9.2 compares the density results manipulated from the brightness data obtained from Glab's 100 seconds time average image and the ten 10 seconds images using the manual averaging method.

From the graphs shown in Figure 9.2, a definite difference can be seen as the Glab's time average images produce lower density ("darker") profiles. This is not a surprise for the truncation error involved. The loss of accuracy in the Glab average increases with the height of the spilling plume. The reason for this is that the plume at a greater height is greatly diluted and hence low brightness data integers. With the truncation of these small value integers, the overall percentage errors are tremendous. This could be realised from Figure 9.2 (d). Thus, the manual averaging method was the preferable method to obtain the density data from the flow images taken during the experiments.

9.4 COMMENTS ON SALT WATER MODELLING

As discussed in the previous chapter, although applying salt water modelling with LIF technique allowed good visualisation of the flow, the conversion from the salt water data to fire data was unsuccessful. For this reason, the salt water data sets were under-used. This unsuccessful conversion has been the major obstacle in limiting the potential use of the data collected at this stage.

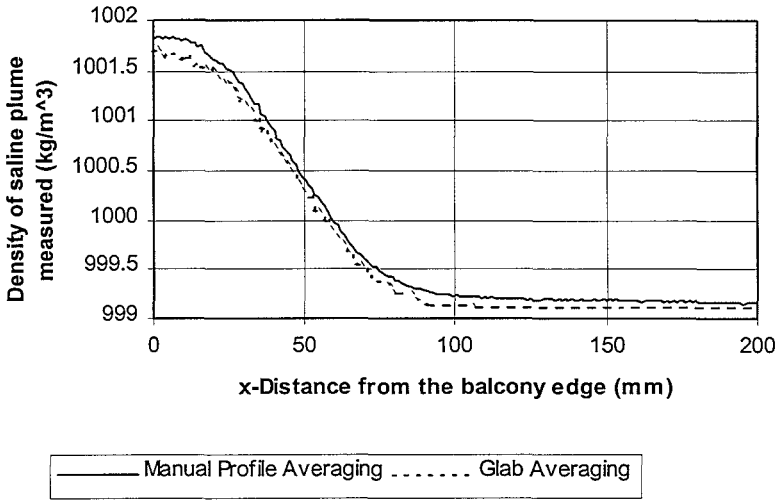

(a) At height of y=0mm

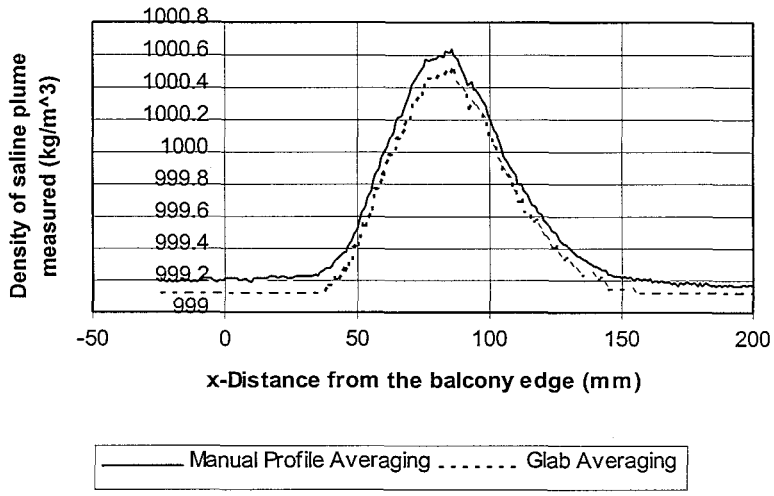

(b) At height of y=50mm

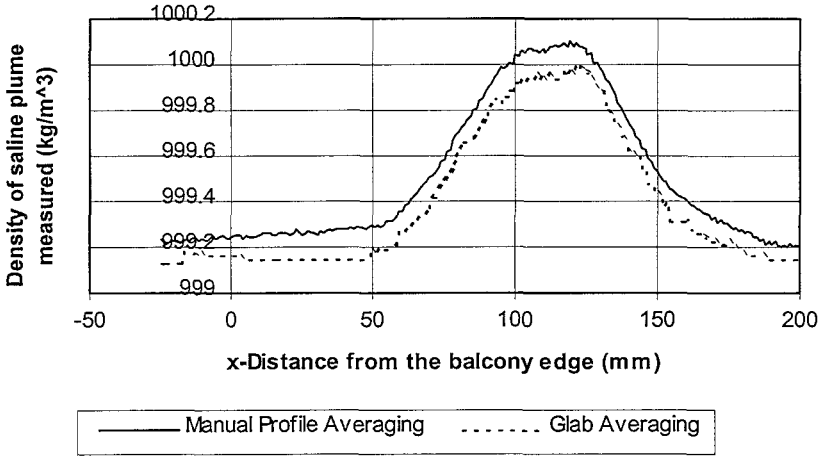

(c) At height of y=100mm

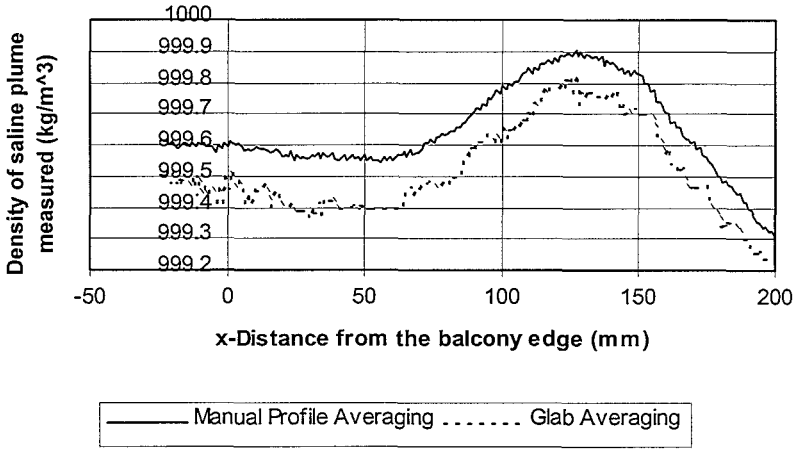

(d) At height of y=150mm

Figure 9.2 Comparison of density results obtained using Manual Profile Averaging and Glab Averaging methods in experimental series SP-B01.

However, the salt water modelling could provide good flow visualisation. With the LIF technique, it could provide experimental data to verify the flow aspects assumed in the derivation of correlations or mathematical models. It is also a relatively inexpensive and easy technique to obtain the smoke flow behaviours compared to the use of conventional smoke flow visualisation techniques. These techniques include carbon dioxide smoke generator and titanium chloride for tracing the smoke behaviours in small scale fire tests. Recently, helium gas has been used as an alternative buoyant source to heated air for studying the flow of gases within small scale models (Marshall and Harrison, 1996). This new method is claimed to give good flow visualisation. However, the main disadvantage of using the Helium is that it is costly.

Also, with the increasing interest in the CFD (Computational Fluids Dynamic) modelling, salt water data could be used as a qualitative comparator to these CFD results. For instance, the density contours within the plume could be qualitatively compared to the temperature contours as obtained from the CFD results.

Looking through Papps (1995) and Gaskin (1995) buoyant jet works, it seems that another measuring technique, known as Particle Induced Velocimetry (PIV) could be used in conjunction with the salt water modelling. This method would allow both qualitative and quantitative data to be obtained. It involves seeding the ambient fluid with particles which are neutrally suspended within the ambient fluid. With the introduction of the saline plume, these particles would move with the entrainment fluid towards the plume. Their movement would be traced and later retrieved as a velocity vector diagram. This would allow the study of the effective entrainment coefficient, α, on line plumes. Thus, justifying the recent claim of lower α figure of 0.11 (Thomas et al., 1996) than 0.16 found by Lee and Emmons (1961).

Having this experimental velocity vector diagram would be valuable as it could be used as a comparative experimental reference to the velocity flow vectors field obtained from CFD modelling. Cross validation between the results from these two modelling techniques will allow the revision of the physics of the CFD simulations as

well as discovering modifications to Froude number scaling that would account for some of the thermal effects not present in the salt water experiments.

9.5 SUMMARY

The literature survey on salt water modelling shows that direct measurement of entraining mass flow rate into the smoke layer by applying the extraction hood system cannot be achieved. This is bounded by practicality involved in the experimental setup. However, experimental results show that good flow visualisation is readily achieved using the LIF technique. Good quality results can be obtained and the experiments are repeatable. This technique is significantly cheaper and more accurate for observing the smoke behaviour than using the carbon dioxide or titanium chloride to trace the smoke movement in small scale fire tests. The salt water data could also serve as a useful comparator to the CFD modelling qualitatively. The salt water results appears to be under-used at this stage with the scaling equations yet to be developed in the future.

CHAPTER 10

10 CONCLUSIONS

The study showed that the LIF (Laser Induced Fluorescence) technique was a good method to investigate and validate the flow aspects that have been assumed or derived from theoretical models or correlations. It was a relatively inexpensive way to obtain relatively good flow data compared to fire tests (full or small scale) and CFD (Computational Fluids Dynamics) modelling.

The density data collected at the rotation region of the spilling plume showed a small degree of dilution, thus entrainment into that region. These results provide experimental verification for recent theoretical claims about the small degree of entrainment at the rotational region.

The behaviour of the under-balcony flow layer was revealed from the density contour plots. It was found that the presence of the soffit at the opening resulted in significant entrainment into the under-balcony layer, a common behaviour of a rearward facing step flow.

A higher density spilling plume was found to create a greater density distribution along the width of the balcony spill plume.

The smoke logging aspect above the balcony was also investigated. The results showed that the clear heights above the balcony were all greater than 2 meters in full scale equivalent. It was found that a shorter balcony would cause a more severe smoke logging effect on the upper floor, thus reducing the clear height, due to local deepening effects. Although these results satisfied the recommendation by NFPA 101 (1997) of a clear height of 6 feet (~1.85 meter) above the upper most level for life safety purpose, there are still many questions regarding salt water scaling. Therefore practical application of these results is not advised at this time. Hence, any overlapping

boundaries above balconies' edges should be avoided if possible, preferably with the balcony edge protruding into the smoke reservoir allocated. This would prevent any smoke-logging effect on the upper floor which might hinder any evacuation process. However, if this type of geometry is unavoidable, physical barriers such as smoke curtains or airflow should be employed to prevent any smoke logging on the upper floor.

The main advantage of using the salt water modelling technique is the ease in modifying the geometry of the model and testing conditions. Any modification would not result in a lot of changes to the data acquisition systems as in the fire tests. This method would also produce an insight into the appropriate placement of measuring devices such as thermal-couples and bi-directional velocity probes if either full or small scale fire tests are to be conducted.

For the physical model used, it was found its box-shape atrium might have introduced certain disturbances to the physical shape of the spilling plumes. Regarding the counter pumping method used to simulate the counter flows at the doorway of the fire compartment, the results were repeatable. With LIF technique, good flow visualisation was achievable. Further research is required before salt water results can be scaled to predict actual fire generated spill plumes.

For the study presented here, only the flow features of the balcony spill plume were revealed. This was because the Laser Induced Fluorescence (LIF) technique was the only method used for investigation in this study. Since no velocity data were collected, no comments could be made upon the entraining mass flow of the spilling plume. There are other advance techniques available such as the Particle Induced Velocimetery (PIV) technique and Hydrogen Bubble technique that could be employed for studying the entraining mass flow into the plume in the future.

CHAPTER 11

11 RECOMMENDATIONS

Salt water modelling technique provides an opportunity to refine or validate any mathematical model developed for the balcony spill plume experimentally.

It is recommended that the counter action pumping method, ie the injection of saline layer, be retained for future tests. Further research upon the scaling equations is needed.

The physical model may need to be modified as well. Since its box-shape atrium may cause distortion of the plume shape, it is recommended that the model to have its sides stripped away, leaving only the back wall. The roof of the model atrium may also be removed to allow a longer flow distance for the spill plume. With these modifications, reattachment of the spilling plume can be investigated in more detail.

To achieve these investigations, the LIF technique is still useful for its good flow visualisation. There are other techniques such as hydrogen bubbles technique that could be used to measured the velocity inside the plume region. The PIV (Particle Induced Velocimetry) technique that could be used to traced the entraining ambient fluids into the plume. With these combinations of techniques, flow aspects such as entraining constant, height to establish Gaussian distribution within the plume and other aspects could be investigated.

With the possession of these data, a few small scale fire tests could then be performed and compared with these salt water results. CFD modelling of the salt water modelling conditions could also serve as a useful comparator. If turbulence aspects need to be investigated a LES (Large Eddy Simulation) could be performed.

Below is a summary task list that might be carried out in the future.

1) With LIF technique

- Modify the model by removing the sides walls and roofing
- Work on the scaling equations

2) With PIV and Hydrogen Bubble techniques

- Collect the velocity data within the plume region and the entraining fluid
- Ensure the results are repeatable
- Investigate the entrainment constant into the line plume

3) Small scale fire tests

- Perform small scale fire tests with fire size corresponds to the equivalent fire size in salt water modelling.
- Collect velocity and temperature data.
- Compare these data with the salt water data.

4) CFD and LES modellings

- Perform CFD modelling based upon the geometry involved in the experiments.
- Collect results and made comparison.
- Perform LES simulation on the flow.

Finally, compile all the data gathered. Relating to the theoretical derived constants and made any modification if necessary. Refine the salt water modelling technique if appropriate.

REFERENCES

Baum, H.R. and Rehm, R.G. (1984) Calculations of Three Dimensional Buoyant Plumes in Enclosures, *Combustion Science and Technology*, Vol. 40, 55-77

Butcher, E.G. and Parnell, A.C. (1979) *Smoke Control in Fire Safety Design*, E & F N Spon Limited, London, pp 71-106.

Clement, J.M. (1996) Mixing in Fire Induced Doorway Flows: A Review, M.E.(Fire) Thesis, Department of Civil Engineering, University of Canterbury, Christchurch, New Zealand.

Clement, J.M. (1997) Draft Ph.D. Thesis, Fluid Laboratory, Department of Civil Engineering, University of Canterbury, Christchurch, New Zealand.

Drysdale, D. (1992) *An Introduction to Fire Dynamics*. John Wiley and Sons, New York, pp 114-151.

Emmons, H.W. (1995) "Vent Flows". In: *SFPE Handbook of Fire Protection Engineering, 2nd Edition*. Eds: P.J. DiNenno, C.L. Beyler, R.L.P. Custer, W.D. Walton, J.M. Watts, D. Drysdale and J.R. Hall. Quincy, MA, pp 4.20-4.29

Galae, E.R., Berhane, D. and Hoffmann, N. (1995) CFD Analysis of Fire Plumes Emerging from Windows in High-rise Buildings, *Proc of Fire Safety by Design, University of Sunderland*, July 10-12. Published by Tyne and Wear Metropolitan Fire Brigade, Vol. 3, pp 111-120

Gaskin, S.J. (1995) Single Buoyant Jets in a Crossflow and the Advected Line Thermal, Ph.D Thesis, Department of Civil Engineering, University of Canterbury, Christchurch, New Zealand.

Hansell, G.O., Morgan, H.P. and Marshall, N.R. (1993) Smoke Flow Experiments in A Model Atrium, *Building Research Establishment Occasional Paper*, FRS38/93M. Garston, BRE.

Hansell, G.O. and Morgan, H.P. (1994) *Design Approaches for Smoke Control in Atrium Buildings*. Building Research Establishment Report, (BRE Bookshop ref BR258). Garston, BRE.

Hoffmann, N.A., Galae, E.R. and Berhane, D. (1996) CFD Analysis of Fire Plumes Emerging From Windows with External Protrusions in High-rise Buildings, *INTERFLAM'96*, pp 835-839

Law, M. (1986) A Note on Smoke Plumes from Fires in Multi-level Shopping Malls, *Fire Safety Journal*, Vol. 10, pp 197-202

Law, M. (1995) Measurements of Balcony Smoke Flow, *Fire Safety Journal*, Vol. 24, pp 189-195

Lee, S.H. and Emmons, H.W. (1961) A Study of Natural Convection above a live fire, *Fluid Mech.*, Vol. 11, pp 353-368

Marshall N.R., (1986) Air Entrainment into Smoke and Hot Gases in Open Shafts, *Fire Safety Journal*, Vol. 10, pp 37-46

Marshall, N.R. and Morgan, H.P. (1992) User's Guide to BRE Spill Plume Calculations, *Fire Surveyor*, Vol. 21 (6), pp 14-20

Marshall, N.R., Harrison, R. and Morgan, H.P. (1993) A Study of the Mechanisms that Govern the Entrainment of Air into a Thermal Line Plume, *Building Research Establishment Note*, N65/93, Garston, BRE.

Marshall, N.R. and Harrison, R. (1996) Experimental Studies of Thermal Spill Plumes, *Building Research Establishment Occasional Paper*, OP1, Garston, BRE April.

Miles, S., Kumar, S. and Cox, G. (1996) The Balcony Spill Plume- Some CFD Simulations, *Building Research Establishment Publish Document*, PD287/96, Garston, BRE.

Milke, J.A. (1990) Smoke Management for Covered Malls and Atria, *Fire Technology*, Vol. 26 (3), pp 223-243.

Milke, J.A. (1995) "Smoke Management in Covered Malls and Atria". In: *SFPE Handbook of Fire Protection Engineering, 2nd Edition*. Eds: P.J. DiNenno, C.L. Beyler, R.L.P. Custer, W.D. Walton, J.M. Watts, D. Drysdale and J.R. Hall. Quincy, MA, pp 4.246-4.258

Morgan, H.P. and Marshall, N.R. (1975) Smoke Hazards in Covered, Multi-level Shopping Malls: Part 1- An experimentally based theory for smoke production, *Building Research Establishment Current Paper* CP48/75, Garston, BRE.

Morgan, H.P., Marshall, N.R. and Goldstone B.M. (1976) Smoke Hazards in Covered, Multi-level Shopping Malls: Some Studies using a Model 2-Storey Mall, *Building Research Establishment Current Paper*, CP45/76, Garston, BRE.

Morgan, H.P. and Marshall, N.R. (1979) Smoke Control Measures in a Covered Two-storey Shopping Mall having Balconies as Pedestrian Walkways, *Building Research Establishment Current Paper* CP11/79, Garston, BRE.

Morgan, H.P. (1986) The Horizontal Flow of Buoyant Gases Towards an Opening, *Fire Safety Journal*, Vol. 11, pp 193-200

Morgan, H.P. and Hansell, G.O. (1987) Atrium Buildings: Calculating Smoke Flows in Atria for Smoke Control Design, *Fire Safety Journal*, Vol. 12, pp 9-35

Morgan, H.P. (1987) Comment on -A Note on Smoke Plumes from Fires in Multi-level Shopping Malls, *Fire Safety Journal*, Vol. 12, pp 83-84

Morgan, H.P. and Gardner, J.P. (1990) *Design Principles for Smoke Ventilation in Enclosed Shopping Centres.*), Building Research Establishment Report (BRE Bookshop ref BR186). Garston, BRE.

NFPA 92B, (1991) Guide for Smoke Management Systems in Malls, Atria and Large Areas, NFPA, Quincy, MA.

NFPA 101, (1997) Life Safety Code, NFPA, Quincy, MA.

Papps, D.A. (1995) Merging Buoyant Jets in Stationary and Flowing Ambient Fluids, Ph.D Thesis, Department of Civil Engineering, University of Canterbury, Christchurch, New Zealand.

Poreh, M., Morgan, H.P., Marshall, N.R. and Harrison, R. (1997) The Spill Plume in Smoke Control Design, to be published in *Fire Safety Journal.*

Robinson, P. (1982) Atrium Building: A Fire Service View, *Fire Surveyor*, Vol. 11, pp 42-47

Rockett, J.A. (1976) Fire Induced Gas Flow in an Enclosure, *Combustion Science and Technology*, Vol. 12, pp 165-175

Saxon, R. (1983) Atrium buildings- Development and design, *The Architectural Press*, London.

Steckler, K.D., Baum, H.R. and Quintiere, J.G. (1986) Salt Water Modelling of Fire Induced Flows in Multicompartment Enclosures, 21th Symposium (International) on Combustion/The Combustion Institute, pp 143-149

Tangren, E.N., Sargent, W.S. and Zukoski, E.E. (1978) Hydraulic and Numerical Modelling of Room Fires, NSF Grant ENV76-06660 and US Dept. of Commerce, Nat. Bur. of Stand. Grant 5-9004, California Institute of Technology, Pasedena, CA.

Thomas, P.H., Hinkley, P.L., Theobald, C.R. and Simms D.L. (1963) Investigations into the Flow of Hot Gases in Roof Venting, *F.R. Technical Report No.7*, Dept. of Scientific and Industrial Research and Fire Offices' Committee Joint Fire Research Organisation, London.

Thomas, P.H. (1987) On the Upward Movement of Smoke and Related Shopping Mall Problems, *Fire Safety Journal*, Vol. 12, pp 191-203

Thomas, P.H., Morgan, H.P. and Marshall, N.R. (1996) The Spill Plume in Smoke Control Design, *Building Research Establishment Publish Document* PD277/96, Garston, BRE.

Turner, J.S. (1973) *Buoyancy Effects in Fluids*, Cambridge University Press, London, pp 48-90

Waters, R.A. (1989) Stansted Terminal Building and Early Atrium Studies, *J. of Fire Prot. Engr.*, Vol. 1 (2), pp 63-76

Wraight, H.G.H. (1973) Fire Problems in Pedestrian Precincts. Part 4, Experiments with a Glazed Shop Front, *Joint Fire Research Organisation Fire Research Note* 977/1973

Yokoi, S. (1960) Study on the Prevention of Fire-Spread Caused by Hot Upward Current, Report of the Building Research Institute.

Zukoski, E.E. (1995) "Properties of Fire Plumes". In: *Combustion Fundamentals of Fire*. Ed: G. COX. Academic Press, London. pp.101-219.

BIBLIOGRAPHY

Buchanan, A.H., (Editor), (1994), *Fire Engineering Design Guide.* Centre for Advanced Engineering, University of Canterbury, Christchurch, New Zealand.

Butcher, E.G. and Parnell, A.C. (1979*) Smoke Control in Fire Safety Design*, E & F N Spon Limited, London.

Clement, J.M., Personal Communication, Department of Civil Engineering, University of Canterbury, Christchurch, New Zealand.

Drysdale, D. (1992) *An Introduction to Fire Dynamics*. John Wiley and Sons, New York.

Global Lab® Image for Microsoft Windows: User Manual, Data Translation Incorporate, 1992

Klote, J.H. and Milke, J.A. (1992), *Design of Smoke Management Systems*, ASHRAE, Atlanta.

Wood, I.R., Bell, R.G. and Wilkinson, D.L. (1993) *Ocean Disposal of Wastewater*, Advanced Series on Ocean Engineering- Volume 8, World Scientific, London.

APPENDIX A

PHYSICAL MODEL

The physical shape of the model is shown by the photographs below. Its dimensions are indicated in the engineering drawings at the following pages. The source's geometry at the back of the model is also presented.

The model was made of clear perspex sheets. It was covered with black-powder coated metal sheets leaving only the section facing the camera. This was to reduce possible reflected laser light from surrounding which would cause errors in the filming process.

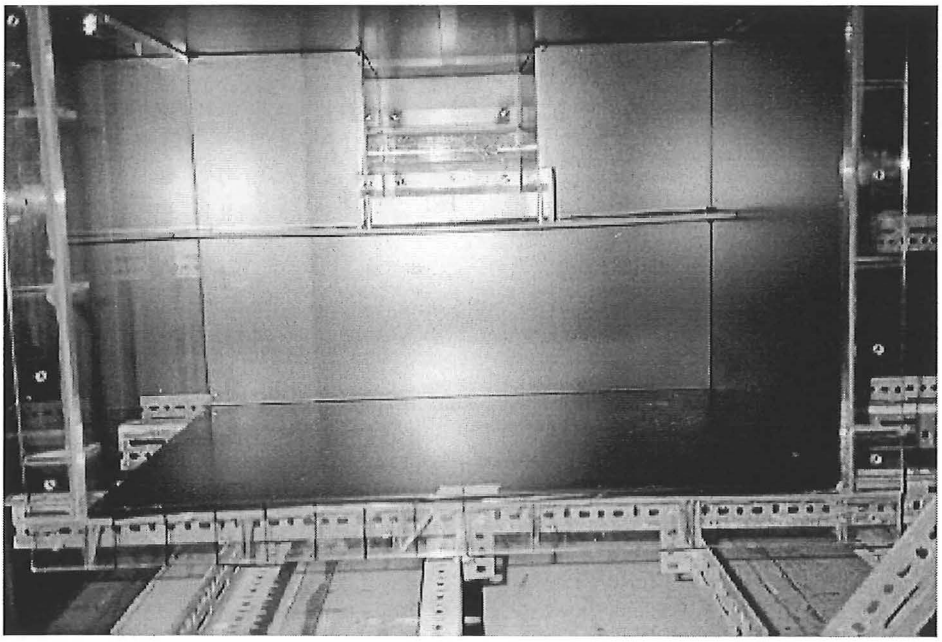

Figure A.1 The front view of the model.

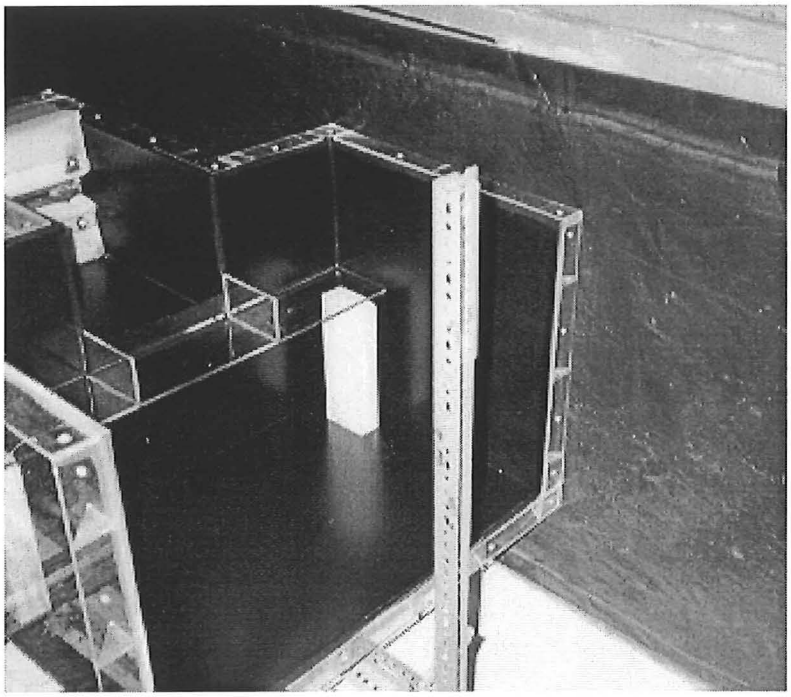

Figure A.2 A closer view of the model with short balcony setting.

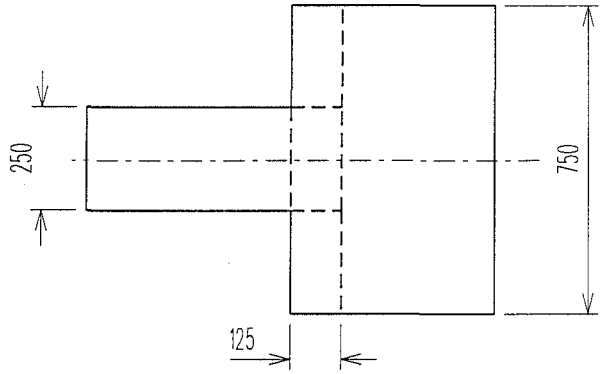

PLAN VIEW

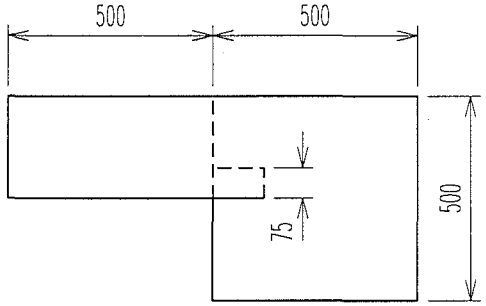

ELEVATION VIEW

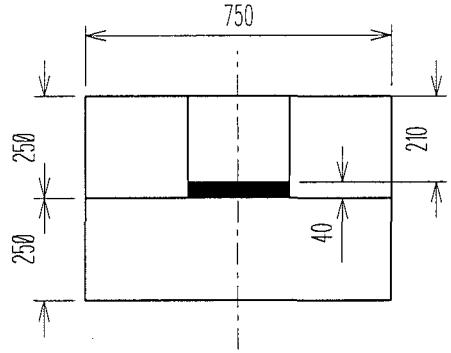

FRONT VIEW

ALL DIMENSIONS IN MM.

ITEM	DESCRIPTION	QUANTITY

PHYSICAL MODEL
-SHORT BALCONY SETTING

SCHOOL OF ENGINEERING
CIVIL ENGINEERING DEPARTMENT

DRN : EE H. YII | DRG No : A-SP-01

SCALES : 1 : 20 | DATE : 19 FEB 1998

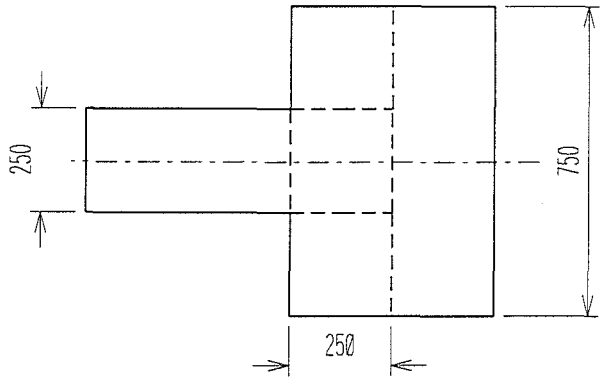

PLAN VIEW

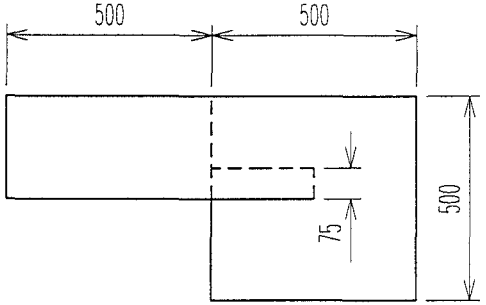

ELEVATION VIEW

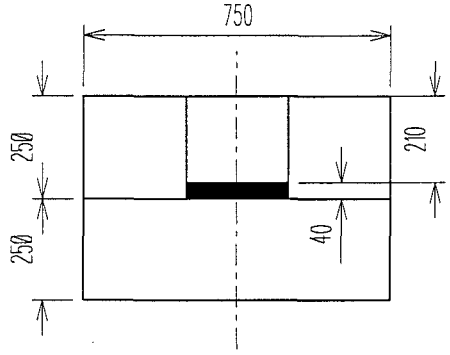

FRONT VIEW

ALL DIMENSIONS IN MM.

ITEM	DESCRIPTION	QUANTITY

PHYSICAL MODEL
-LONG BALCONY SETTING

SCHOOL OF ENGINEERING
CIVIL ENGINEERING DEPARTMENT

DRN : EE H. YII

DRG No : A-SP-02

SCALES : 1 : 20

DATE : 19 FEB 1998

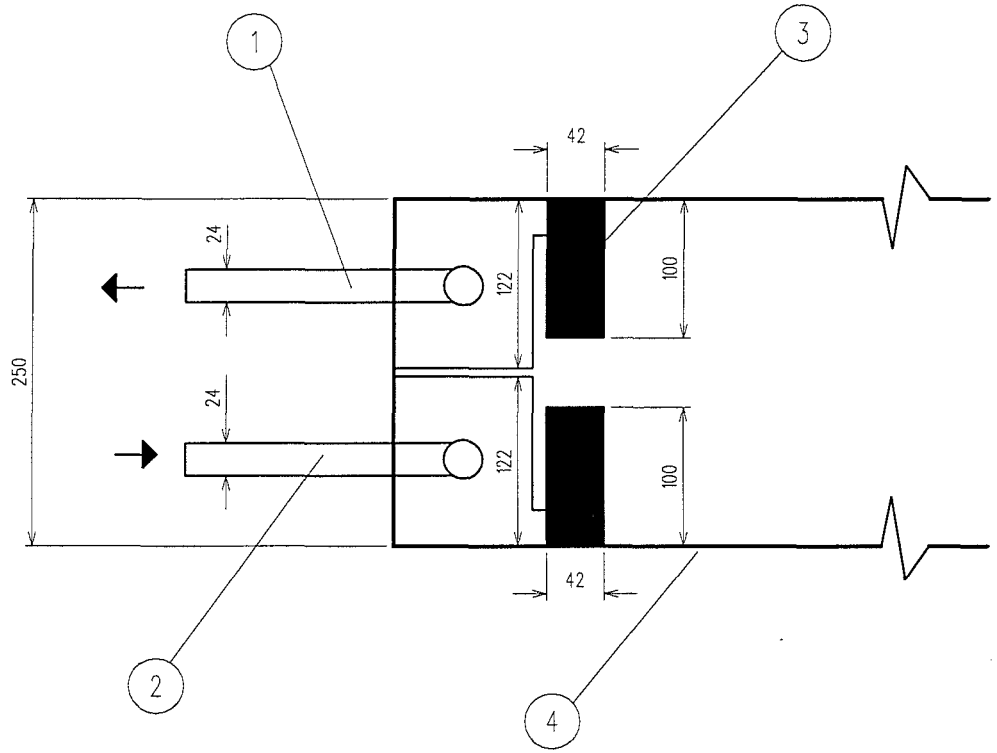

ELEVATION VIEW

ITEM	DESCRIPTION	QUANTITY
4	MODEL	1
3	SPONGE	2
2	INJECTION PORT	1
1	SUCTION PORT	1

ALL DIMENSIONS IN MM.

BACK END OF THE MODEL
-SOURCE

SCALES : 1 : 20

SCHOOL OF ENGINEERING
CIVIL ENGINEERING DEPARTMENT

DRN : EE H. YII

DATE : 19 FEB 1998

DRG No : A-SP-03

APPENDIX B

X-Y FLOW IMAGE PLOTS

These flow image plots are the time average images for the flows generated during the experiments. These images show contours of time averaged flow dilution, measured over 100 seconds. The directional convention is shown in Figure B.(a) below. The coordinate origin is defined at the bottom face at the outer edge of the balcony. The buoyancy force is acting in the positive y direction. The flow parameters for each experimental series are presented in Appendix D. The square grid drawn on the flow image plot has a spacing dimension of 25mm both vertically and horizontally.

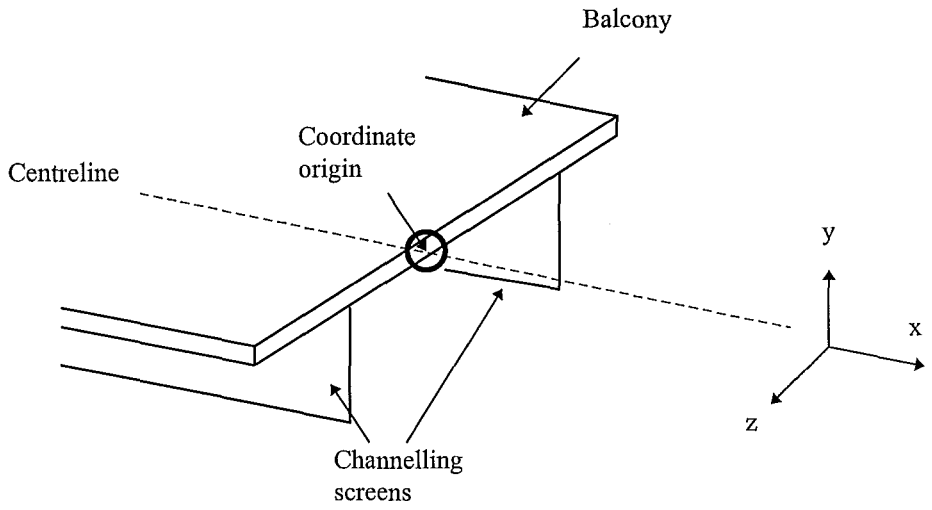

Figure B.(a) Definition for the directional convention used.

Experiment Setting:

Experimental Series	Balcony Setting	% Saline Concentration
SP-B01	125 mm	0.5 %
SP-B02	125 mm	1.0 %
SP-C01	250 mm	0.5 %
SP-C02	250 mm	1.0 %

Sampling Sections: Starting from the centre of the model towards the outside at 50mm spacing interval.

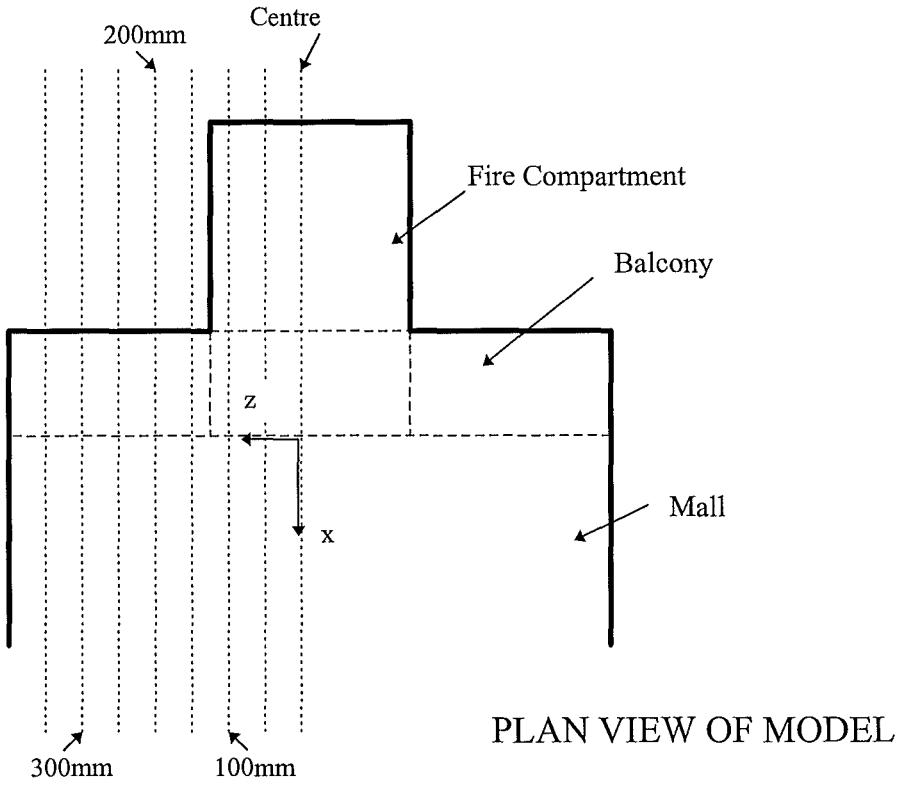

Figure B.(b) Sections sampled.

Notation:

Co/C Dilution ratio

B.1 EXPERIMENTAL SERIES SP-B01

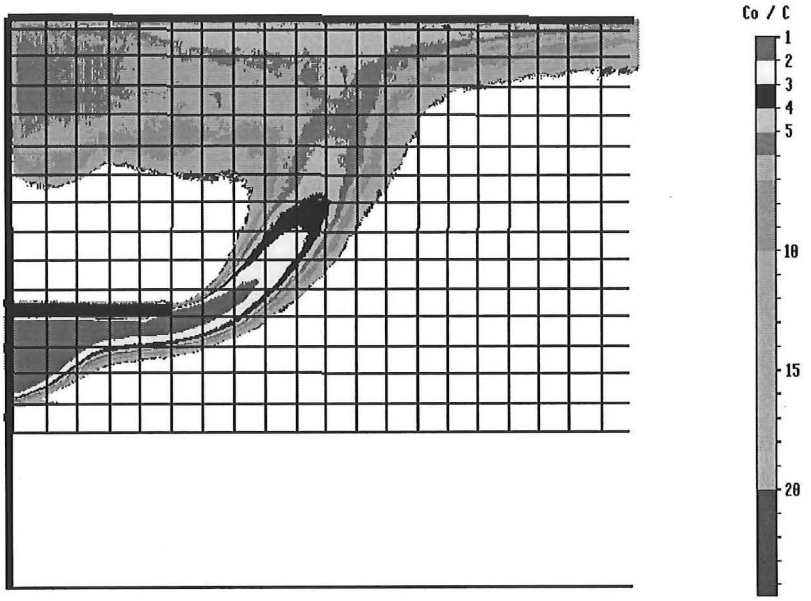

Figure B.1 The density profile of the balcony spill plume at centre section (z=0mm).

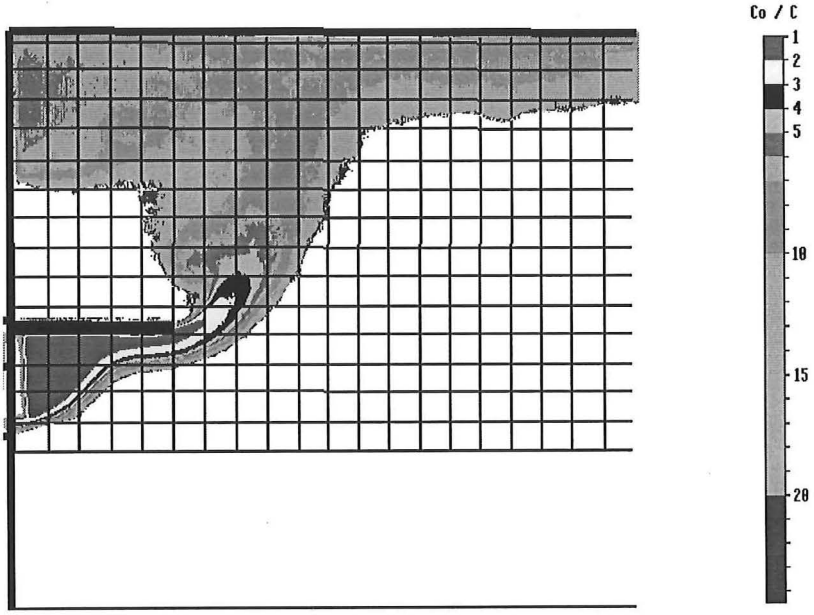

Figure B.2 The density profile of the balcony spill plume at 100mm section (z=100mm).

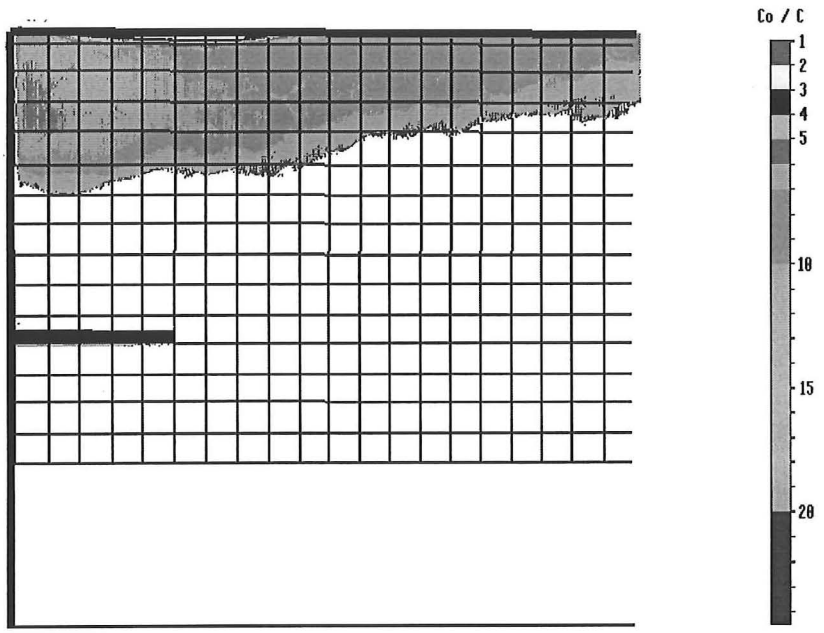

Figure B.3 The density profile of the balcony spill plume at 200mm section (z=200mm).

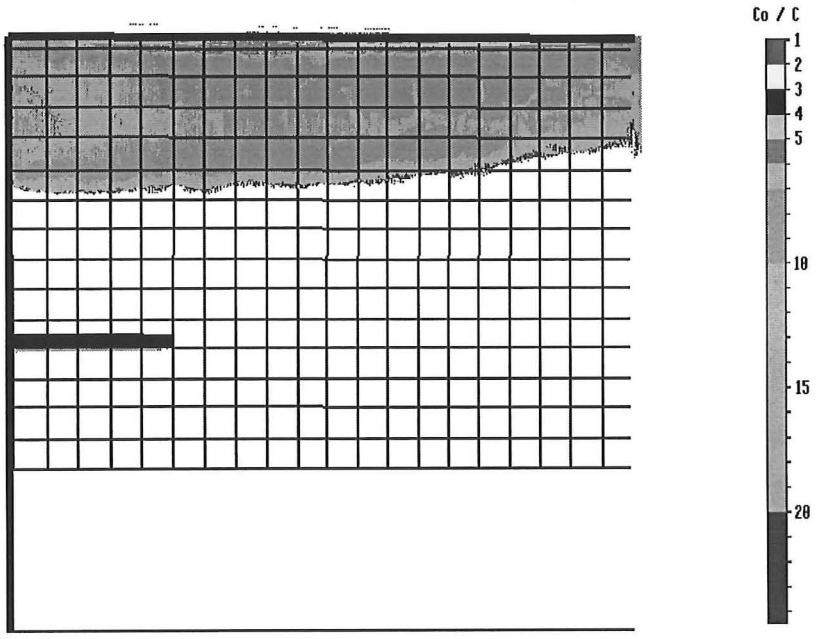

Figure B.4 The density profile of the balcony spill plume at 300mm section (z=300mm).

B.2 EXPERIMENTAL SERIES SP-B02

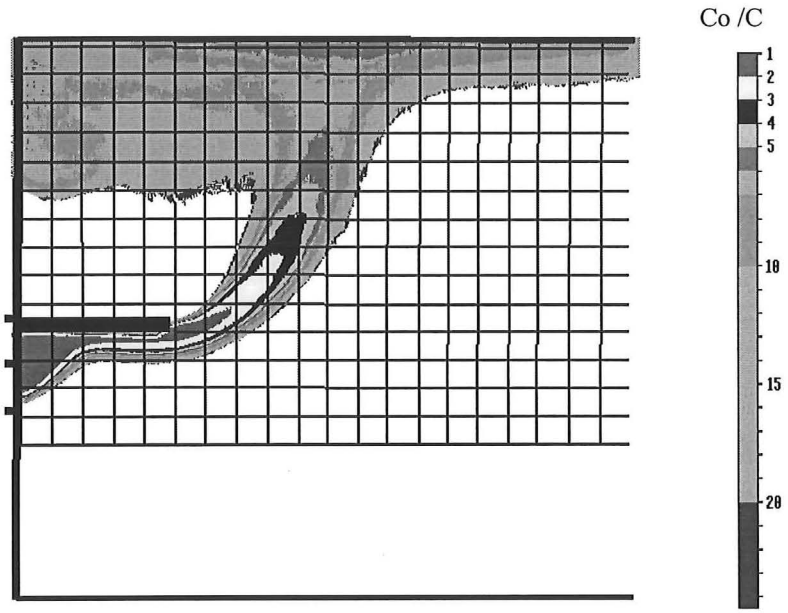

Figure B.5 The density profile of the balcony spill plume at centre section (z=0mm).

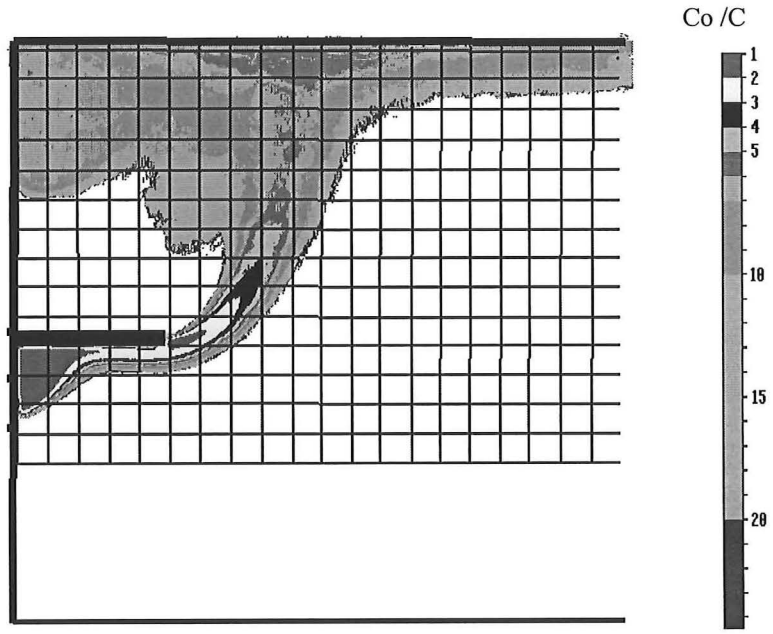

Figure B.6 The density profile of the balcony spill plume at 50mm section (z=50mm).

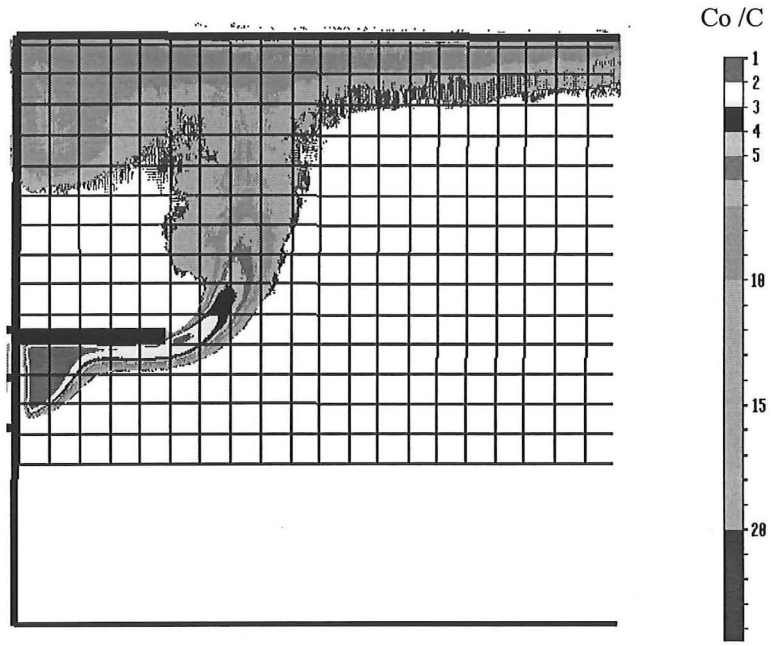

Figure B.7 The density profile of the balcony spill plume at 100mm section (z=100mm).

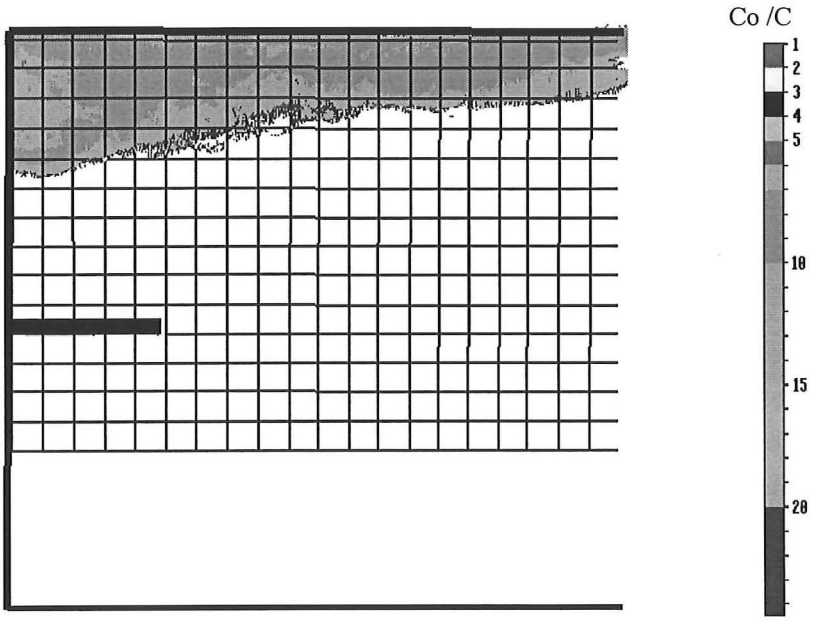

Figure B.8 The density profile of the balcony spill plume at 150mm section (z=150mm).

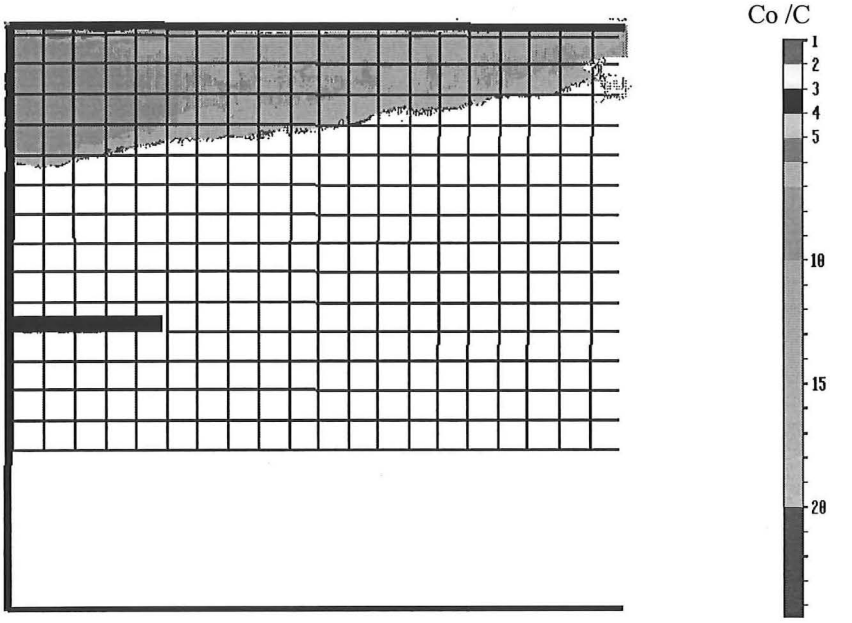

Figure B.9 The density profile of the balcony spill plume at 200mm section (z=200mm).

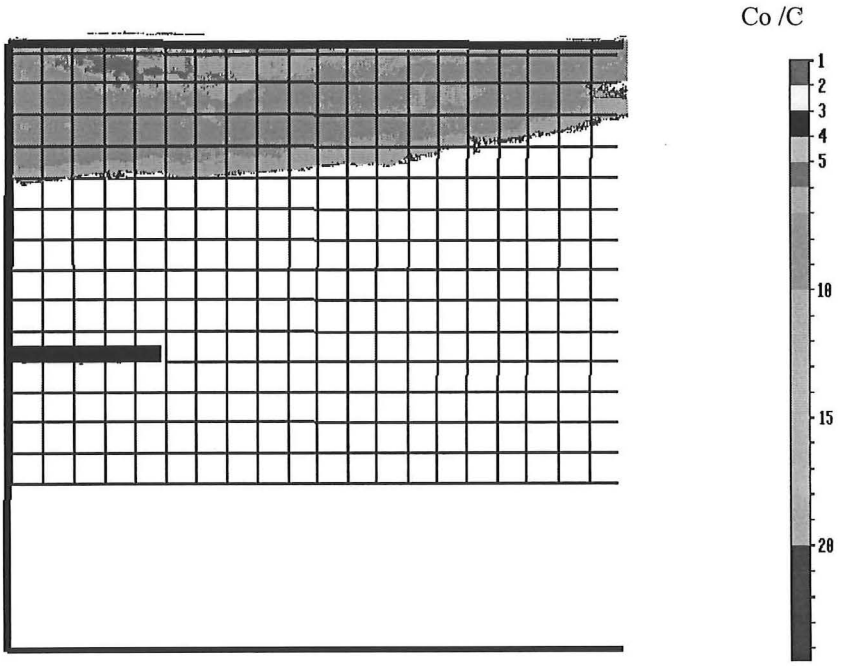

Figure B.10 The density profile of the balcony spill plume at 250mm section (z=250mm).

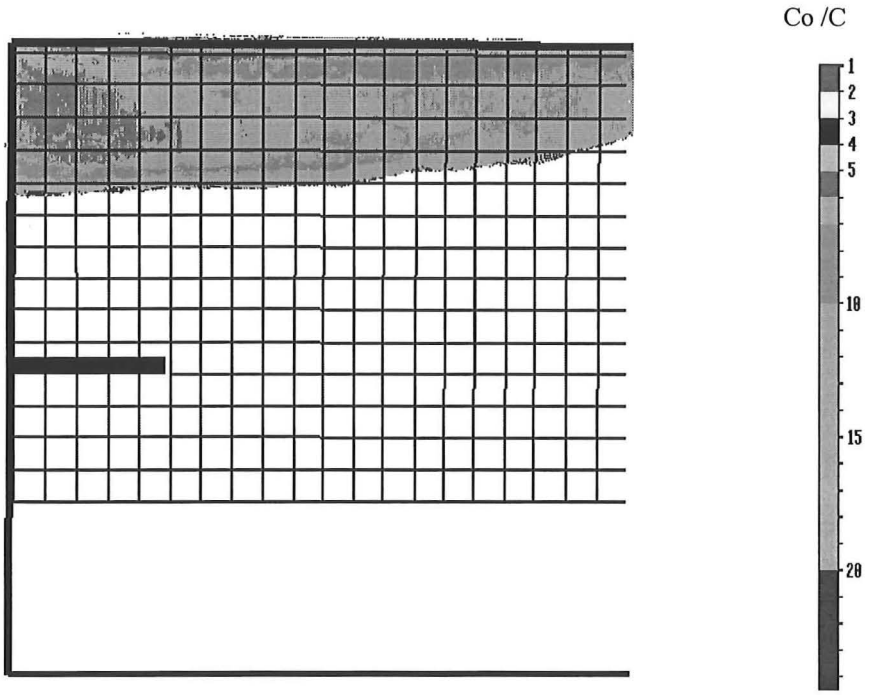

Figure B.11 The density profile of the balcony spill plume at 300mm section (z=300mm).

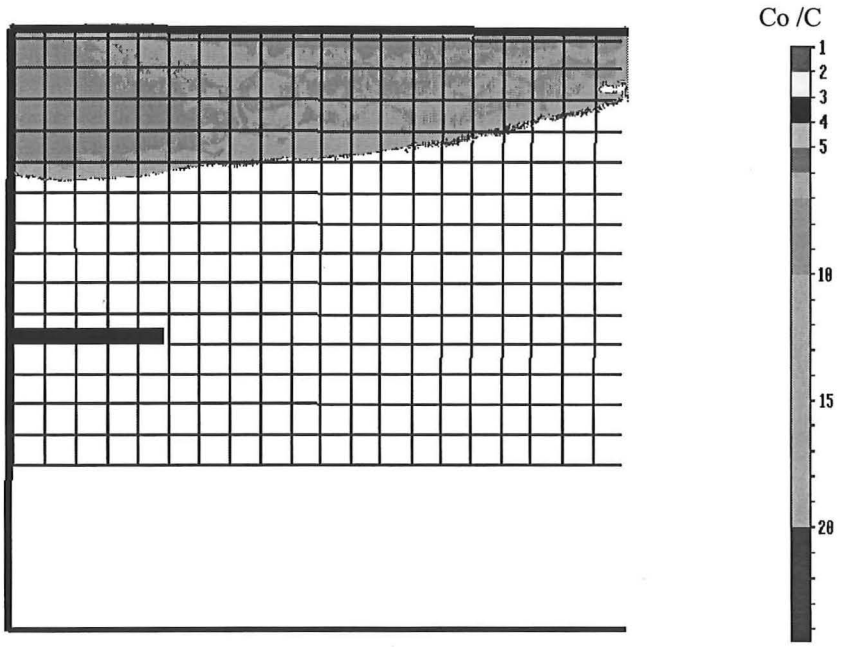

Figure B.12 The density profile of the balcony spill plume at 350mm section (z=350mm).

B.3 EXPERIMENTAL SERIES SP-C01

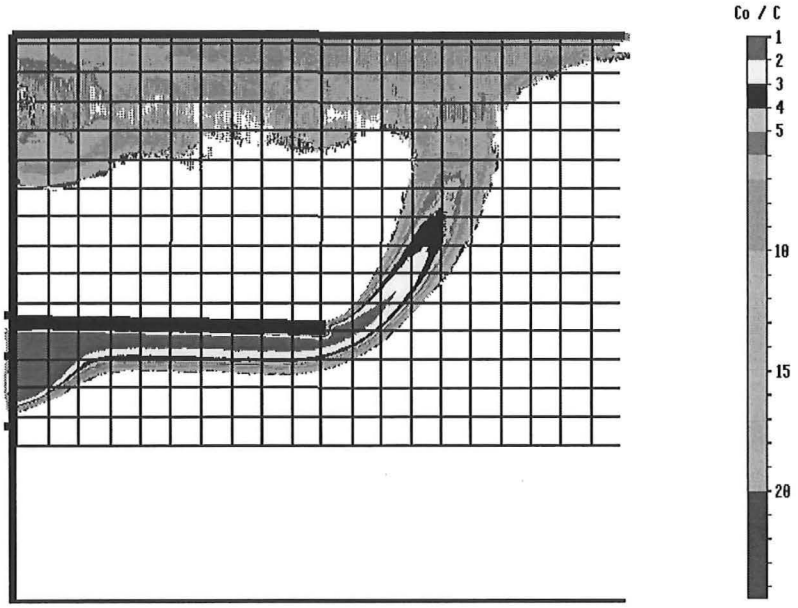

Figure B.13 The density profile of the balcony spill plume at centre section (z=0mm).

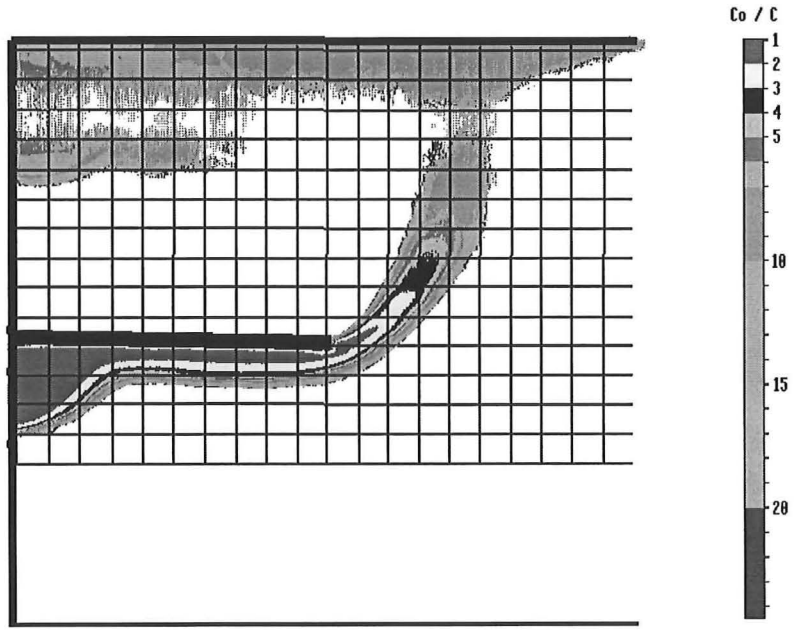

Figure B.14 The density profile of the balcony spill plume at 50mm section (z=50mm).

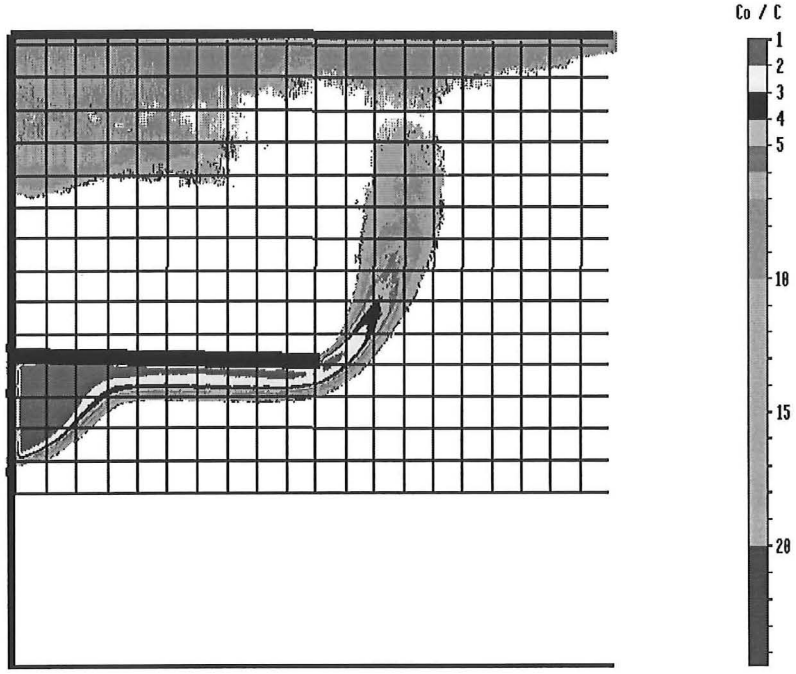

Figure B.15 The density profile of the balcony spill plume at 100mm section (z=100mm).

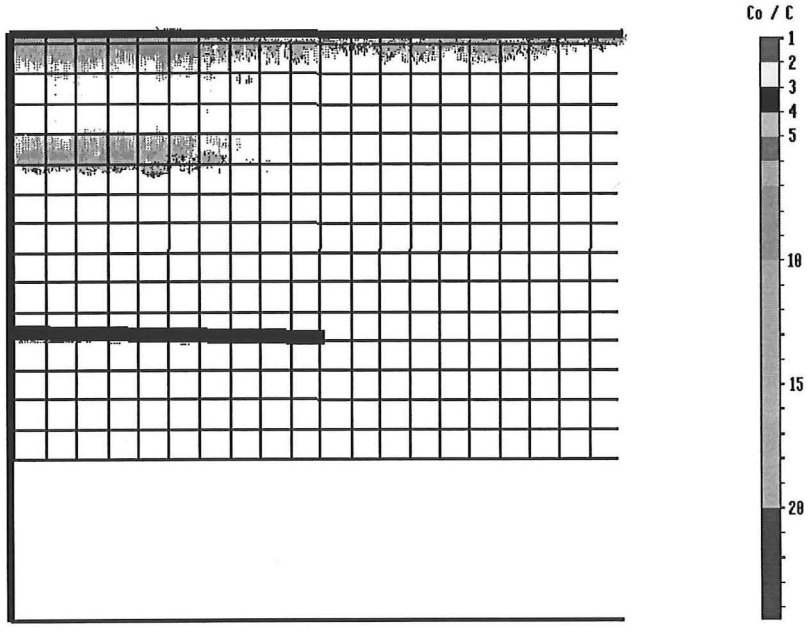

Figure B.16 The density profile of the balcony spill plume at 150mm section (z=150mm).

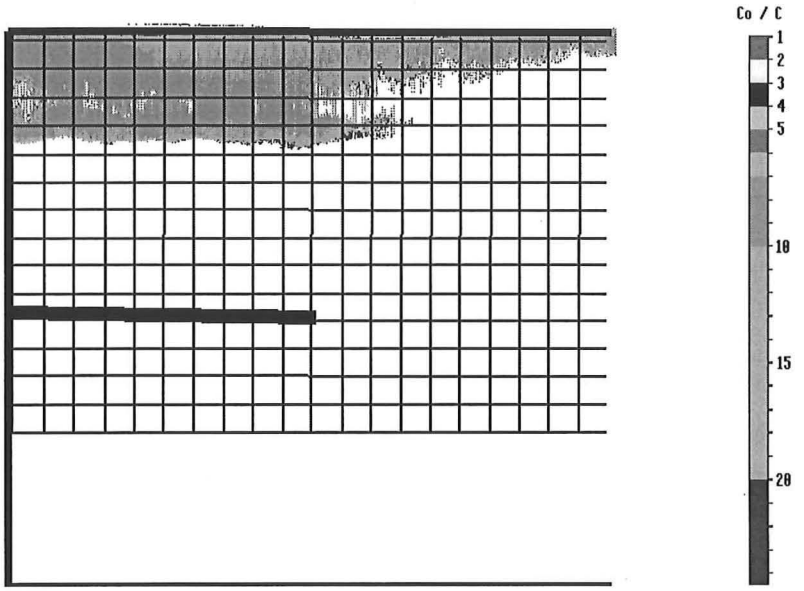

Figure B.17 The density profile of the balcony spill plume at 200mm section (z=200mm).

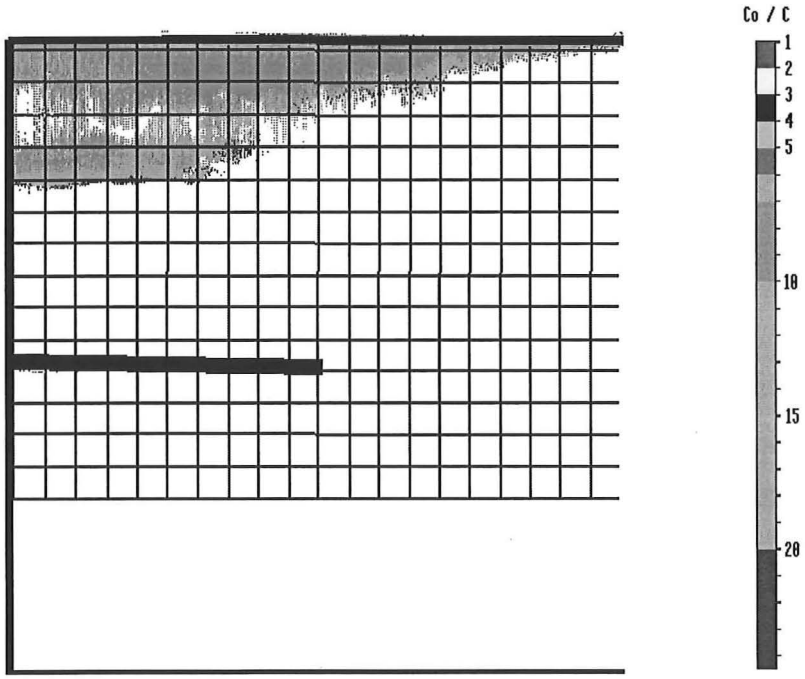

Figure B.18 The density profile of the balcony spill plume at 250mm section (z=250mm).

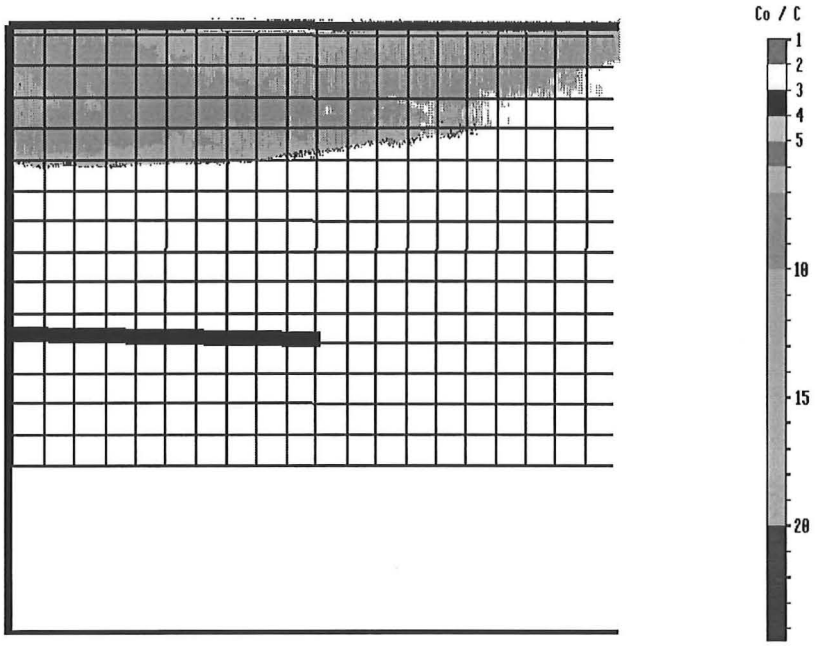

Figure B.19 The density profile of the balcony spill plume at 300mm section (z=300mm).

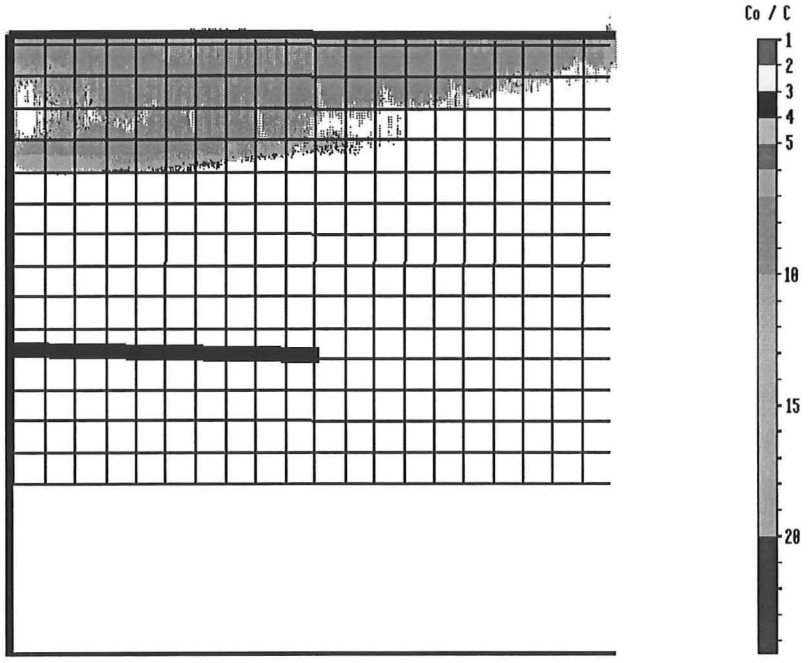

Figure B.20 The density profile of the balcony spill plume at 350mm section (z=350mm).

B.4 EXPERIMENTAL SERIES SP-C02

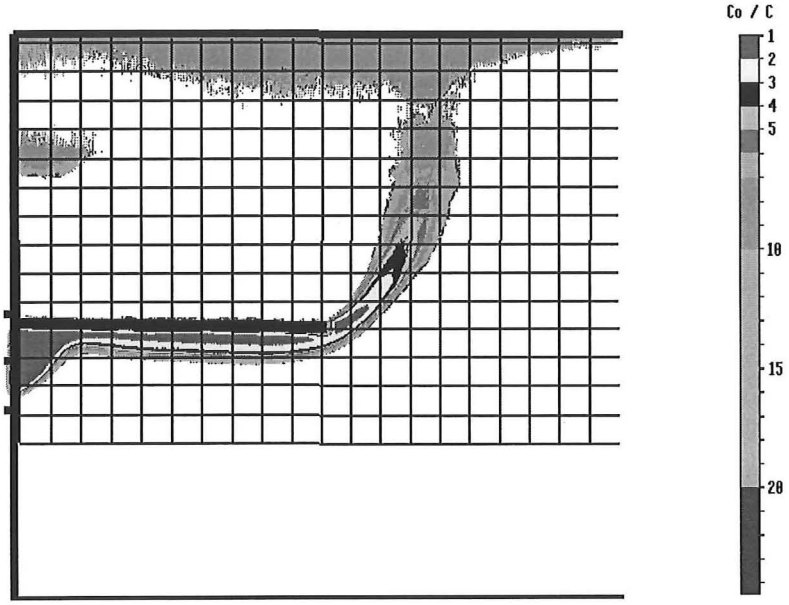

Figure B.21 The density profile of the balcony spill plume at centre section (z=0mm).

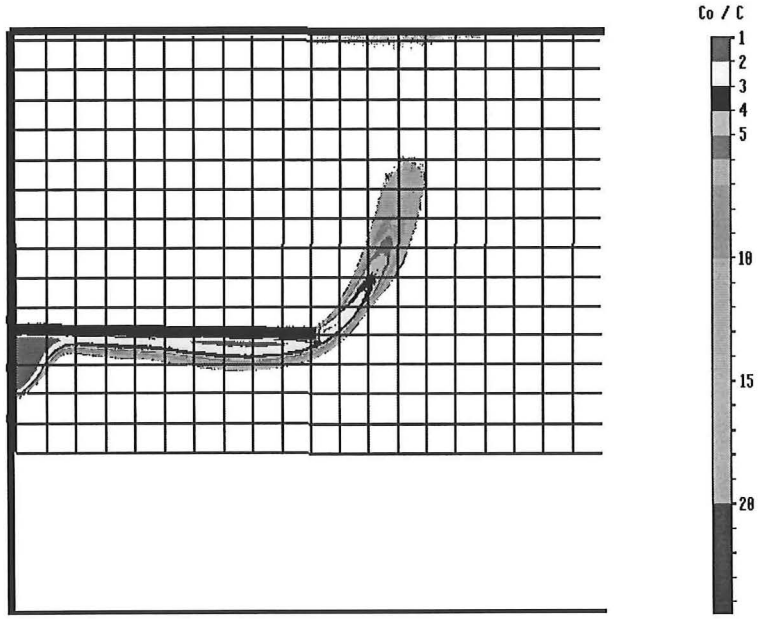

Figure B.22 The density profile of the balcony spill plume at 50mm section (z=50mm).

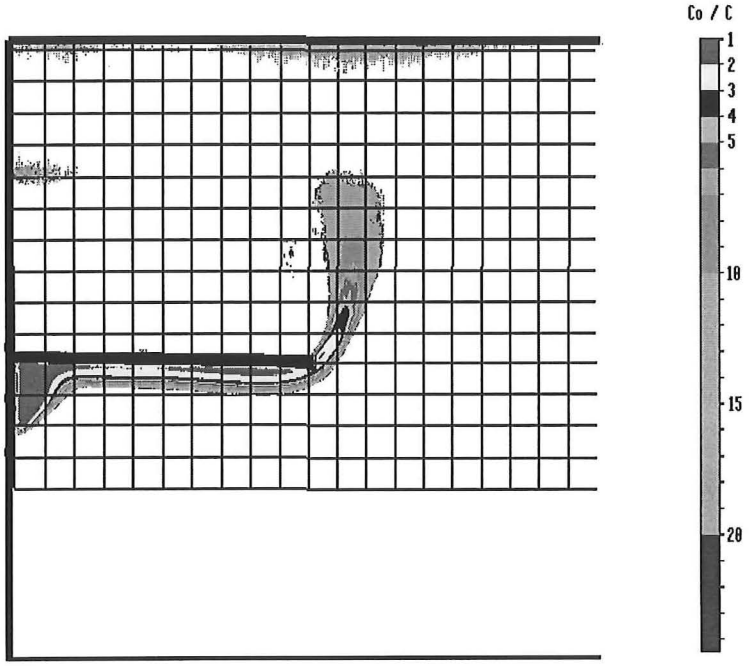

Figure B.23 The density profile of the balcony spill plume at 100mm section (z=100mm).

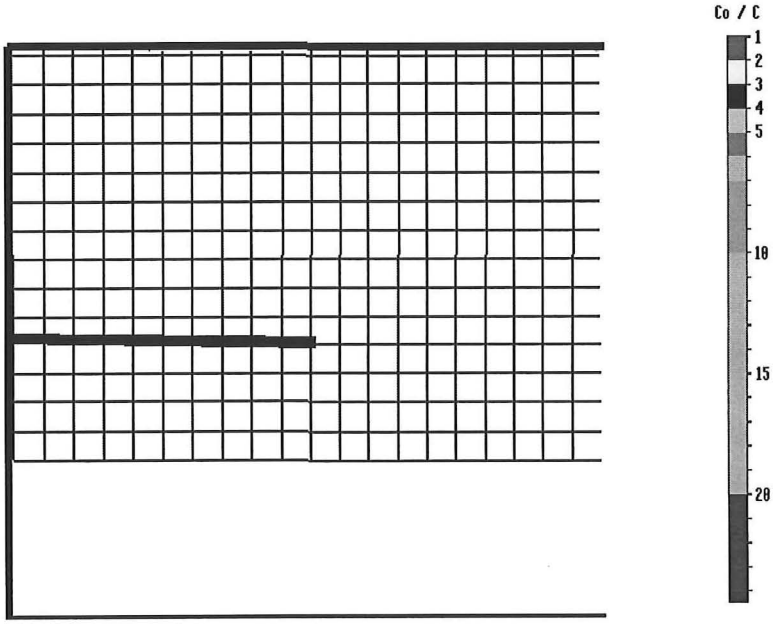

Figure B.24 The density profile of the balcony spill plume at 150mm section (z=150mm).

B.5 EXPERIMENTAL SERIES SP-D01(Same setting as in SP-C02 with 250mm balcony and 1.0% saline solution)

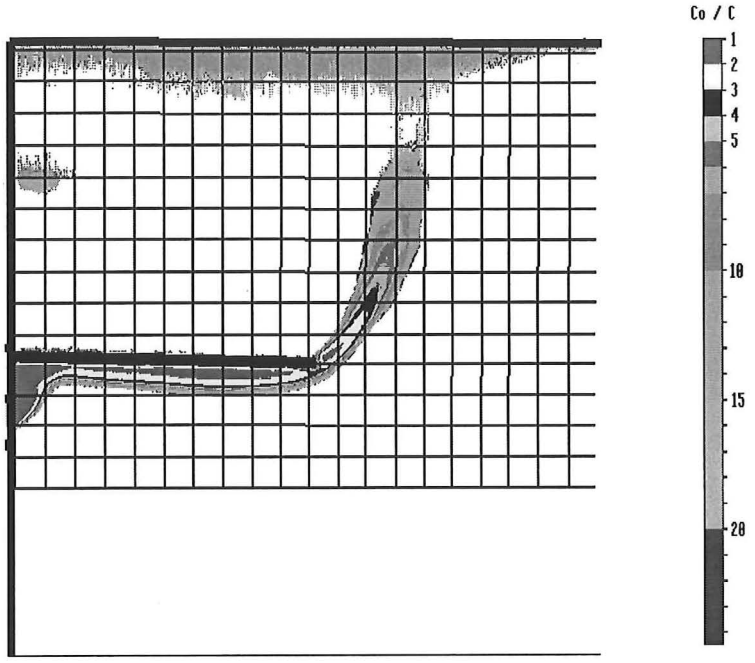

Figure B.25 The density profile of the balcony spill plume at centre section (z=0mm).

APPENDIX C

X-Z CONTOUR PLOTS

Application: These contour plots provide the basic shape and density distribution of the plume at various heights.

Input Data:

- The data sets were collected at single pixel interval along the x-axis from the 100 seconds averaged image. They were mapped with corresponding data sets at section intervals along z-axis collected during experiment.
- The data sets were presented as a matrix for mapping purpose.
- *Matlab® for Windows*, Classroom Version 4.2c.1 (1994) was used to perform the mapping for these contours.

Table C.1 Sections of plume used for mapping.

Experimental Series	Plume Data Collected at Section
SP-B01	centre, 100mm
SP-B02	centre, 50mm, 100mm
SP-C01	centre, 50mm, 100mm
SP-C02	centre, 50mm, 100mm

Disclaimer: These contour plots are interpolated using Matlab software. The author does not and has not validated or justified the accuracy of any data point within the interpolation region.

C.1 EXPERIMENTAL SERIES SP-B01

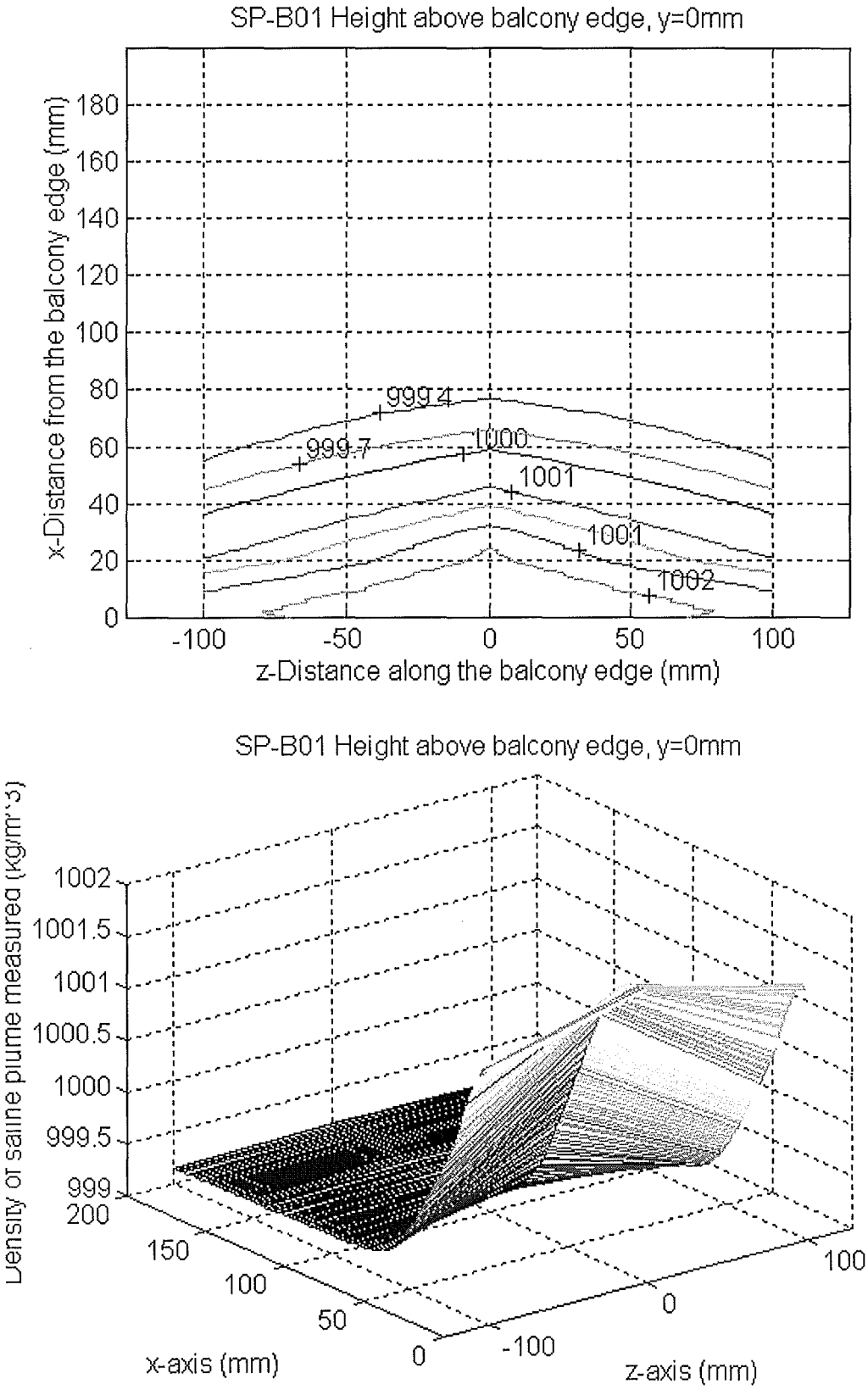

Figure C.1 The x-z contour plot and 3-D density distribution for experimental series SP-B01 at a height of 0mm above balcony edge.

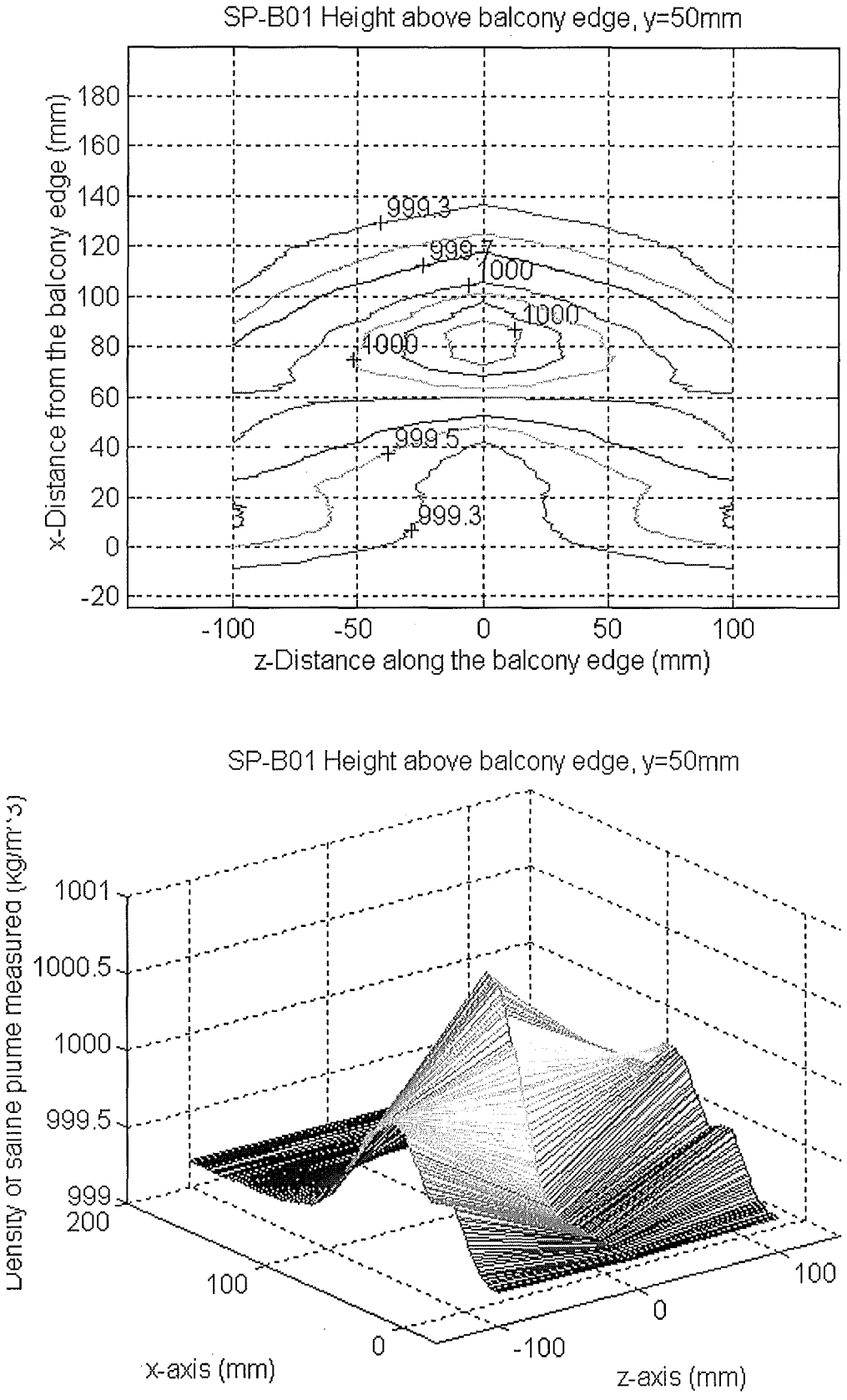

Figure C.2 The x-z contour plot and 3-D density distribution for experimental series SP-B01 at a height of 50mm above balcony edge.

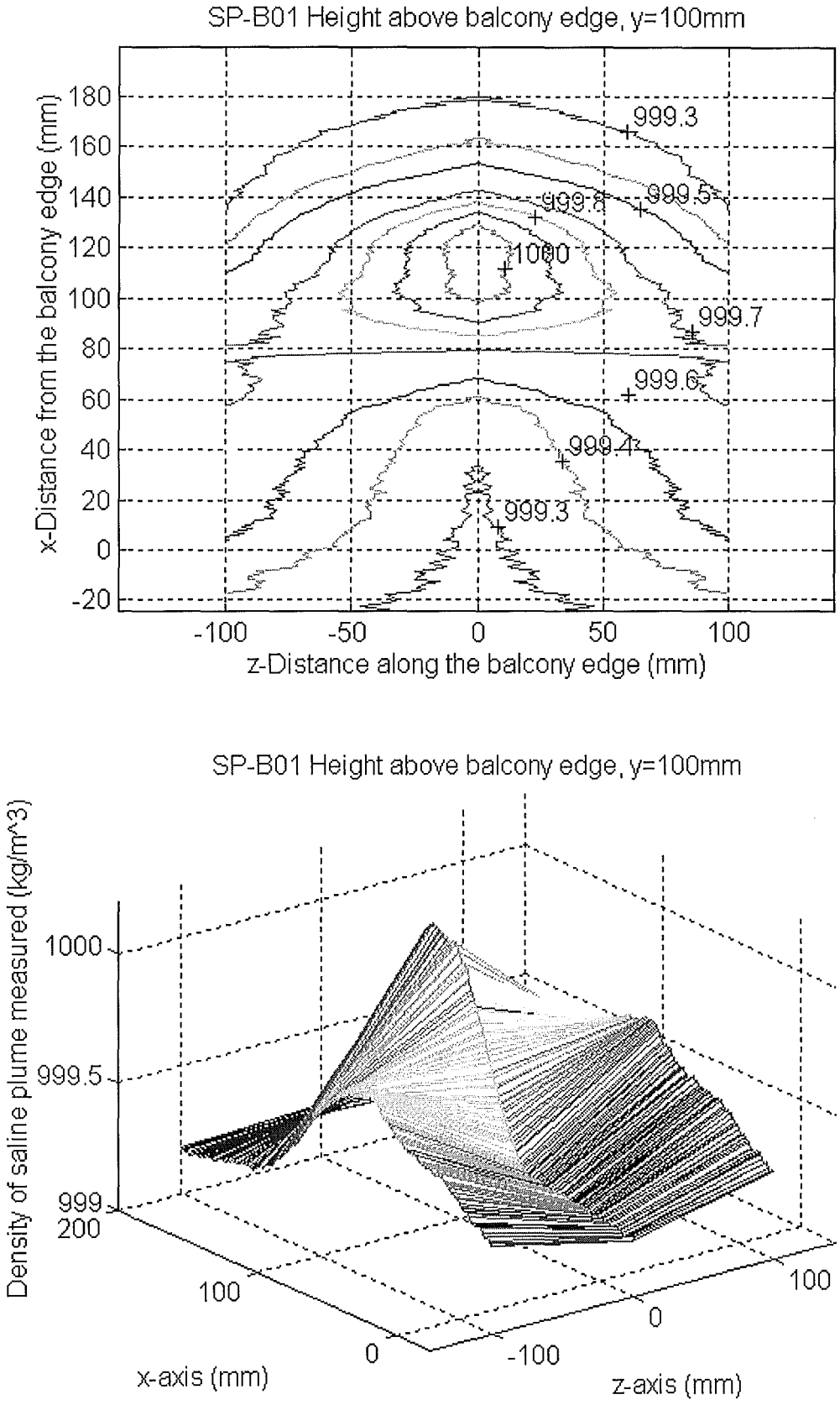

Figure C.3 The x-z contour plot and 3-D density distribution for experimental series SP-B01 at a height of 100mm above balcony edge.

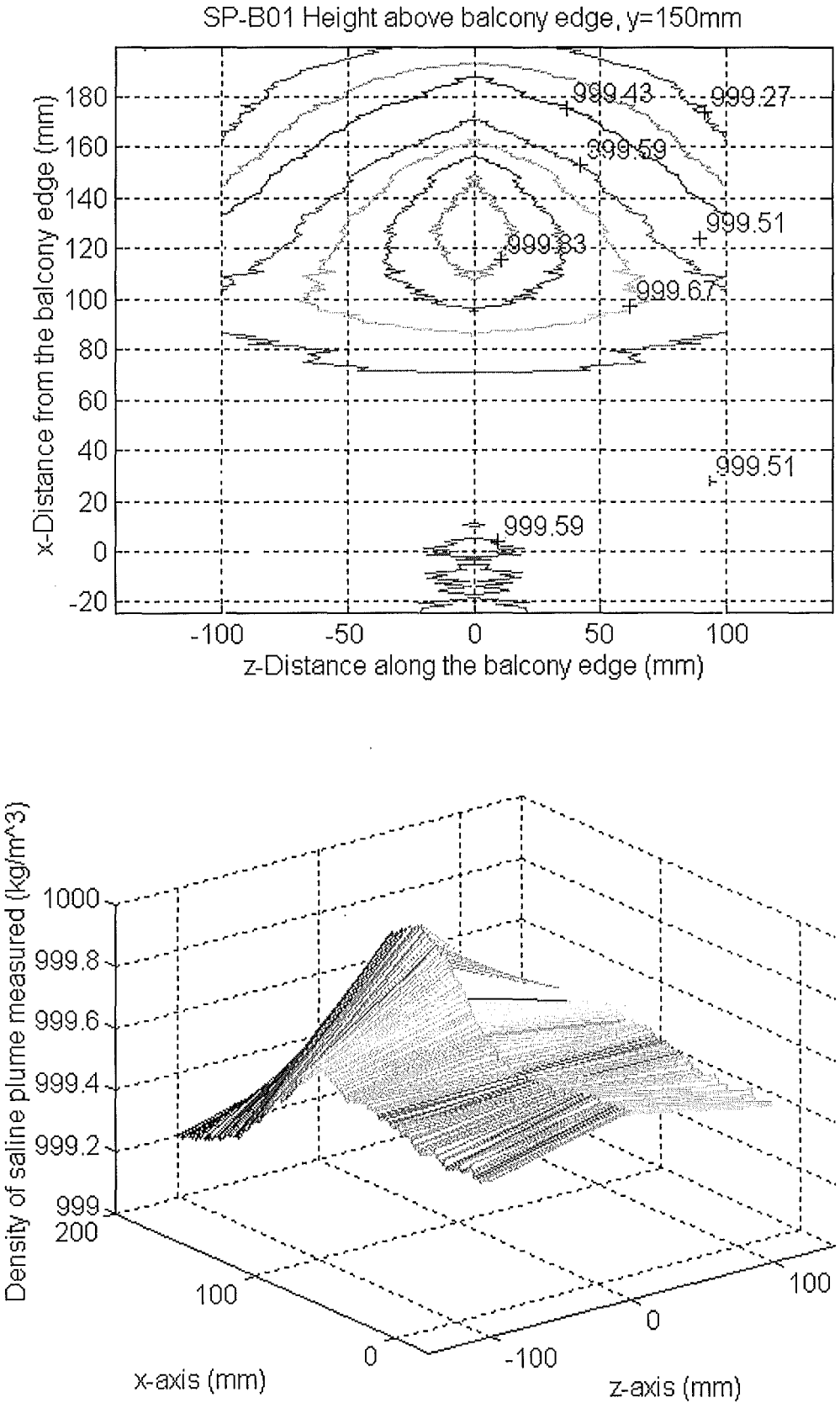

Figure C.4 The x-z contour plot and 3-D density distribution for experimental series SP-B01 at a height of 150mm above balcony edge.

C.2 EXPERIMENTAL SERIES SP-B02

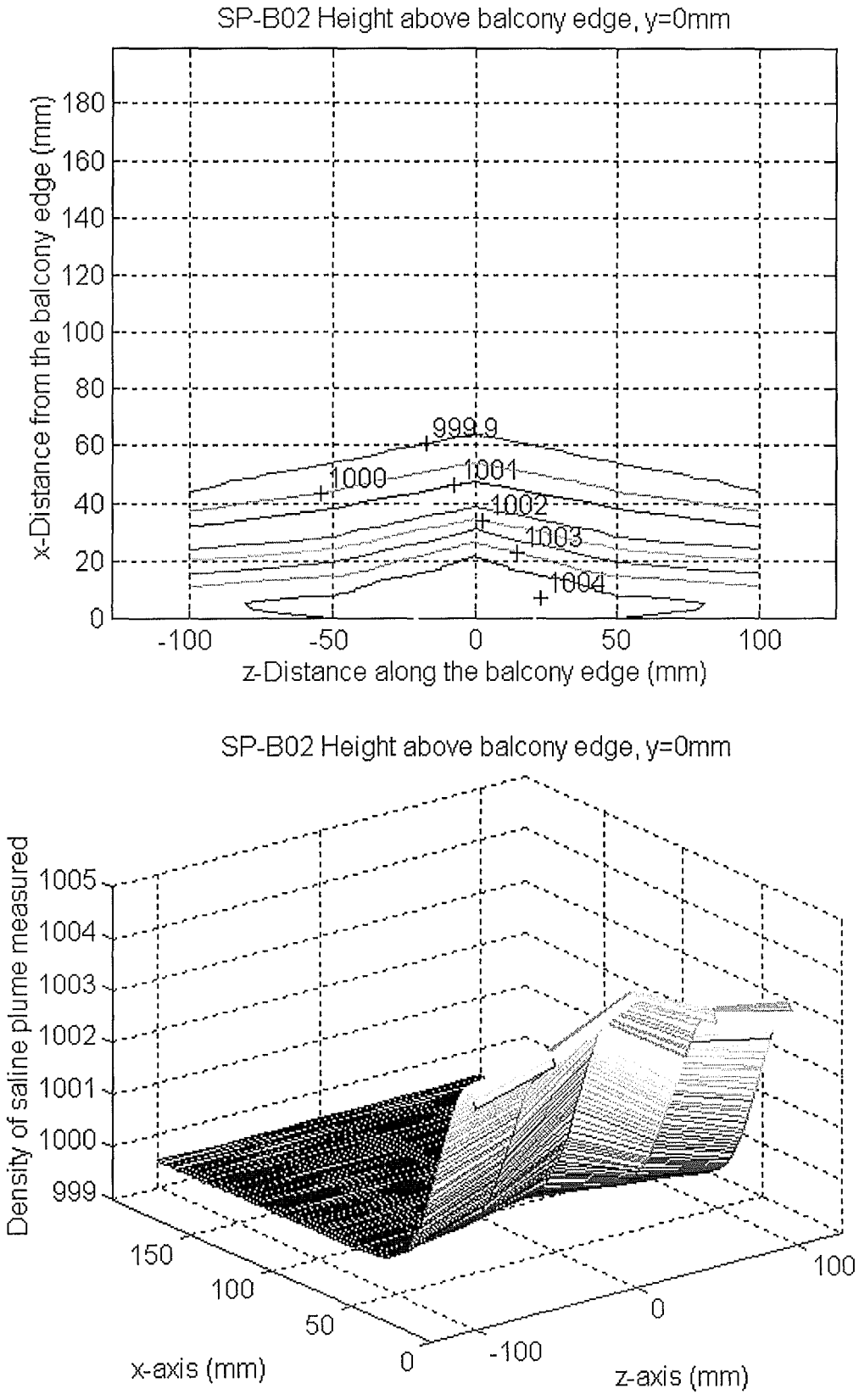

Figure C.5 The x-z contour plot and 3-D density distribution for experimental series SP-B02 at a height of 0mm above balcony edge.

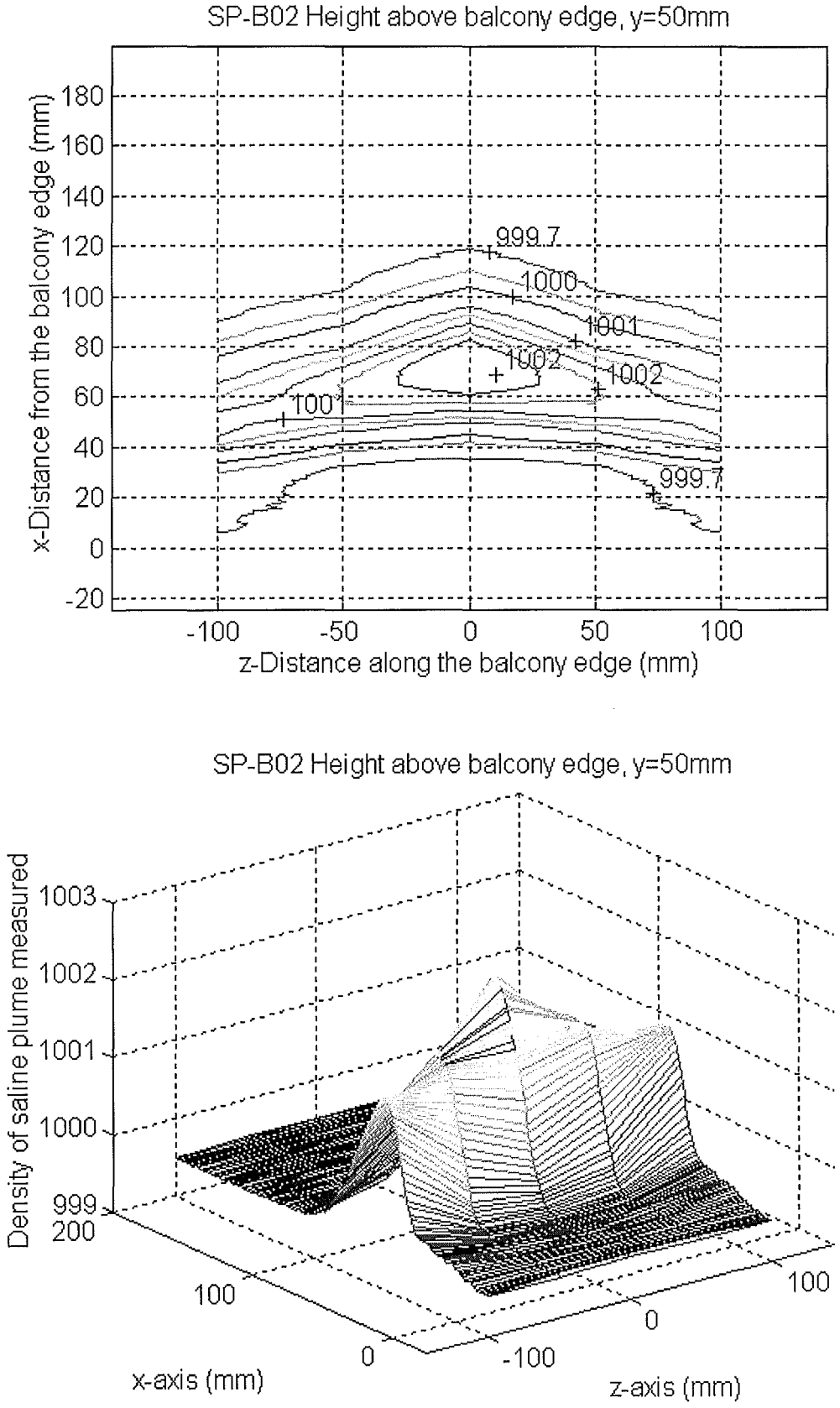

Figure C.6 The x-z contour plot and 3-D density distribution for experimental series SP-B02 at a height of 50mm above balcony edge.

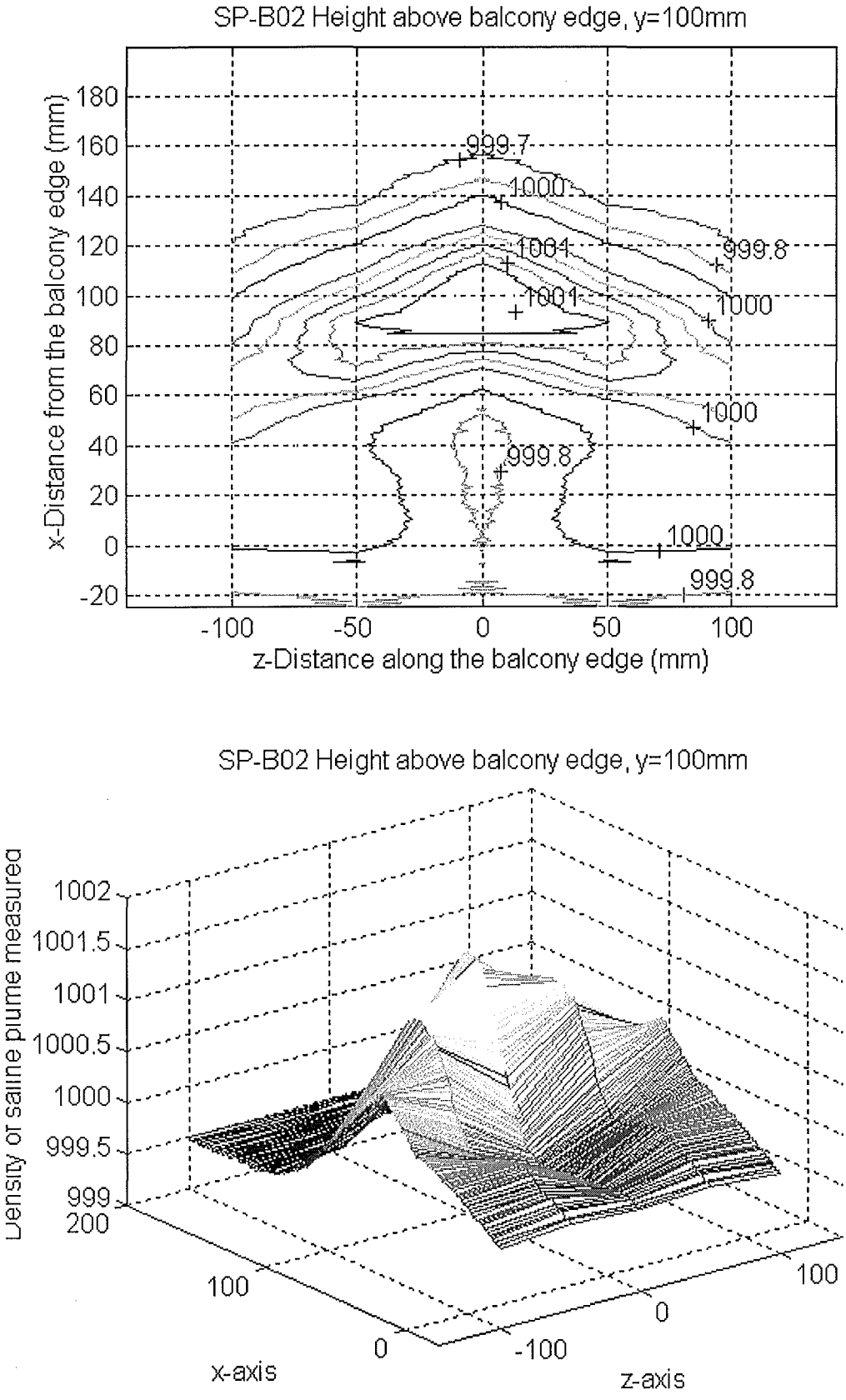

Figure C.7 The x-z contour plot and 3-D density distribution for experimental series SP-B02 at a height of 100mm above balcony edge.

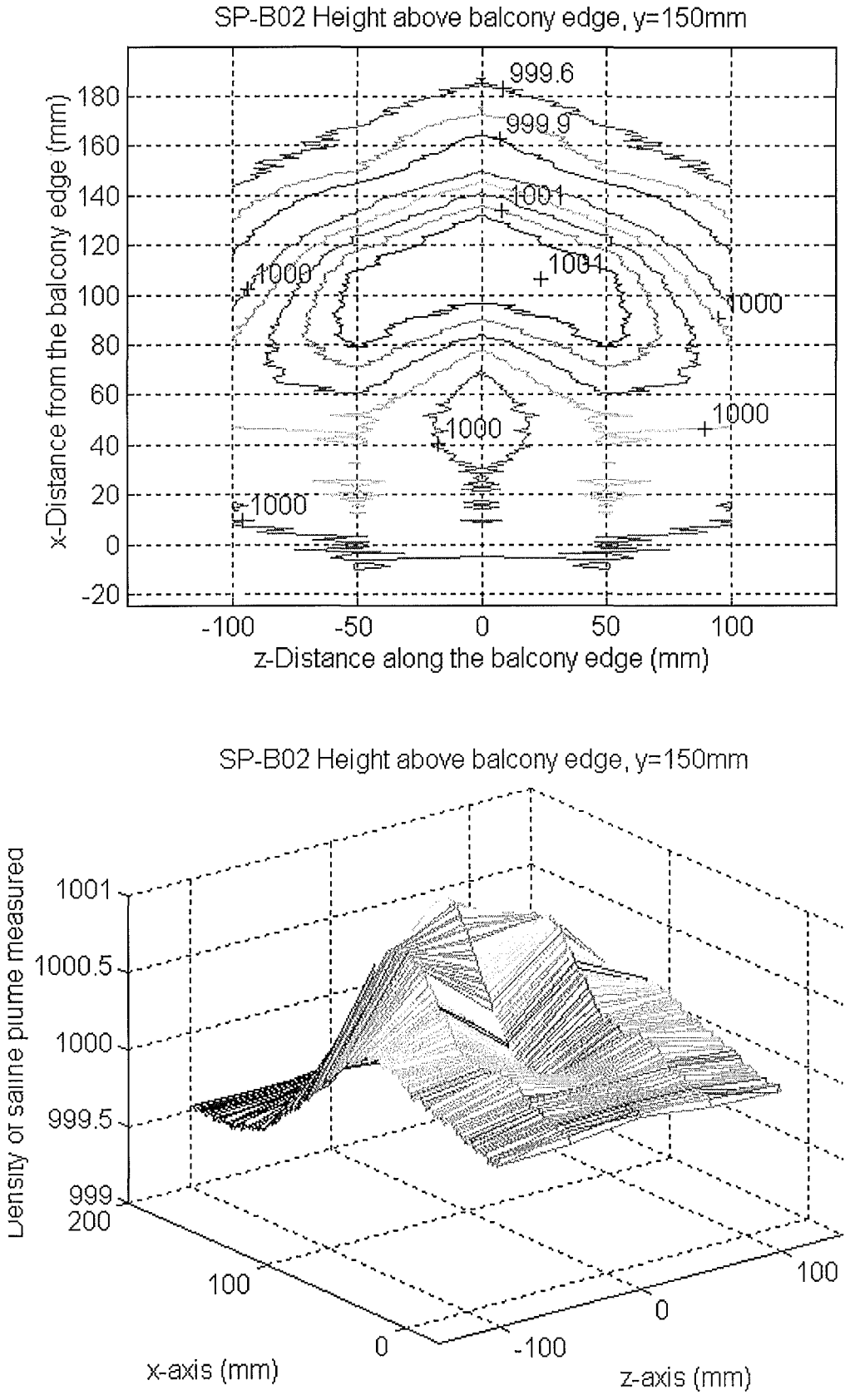

Figure C.8 The x-z contour plot and 3-D density distribution for experimental series SP-B02 at a height of 150mm above balcony edge.

C.3 EXPERIMENTAL SERIES SP-C01

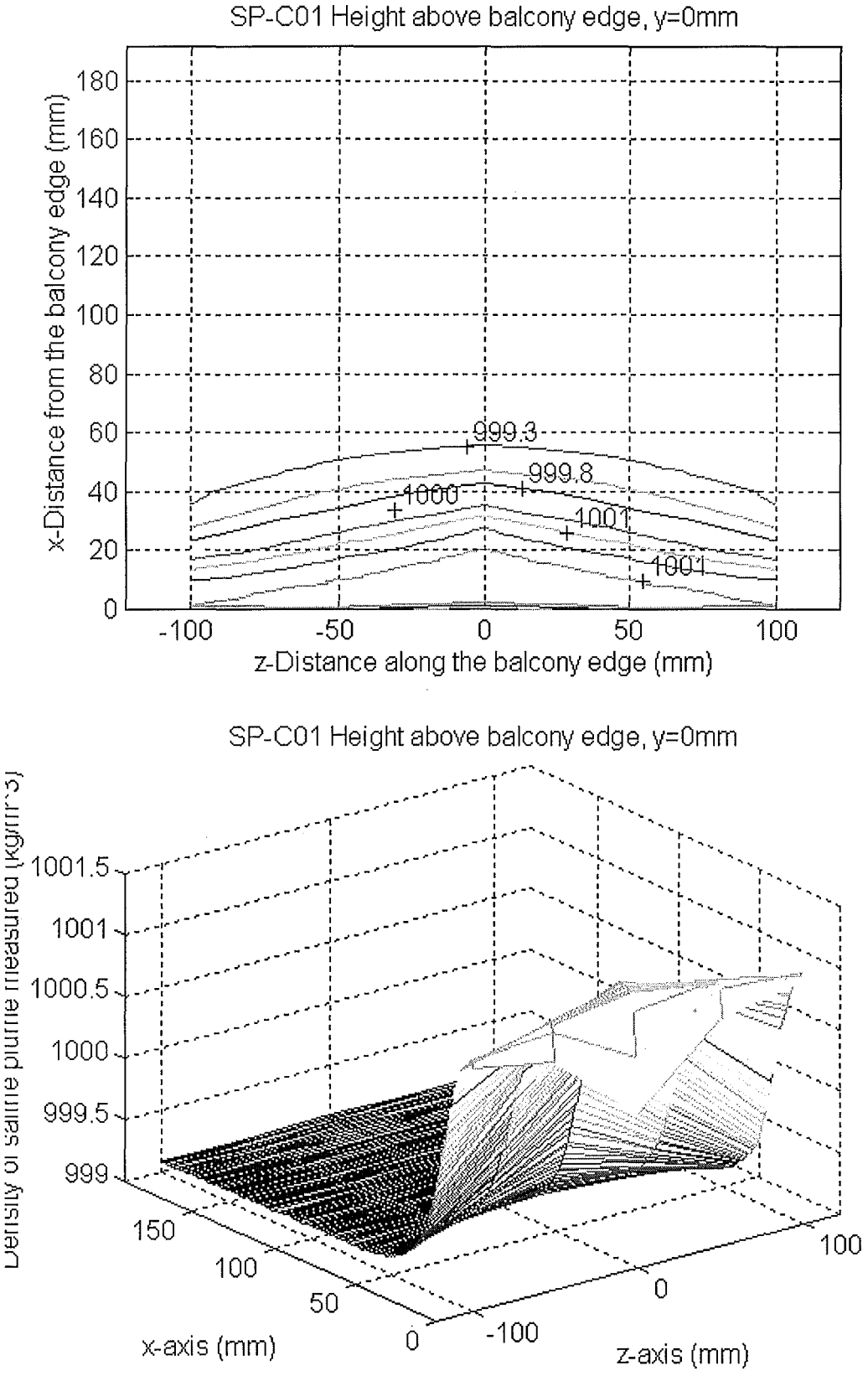

Figure C.9 The x-z contour plot and 3-D density distribution for experimental series SP-C01 at a height of 0mm above balcony edge.

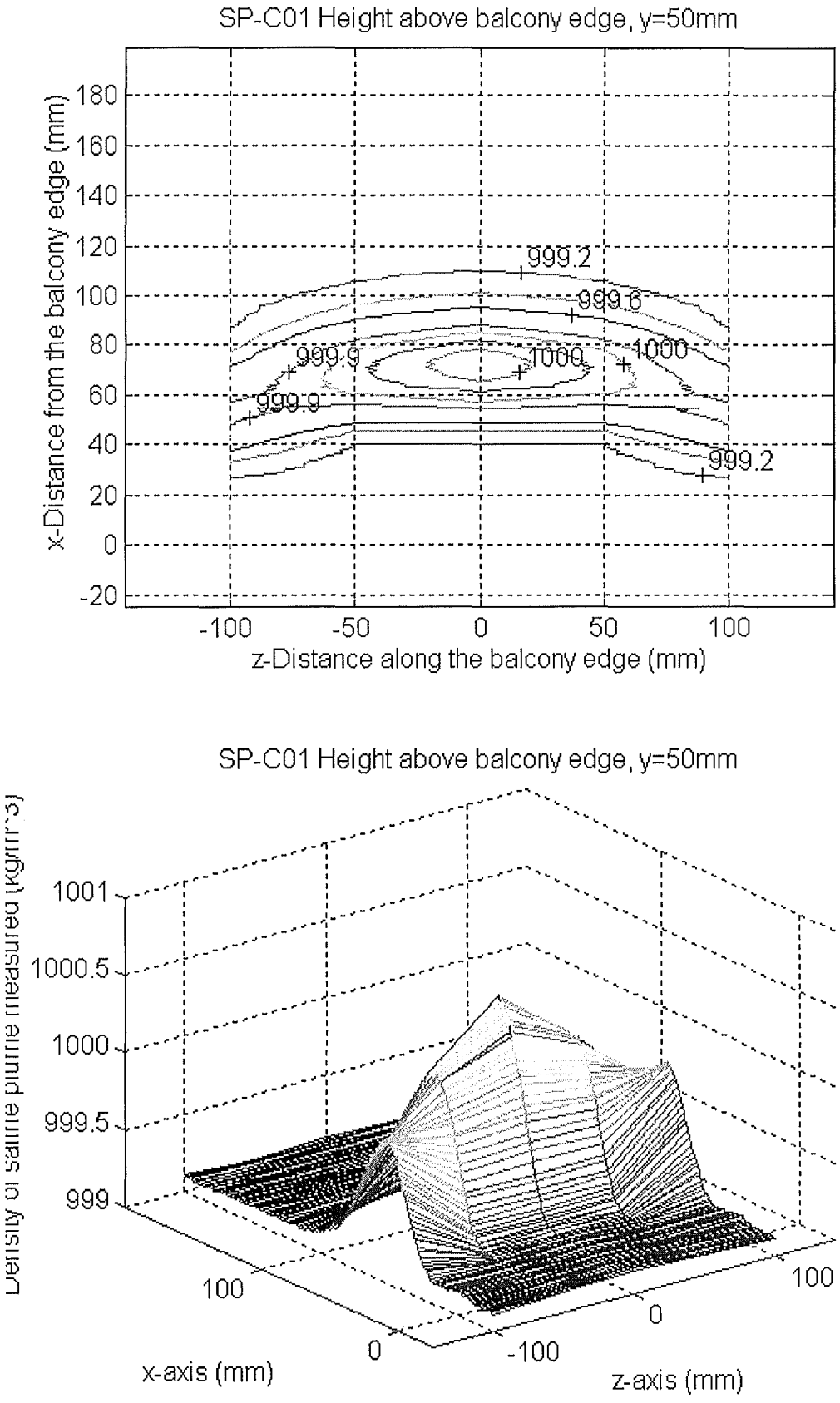

Figure C.10 The x-z contour plot and 3-D density distribution for experimental series SP-C01 at a height of 50mm above balcony edge.

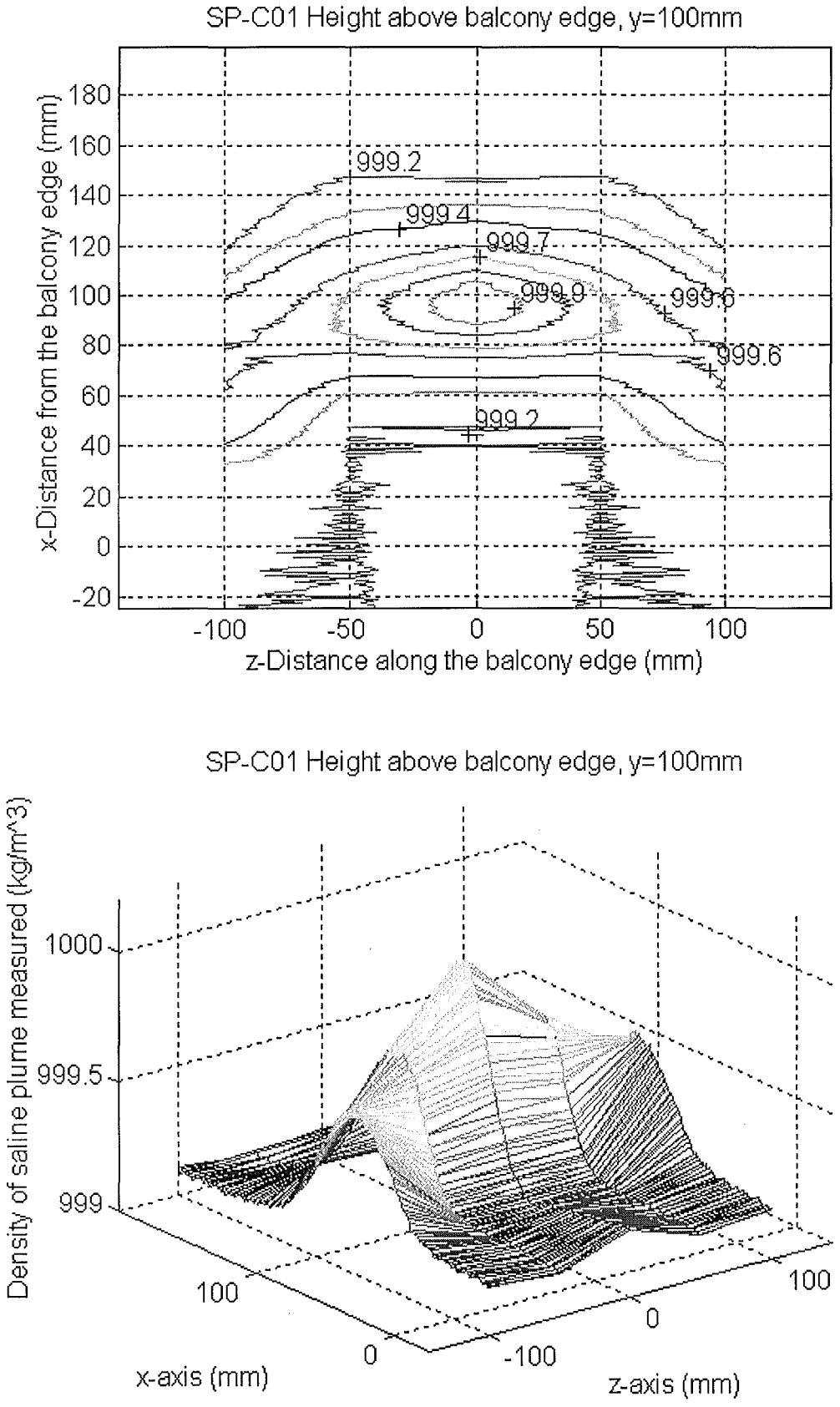

Figure C.11 The x-z contour plot and 3-D density distribution for experimental series SP-C01 at a height of 100mm above balcony edge.

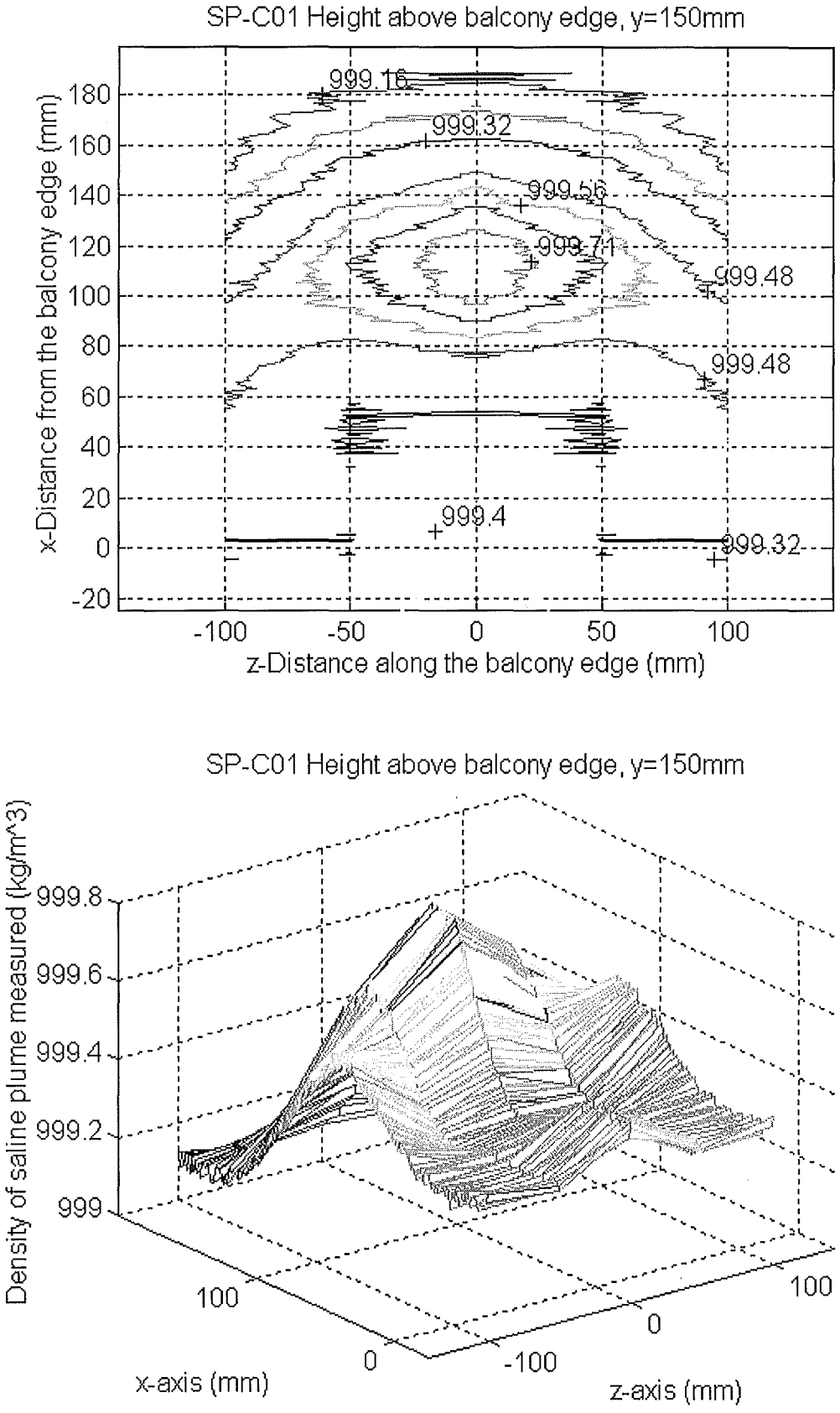

Figure C.12 The x-z contour plot and 3-D density distribution for experimental series SP-C01 at a height of 150mm above balcony edge.

C.4 EXPERIMENTAL SERIES SP-C02

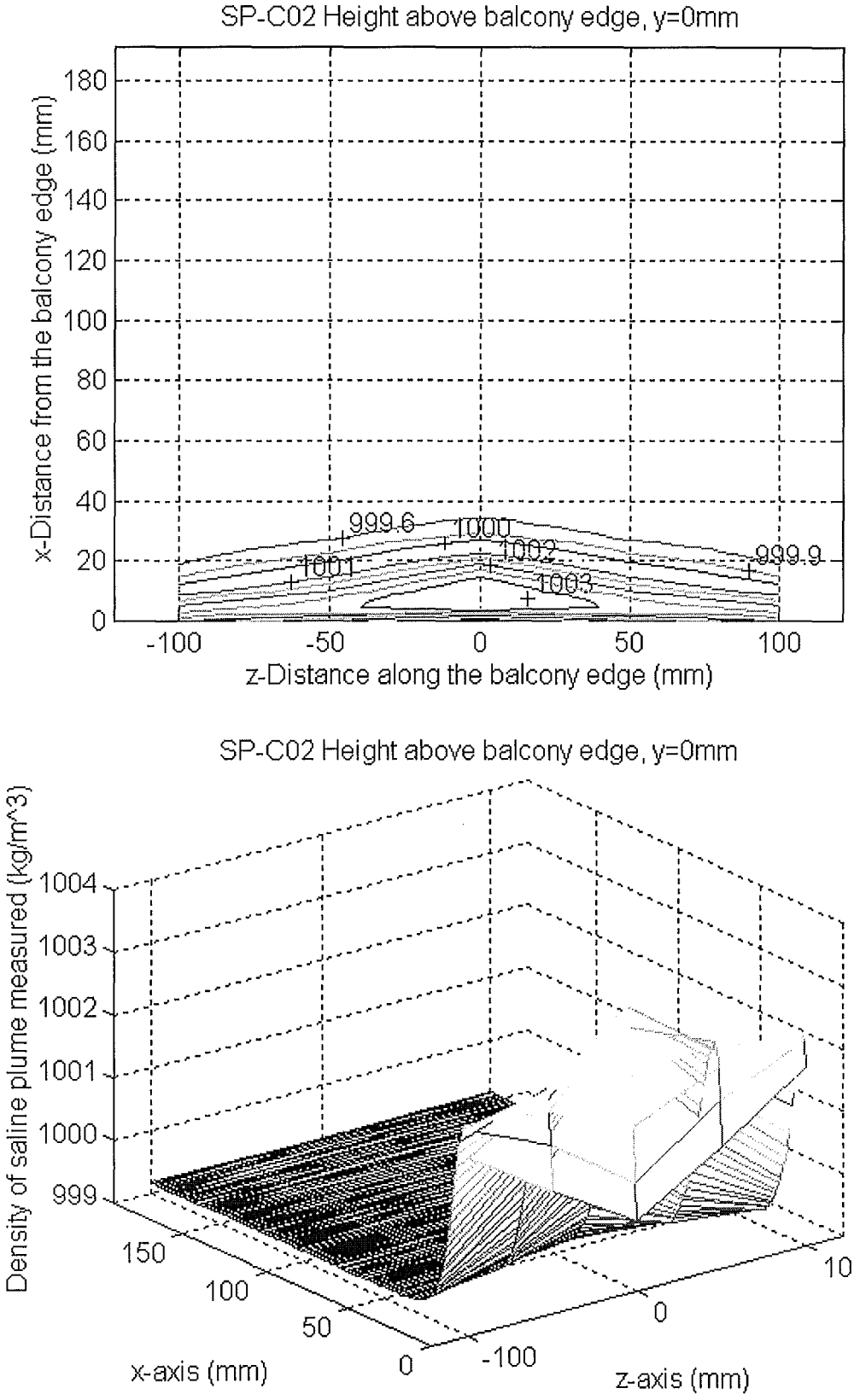

Figure C.13 The x-z contour plot and 3-D density distribution for experimental series SP-C02 at a height of 0mm above balcony edge.

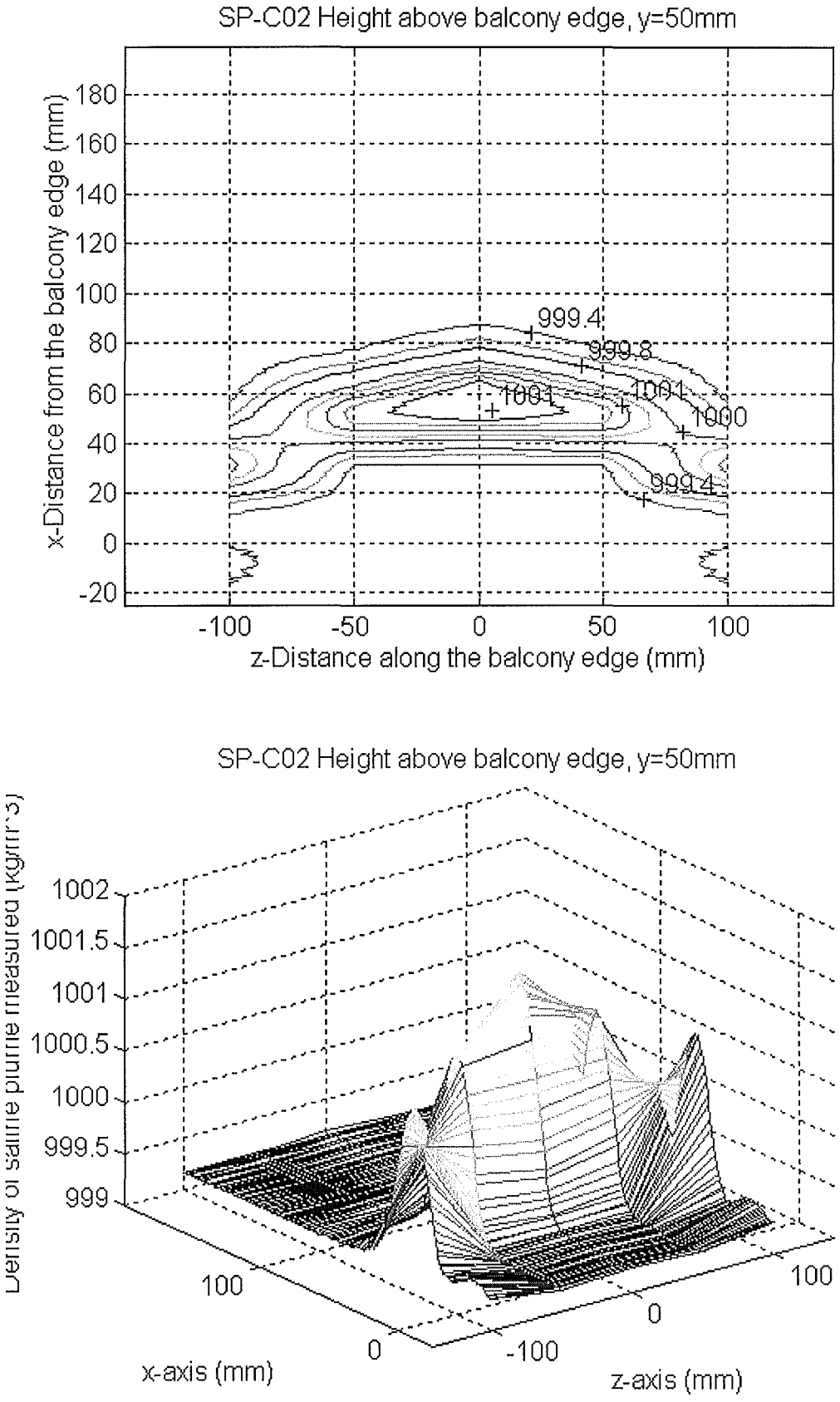

Figure C.14 The x-z contour plot and 3-D density distribution for experimental series SP-C02 at a height of 50mm above balcony edge.

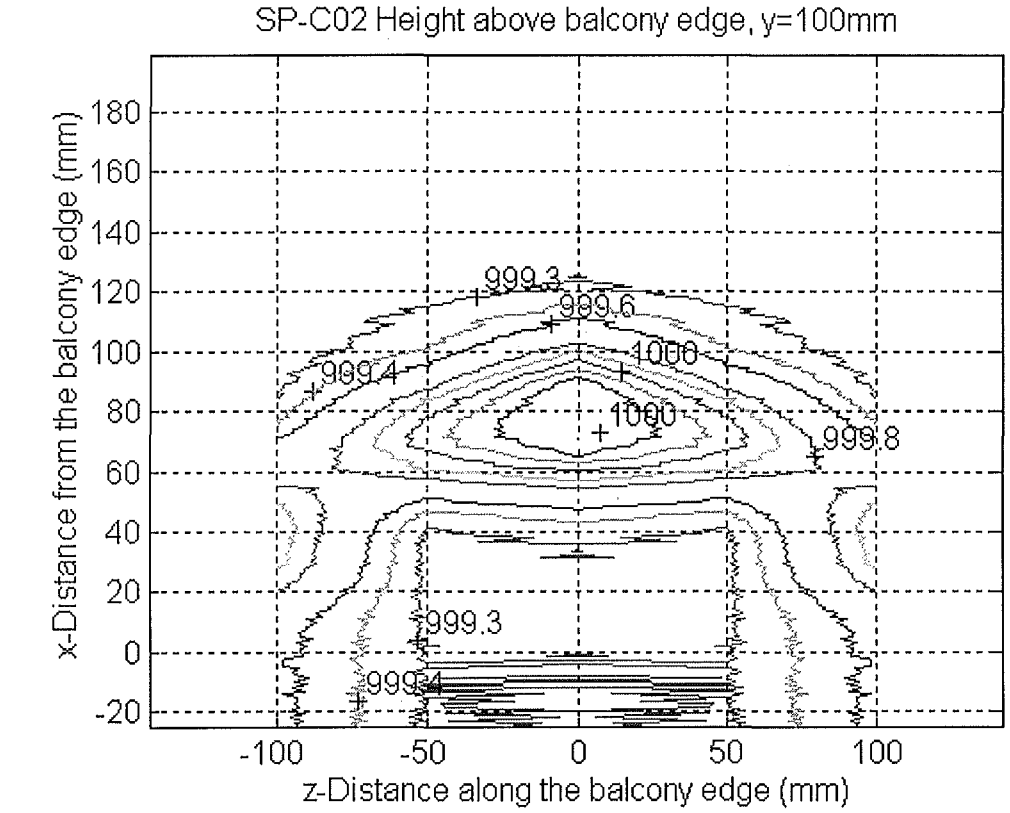

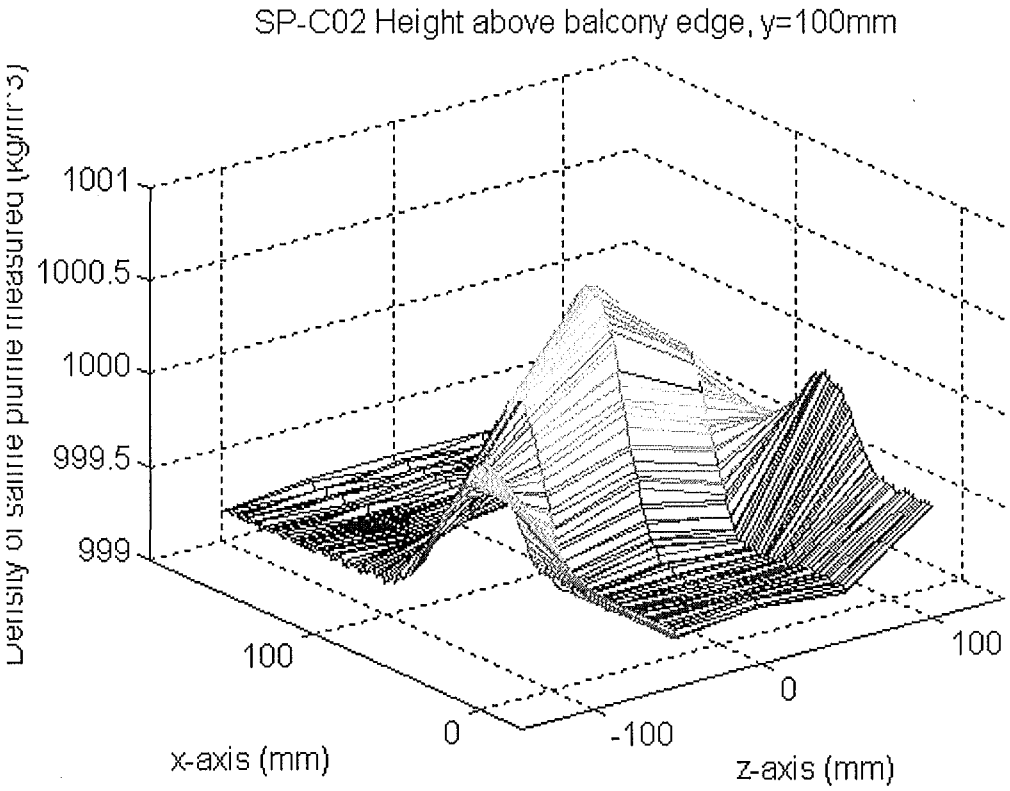

Figure C.15 The x-z contour plot and 3-D density distribution for experimental series SP-C02 at a height of 100mm above balcony edge.

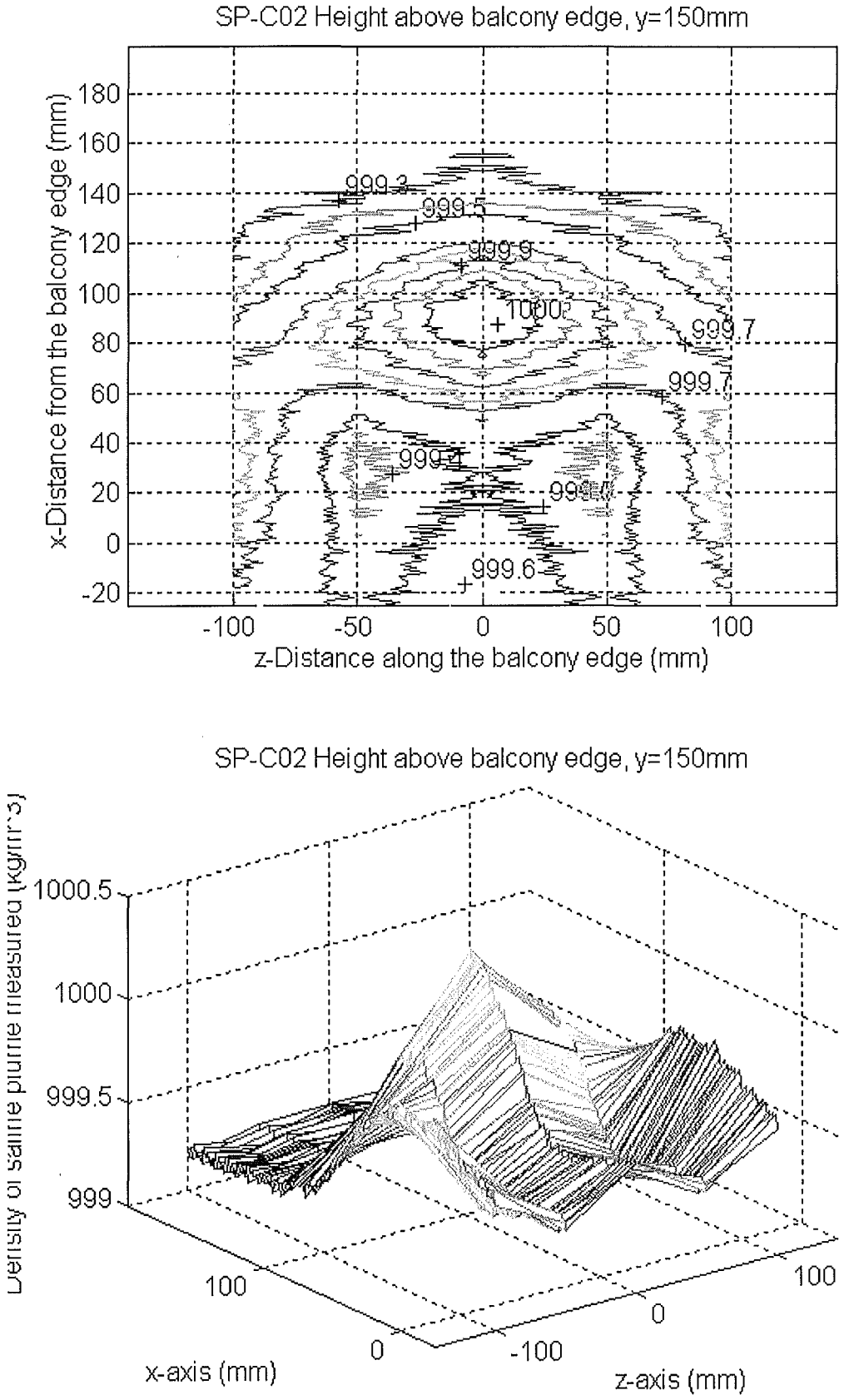

Figure C.16 The x-z contour plot and 3-D density distribution for experimental series SP-C02 at a height of 150mm above balcony edge.

APPENDIX D

FLOW PARAMETERS

References: TURNER, J.S. (1973) *Buoyancy Effects in Fluids*, Cambridge University Press, London, pp 48-90

EMMONS, H.W. (1995) "Vent Flows". In: *SFPE Handbook of Fire Protection Engineering, 2nd Edition.* Eds: P.J. DiNenno, C.L. Beyler, R.L.P. Custer, W.D. Walton, J.M. Watts, D. Drysdale and J.R. Hall. Quincy, MA, pp 4.20-4.29

Notations:

ρ_1	Density of heavy fluid (kg/m^3)- ie Saline solution in this case
ρ_2	Density of lighter fluid (kg/m^3)- ie Ambient fresh water in this case
h_1	Layer depth of the heavy fluid at the vent opening (m)
Q	Volume flow rate (m^3/s)
Q_o	Volume flux per unit width of heavy fluid (m^3/s m)
U	Average velocity of the approaching heavy fluid (m/s)
g	Gravitational constant, 9.81 m/s^2
W	Width of the heavy layer at the vent opening (m)
D	Hydraulic diameter for square vent (m)
μ	Viscosity of the fluid (kg/m s^2)
F	Froude number
Re	Reynolds number

For a heavy layer flowing over an obstacle and under a deep lighter layer at rest, its behaviour depends on the internal Froude number defined in Eq. (D.1) (Turner, 1973).

$$F = \left(\frac{Q_o^2}{g' h_1^3} \right)^{\frac{1}{2}} = \frac{U}{(g' h_1)^{\frac{1}{2}}} \tag{D.1}$$

where g' an effective gravitational term as defined in Eq. (D.2).

$$g' = g \cdot \frac{(\rho_1 - \rho_2)}{\rho_1} \tag{D.2}$$

and average flow velocity, U as in Eq. (D.3).

$$U = \frac{Q}{W \cdot h_1} \tag{D.3}$$

As for the hydraulic diameter, D, for rectangular vent type, it is defined in Eq. (D.4) (Emmons, 1995).

$$D = \frac{2Wh_1}{(W + h_1)} \tag{D.4}$$

and hence Reynolds number is defined as in Eq. (D.5).

$$\mathrm{Re} = \frac{UD\rho_1}{\mu} \tag{D.5}$$

All the experiments were conducted under same flow rate, Q, of 16.25 litre/second and same vent width, W, of 0.250 m. The volume flux per unit width, Q_0, is a constant of 1.083×10^{-3} m^3/s m.

Table D.1 Evaluation of Froude Numbers

	SP-B01	**SP-B02**	**SP-C01**	**SP-C02**
Q_O	1.083×10^{-3}	1.083×10^{-3}	1.083×10^{-3}	1.083×10^{-3}
ρ_1	1002.28	1006.2	1002.07	1005.56
ρ_2	999.13	999.47	999.08	999.16
h_1	0.043	0.033	0.040	0.030
g'	0.0308	0.0656	0.0293	0.0624
Froude No.†	0.692	0.705	0.792	0.834

Table D.2 Evaluation of Reynolds Numbers

	SP-B01	**SP-B02**	**SP-C01**	**SP-C02**
ρ_1	1002.28	1006.2	1002.07	1005.56
h_1	0.043	0.033	0.040	0.030
μ	1.11×10^{-3}	1.12×10^{-3}	1.10×10^{-3}	1.11×10^{-3}
U	0.0252	0.0328	0.0271	0.0361
D	0.0734	0.0583	0.0690	0.0536
Reynolds No.†	1666	1720	1705	1757

† These non-dimensional numbers are all evaluated at the vent opening of the fire compartment.

APPENDIX E

X-Y CONTOUR PLOTS

Application: These contour plots are similar to the flow image plots. They provide the basic shape and density distribution of the rising plume.

Input Data:

- The data sets were collected at single pixel interval along the x-axis from the 100 seconds averaged flow image. They were mapped with corresponding data sets collected along the y-axis at an interval of 12.5mm on the same image.
- Only centre section flow images were manipulated in this Appendix.
- The data sets were presented as a matrix for mapping purpose.
- *Matlab® for Windows*, Classroom Version 4.2c.1 (1994) was used to perform the mapping for these contours.

Table E.1 Experimental settings.

Experimental Series	Balcony Setting	Initial Saline Density (kg/m^3)	Ambient Water Density (kg/m^3)
SP-B01	125 mm	1002.28	999.13
SP-B02	250 mm	1006.20	999.47
SP-C01	125 mm	1002.07	999.08
SP-C02	250 mm	1005.56	999.16

Disclaimer: These contour plots are interpolated using Matlab software. The author does not and has not validated or justified the accuracy of any data point within the interpolation region.

E.1 EXPERIMENTAL SERIES SP-B01

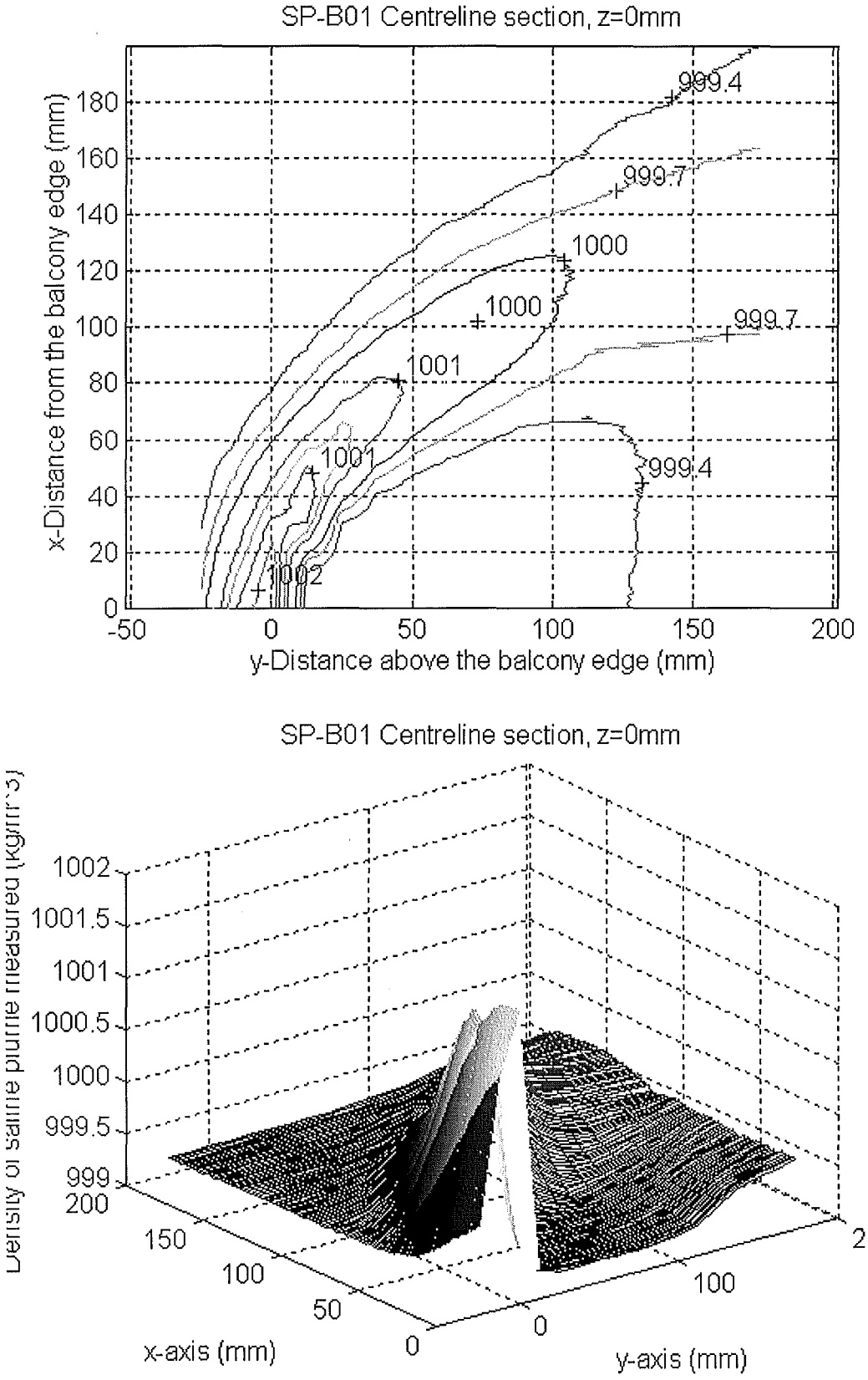

Figure E.1 The x-y contour plot and 3-D density distribution for experimental series SP-B01 at centre section (z=0mm).

E.2 EXPERIMENTAL SERIES SP-B02

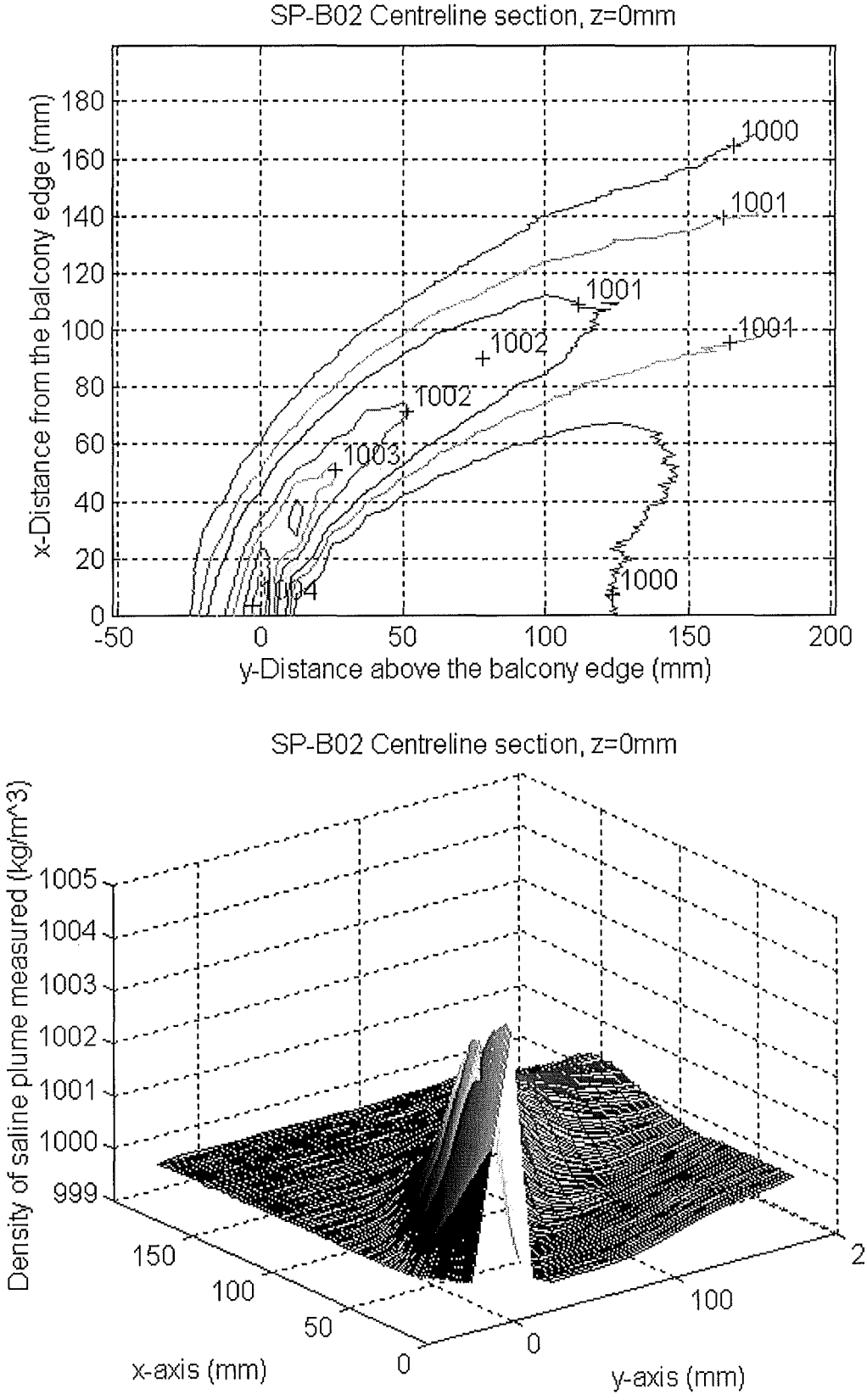

Figure E.2 The x-y contour plot and 3-D density distribution for experimental series SP-B02 at centre section (z=0mm).

E.3 EXPERIMENTAL SERIES SP-C01

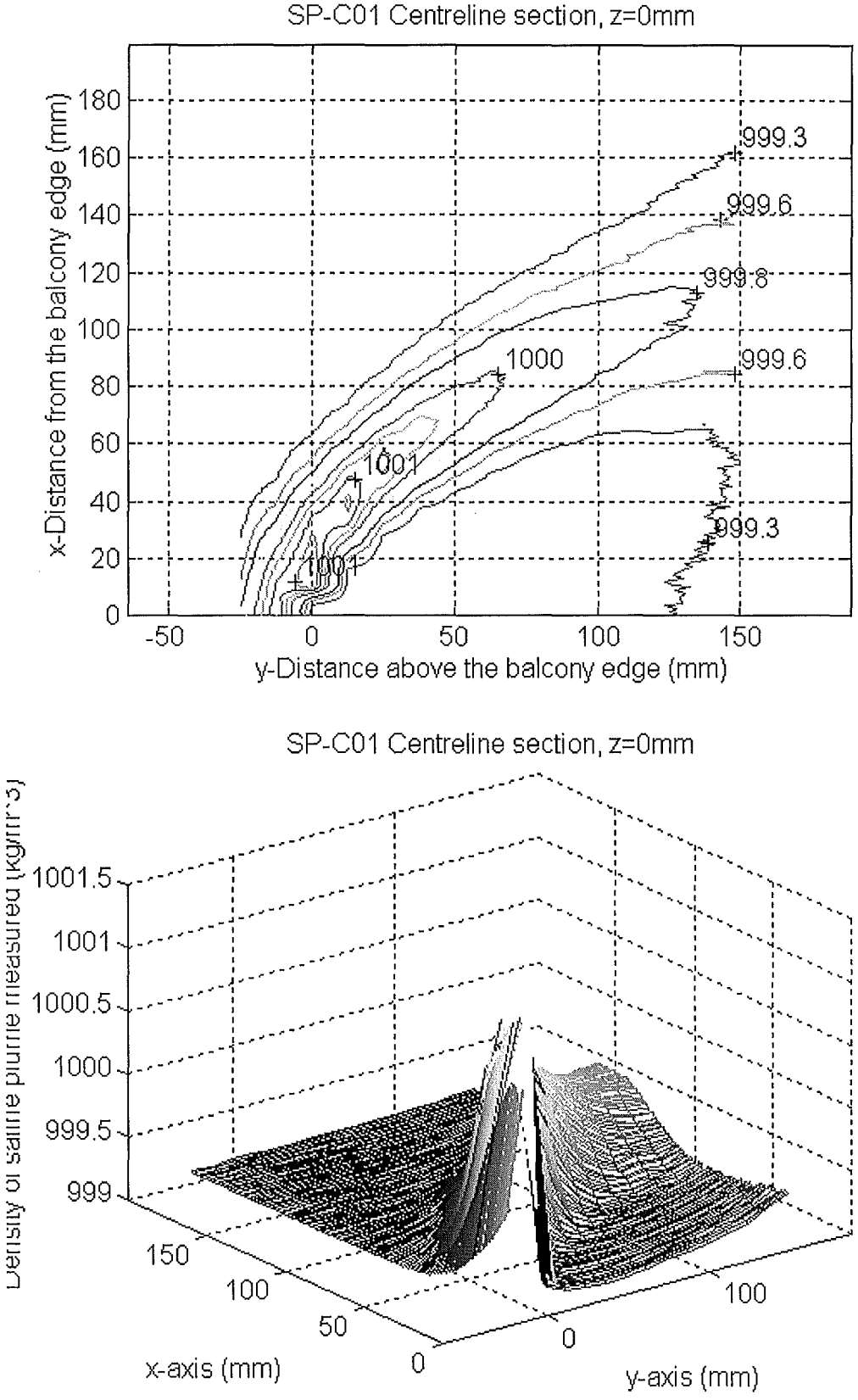

Figure E.3 The x-y contour plot and 3-D density distribution for experimental series SP-C01 at centre section (z=0mm).

E.4 EXPERIMENTAL SERIES SP-C02

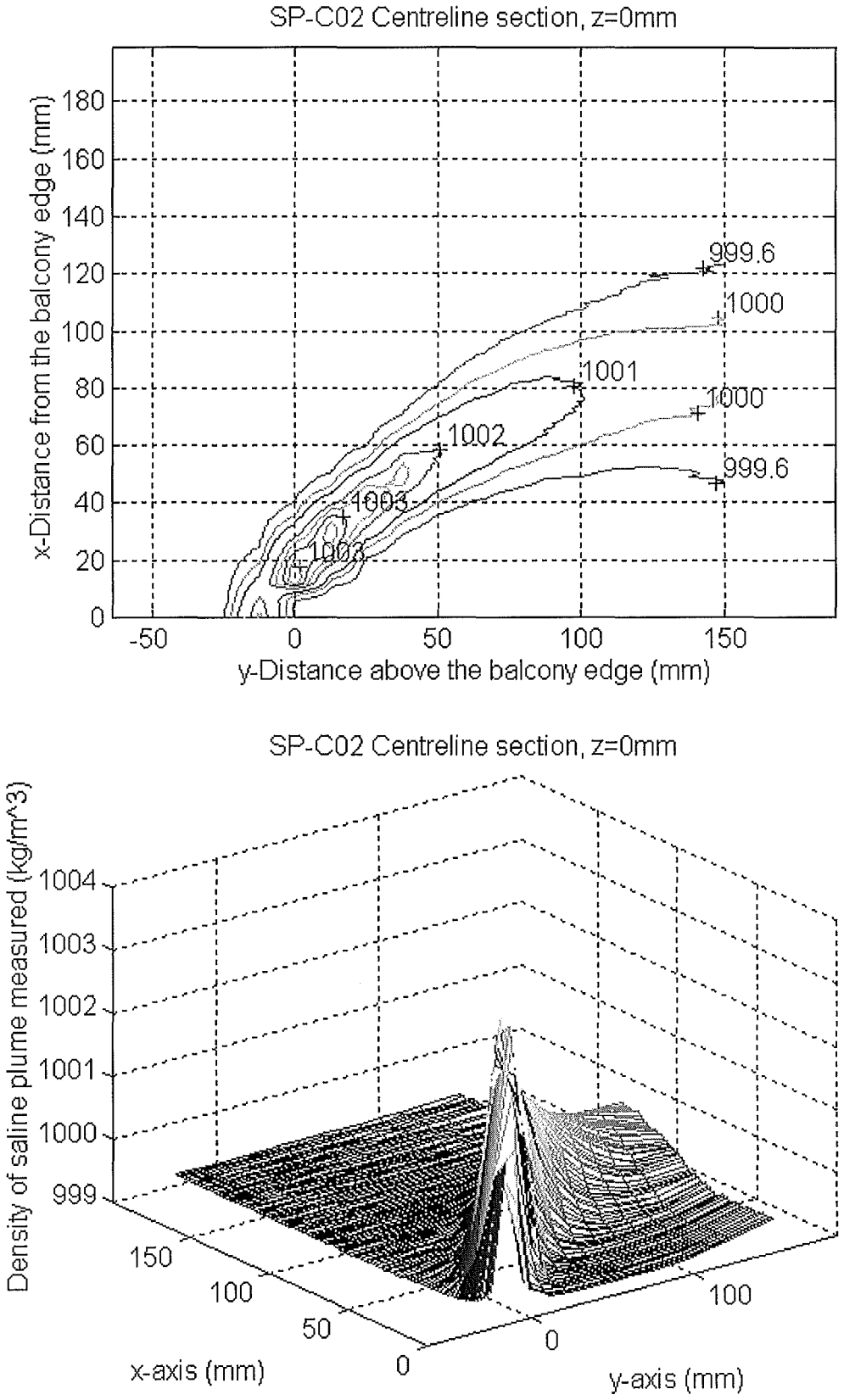

Figure E.4 The x-y contour plot and 3-D density distribution for experimental series SP-C02 at centre section (z=0mm).

FIRE ENGINEERING RESEARCH REPORTS

95/1	Full Residential Scale Backdraft	I B Bolliger
95/2	A Study of Full Scale Room Fire Experiments	P A Enright
95/3	Design of Load-bearing Light Steel Frame Walls for Fire Resistance	J T Gerlich
95/4	Full Scale Limited Ventilation Fire Experiments	D J Millar
95/5	An Analysis of Domestic Sprinkler Systems for Use in New Zealand	F Rahmanian
96/1	The Influence of Non-Uniform Electric Fields on Combustion Processes	M A Belsham
96/2	Mixing in Fire Induced Doorway Flows	J M Clements
96/3	Fire Design of Single Storey Industrial Buildings	B W Cosgrove
96/4	Modelling Smoke Flow Using Computational Fluid Dynamics	T N Kardos
96/5	Under-Ventilated Compartment Fires - A Precursor to Smoke Explosions	A R Parkes
96/6	An Investigation of the Effects of Sprinklers on Compartment Fires	M W Radford
97/1	Sprinkler Trade Off Clauses in the Approved Documents	G J Barnes
97/2	Risk Ranking of Buildings for Life Safety	J W Boyes
97/3	Improving the Waking Effectiveness of Fire Alarms in Residential Areas	T Grace
97/4	Study of Evacuation Movement through Different Building Components	P Holmberg
97/5	Domestic Fire Hazard in New Zealand	KDJ Irwin
97/6	An Appraisal of Existing Room-Corner Fire Models	D C Robertson
97/7	Fire Resistance of Light Timber Framed Walls and Floors	G C Thomas
97/8	Uncertainty Analysis of Zone Fire Models	A M Walker
97/9	New Zealand Building Regulations Five Years Later	T M Pastore
98/1	The Impact of Post-Earthquake Fire on the Built Urban Environment	R Botting
98/2	Full Scale Testing of Fire Suppression Agents on Unshielded Fires	M J Dunn
98/3	Full Scale Testing of Fire Suppression Agents on Shielded Fires	N Gravestock
98/4	Predicting Ignition Time Under Transient Heat Flux Using Results from Constant Flux Experiments	A Henderson
98/5	Comparison Studies of Zone and CFD Fire Simulations	A Lovatt
98/6	Bench Scale Testing of Light Timber Frame Walls	P Olsson
98/7	Exploratory Salt Water Experiments of Balcony Spill Plume Using Laser Induced Fluorescence Technique	E Y Yii

School of Engineering
University of Canterbury
Private Bag 4800, Christchurch, New Zealand

Phone 643 364-2250
Fax 643 364-2758